



<https://theses.gla.ac.uk/>

Theses Digitisation:

<https://www.gla.ac.uk/myglasgow/research/enlighten/theses/digitisation/>

This is a digitised version of the original print thesis.

Copyright and moral rights for this work are retained by the author

A copy can be downloaded for personal non-commercial research or study,  
without prior permission or charge

This work cannot be reproduced or quoted extensively from without first  
obtaining permission in writing from the author

The content must not be changed in any way or sold commercially in any  
format or medium without the formal permission of the author

When referring to this work, full bibliographic details including the author,  
title, awarding institution and date of the thesis must be given

Enlighten: Theses

<https://theses.gla.ac.uk/>  
[research-enlighten@glasgow.ac.uk](mailto:research-enlighten@glasgow.ac.uk)

DOPANT INCORPORATION, DESORPTION AND MIGRATION IN  
MBE GROWN InP AND  $\text{Al}_x\text{Ga}_{1-x}\text{As/GaAs}$

A Thesis,  
submitted to the Faculty of Engineering  
of the University of Glasgow  
for the degree of

Doctor of Philosophy

by

Veli-Matti Airaksinen, M.Sc.

© Veli-Matti Airaksinen, February 1987.

ProQuest Number: 10991923

All rights reserved

INFORMATION TO ALL USERS

The quality of this reproduction is dependent upon the quality of the copy submitted.

In the unlikely event that the author did not send a complete manuscript and there are missing pages, these will be noted. Also, if material had to be removed, a note will indicate the deletion.



ProQuest 10991923

Published by ProQuest LLC (2018). Copyright of the Dissertation is held by the Author.

All rights reserved.

This work is protected against unauthorized copying under Title 17, United States Code  
Microform Edition © ProQuest LLC.

ProQuest LLC.  
789 East Eisenhower Parkway  
P.O. Box 1346  
Ann Arbor, MI 48106 – 1346

# CONTENTS

ABSTRACT

ACKNOWLEDGEMENTS

CHAPTER 1: INTRODUCTION.....1

CHAPTER 2: SOME ASPECTS OF THE MBE GROWTH OF InP

2.1 Introduction.....	9
2.2 Experimental.....	10
2.3 The calibration of beam equivalent pressures	
2.3.1 The calibration of the In-flux.....	13
2.3.2 The calibration of the $P_2$ -flux.....	15
2.4 The $P_2$ -stabilisation of InP.....	16
2.5 The desorption of In during the growth of InP.....	18
2.6 Oval defects.....	20
2.7 Conclusions.....	23
2.8 References.....	24

CHAPTER 3: THE EFFECT OF GROWTH CONDITIONS ON THE  
INCORPORATION AND DESORPTION OF SULPHUR IN  
MBE GROWN InP

3.1 Introduction.....	26
3.2 Experimental.....	29
3.3. Results and discussion	
3.3.1 The effect of the growth temperature on $C_B$ .....	31
3.3.2 $C_B$ vs. incident sulphur flux.....	32
3.3.3 $C_B$ as a function of the growth rate.....	33
3.3.4 $C_B$ vs. the $P_2$ :In flux ratio.....	33
3.4 A thermodynamic analysis of sulphur incorporation and desorption.....	34
3.5 Conclusions.....	38
3.6 References.....	39

CHAPTER 4: A KINETIC MODEL OF DOPANT INCORPORATION AND  
DESORPTION IN MBE GROWN InP AND GaAs

4.1 Introduction.....	41
4.2 The concentration of incorporated dopant atoms vs. incident flux.....	42
4.3 Growth rate dependence of $C_B$ .....	44
4.4 The dependence of $C_B$ on the group V pressure.....	45
4.5 The activation energy of desorption .....	48
4.6 Conclusions.....	52
4.7 References.....	53

CHAPTER 5: A THERMODYNAMIC MODEL FOR THE CALCULATION OF  
NATIVE DEFECT CONCENTRATIONS IN InP AND GaAs

5.1 Introduction.....	55
5.2 The partitioning of the virtual free energies.....	60
5.3 Enthalpies of formation of neutral defects	
5.3.1 Vacancies and divacancies.....	69
5.3.2 Antisite and antistructure defects.....	70
5.4 Entropies of formation of neutral defects.....	74
5.5 Enthalpies and entropies of ionisation	
5.5.1 Ionisation energies of vacancies.....	76
5.5.2 Ionisation energies of antisite defects.....	77
5.5.3 The entropy of ionisation.....	78
5.6 The calculation of defect concentrations	
5.6.1 The thermodynamic model.....	81
5.6.2 Defect concentrations in InP and GaAs.....	83
5.7 Conclusions.....	84
5.8 References.....	89

**CHAPTER 6: SILICON MIGRATION IN MODULATION DOPED  
Al<sub>x</sub>Ga<sub>1-x</sub>As/GaAs HETEROJUNCTIONS**

6.1 Introduction.....93  
6.1.2 Interface roughness.....94  
6.1.3 Impurity accumulation.....95  
6.1.4 Silicon migration.....95  
6.1.5 The improvement of inverted  
heterostructures.....97  
6.2 On the purpose of the experiment.....98  
6.3 Experimental.....100  
6.4 The electron density in the undistorted  
quantum well.....102  
6.5 The distortion of the asymmetrically  
doped well.....104  
6.6 The mobility limiting mechanisms  
in GaAs/AlGaAs quantum wells.....107  
6.6.1 Scattering by remote ionised impurities....108  
6.6.2 Ionised impurity scattering due to  
interface charge.....109  
6.6.3 Interface roughness scattering.....110  
6.6.4 Scattering by acoustic phonons.....112  
6.7 Results and discussion  
6.7.1 Shubnikov-de Haas measurements .....113  
6.7.2 The Hall scattering coefficient.....115  
6.7.3 Mobility vs. temperature.....117  
6.7.4 Annealing experiments.....118  
6.7.5 The mobility vs. the 2D electron  
density.....119  
6.8 Proposals for future work.....120  
6.9 Conclusions.....122  
6.10 References.....123

**CHAPTER 7: CONCLUSIONS AND PROPOSALS FOR  
FUTURE WORK.....127**  
7.2 References.....133

## ABSTRACT

The incorporation, desorption and migration behaviour of sulphur and silicon dopants in MBE-grown InP and GaAs/AlGaAs was investigated.

Some of the more general aspects of the MBE of InP are also discussed to aid the interpretation of the doping studies. Specifically, data is presented on the calibration of the In and  $P_2$  pressures, the stabilisation of InP against the desorption of phosphorus and the sticking coefficient of In at the usual growth temperatures.

A thorough study of the effect of growth conditions on the sulphur doping of InP was completed. A sound theoretical framework based on both thermodynamic equilibrium calculations and a kinetic model was developed to enhance the understanding of the incorporation and desorption processes. Thermodynamic calculations are used to identify the desorbing sulphur species, and to show that the activation energy of desorption can be estimated from the thermochemical constants. The kinetic orders of the reactions are deduced from the experimental data.

In a related application of thermodynamics, a model for the calculation of the concentrations of native defects was developed. The definition of the virtual reactions is discussed. The available experimental and theoretical thermochemical data is reviewed and used for calculating the defect concentrations.

The thesis concludes with a study of silicon migration in modulation doped GaAs/AlGaAs heterostructures. Low temperature Hall measurements of annealed samples were used to show that silicon diffusion can degrade the electron mobility. Evidence is presented of the strong localisation of the 2 dimensional electrons in the unannealed samples.

## ACKNOWLEDGEMENTS

This work would not have been possible without the contributions of a number of people.

I wish to express my gratitude to Professor J. Lamb for the provision of research facilities, and to my supervisor Dr. C. R. Stanley, whose guidance and suggestions proved invaluable.

For the technical assistance at the Department of Electronics, I would like to thank Messrs. J. Cochrane, J. Young, G. Boyle, R. Darkin and J. Clark.

Warmest thanks are due to my flatmates, Messrs. L. Bradley, J. Duffy and D. Halliday for their, usually unscientific, contributions.

I would also like to thank Mr. K. Y. Lee for numerous useful suggestions, primarily in the field of oriental cuisine.

Best of thanks to my fellow MBE students, J. Frost and I. McIntyre and especially T. S. Cheng, with whom I shared the joys of growing InP.

In June 1986 the MBE laboratory was destroyed in a fire, a rather severe misfortune even by the standards of molecular beam epitaxy. For me, however, there was an unexpected bonus: I got the opportunity to work at Philips Research Laboratories for three months (Chapter 6). Best of thanks to Dr. C.T. Foxon and Dr. J.J. Harris I would also like to thank Dr. R. Beall for growing the samples, Dr. D. Hinton for the annealing, Mrs. C. White for preparing the Hall samples, Mr. J. Hewitt for his help with the Hall measurements and Dr. D. Lacklison for the mobility vs. temperature measurements.

Financial support by the Finnish Academy of Technical Sciences is gratefully acknowledged, likewise the support by the Ministry of Education (Finland).

It is perhaps unusual to acknowledge the contribution of a dog in a thesis. I can say truthfully, however, that without the pestering of our Border Collie, Tim, Chapter 5 would probably have stayed unfinished. When the choice was between taking him for a walk in the rain and sleet or staying in to write up, the writing up won often enough. Thanks Tim.

I also wish to express my gratitude to my parents and parents-in-law, who have always been ready to help in every possible way. Last, but not most, I thank my wife Janice for her patience and support, without which this work would have been immeasurably harder.

## CHAPTER 1

### INTRODUCTION

During the past few years the heterostructures of III-V compounds have become increasingly important for both basic research and the development of advanced semiconductor components. The need for the heterostructure devices is steadily increasing because of their superior and often unique optical and electrical properties.

Heterojunctions, quantum wells and superlattices can be used to modify the band structure of the III-V compounds to effectively create new materials with unique properties. These can be used for either enhancing the performance of semiconductor devices or for devising totally new kinds of components. Heterostructure devices offer high electron mobilities for faster components, such as high electron mobility transistors (HEMTs) [1], two dimensional electron gas field effect transistors [2] or ballistic transistors [3],[4]. The optical properties of many III-V compounds make them very attractive as light sources, for instance multiple quantum well (MQW) [5] lasers and detectors such as solid state photomultipliers [6] in optical communications systems.

As the lateral dimensions of semiconductor devices continue to diminish towards the de Broglie wavelength of free electrons, devices based on entirely new physical principles become possible. As an example, quantum interference switching devices based on the Aharonov-Boehm effect can be mentioned [7]. The properties of such quantum mechanical devices are still open to speculation. However, they are likely to offer a way of avoiding the physical limits of conventional

technologies and to provide the next stage in the rapid improvement in the performance of semiconductor devices.

The demand for the heterostructure devices is increased further by the steady improvement of the different epitaxial growth methods, which makes new, more complicated structures feasible. Of the several competing technologies, metal-organic chemical vapour deposition (MOCVD) and molecular beam epitaxy (MBE) have emerged as the most promising during the past decade. The MOCVD seems to have a higher throughput making the scaling up of the growth process for large scale production easier, but the MBE has the advantage of slow growth rates which allow extremely abrupt interfaces to be grown.

Interestingly, it seems that the advantages of different materials and epitaxial technologies can be combined. Hence, the new techniques of growing polar semiconductors on non-polar substrates, i.e. GaAs on Si [8], allow more latitude for choosing the correct material for each purpose on the same wafer. It seems possible that - in another example of technological convergence - the MBE and MOCVD can be successfully combined by using gaseous sources in processes called chemical beam epitaxy (CBE) or metal-organic MBE (MOMBE) [9],[10].

In spite of its considerable advantages, MBE has several unresolved problems which need to be addressed. Amongst these are the high cost per wafer - both in money and skilled manpower - which mainly results from the relatively low reliability, throughput and yield, and the numerous problems which often hamper routine growth. These include the spatial and temporal non-uniformity of the incident beams, unreliable flux calibration methods for the group V species and the accurate measurement of the growth temperature. Even though, at the expense of added complexity, all of these problems can be solved or their effects can be reduced,

they still continue to affect the reproducibility of the MBE growth. For instance, every laboratory seems to have its own temperature scale, which has usually not been calibrated very accurately thus making meaningful comparisons between experiments performed in different MBE systems very difficult.

More important and potentially more serious than the growth system related problems are the deviations of the actual MBE growth process from the ideal model. Ideally MBE would have

- constant sticking coefficients for all matrix and dopant species and a zero sticking coefficient for all background impurities,
- facile surface kinetics for the incorporation and migration of the atoms on the surface to allow the growth of layers with a crystal perfection similar to such near equilibrium techniques as liquid phase epitaxy (LPE) or vapour phase epitaxy (VPE).
- no diffusion, surface accumulation or segregation effects of either the matrix or the dopant species to allow the growth of abrupt interfaces and
- dopants which show no compensation or self-compensation effects and which allow doping levels up to  $10^{20} \text{ cm}^{-3}$ .

In the real growth process there are of course many deviations from the ideal model. This thesis is mainly concerned with the incorporation, desorption and migration behaviour of dopants in MBE-grown InP and GaAs/AlGaAs. The original aim of the work was to investigate the doping behaviour of sulphur and magnesium in InP, extend the work to GaInAs on InP, with GaInAsP/InP as the ultimate goal. As it turned out, the research programme had to be modified due to both "the usual" practical difficulties (Murphy's Law works overtime in MBE) and the more unusual two fires which occurred in 1984 and 1986. Therefore, the

GaInAs/InP and GaInAsP/InP studies were never started. However, it should be noted that chemical beam epitaxy allows much easier and more accurate control of the group V beam fluxes [9]. Hence, the growth of quaternaries with two group V constituents by solid source MBE does not in any case seem attractive.

However, a thorough study of sulphur doping of InP was completed. A sound theoretical framework based on both thermodynamic equilibrium calculations [11] and a kinetic model was developed to enhance the understanding of the incorporation and desorption processes. In a related application of thermodynamics, a model for the calculation of the concentrations of native defects is presented. The thesis concludes with a study of silicon migration in GaAs/AlGaAs heterostructures undertaken at Philips Research Laboratories.

In Chapter 2 some of the more general aspects of the MBE of InP are discussed. Especially, the calibration of the In and P<sub>2</sub> pressures, the stabilisation of InP against the desorption of phosphorus and the sticking coefficient of In at the usual growth temperatures are discussed to aid the interpretation of the doping studies and the thermodynamic calculations of later Chapters. Also, the effect of the oval defects on the electrical and optical properties of InP is explored in Chapter 2.

According to Martin et al. [12] sulphur originating in the red phosphorus charge of the phosphorus cell is the main background impurity in InP grown by MBE. Sulphur is also a useful dopant of both GaAs and InP [13],[14],[15]. Therefore a better understanding of the doping behaviour of sulphur is needed for both its use as an intentional dopant and to optimise the growth parameters for the growth of high quality undoped InP. In Chapter 3 extensive experimental data of the effect

of growth conditions on the incorporation and desorption behaviour of sulphur in InP is presented. Thermodynamic equilibrium calculations first proposed by Heckingbottom [11] are used to identify the desorbing sulphur species, and to show that the activation energy of desorption can be estimated from the thermochemical constants.

To gain information about the kinetics of the incorporation and desorption reactions, the results of Chapter 3 are analysed in Chapter 4. The analysis is based on the basic kinetic model by Wood and Joyce [16], according to which the dopant incorporation occurs from a surface layer. It is shown how the kinetic orders of the reactions can be deduced from the experimental data, and how the In flux affects the incorporation and desorption rates.

Thermodynamic calculations can be used for estimating the concentration<sup>of</sup> native point defects in semiconductors grown near thermodynamic equilibrium [17],[18],[19],[20],[21]. In Chapter 5 a model for the calculation of the concentrations of native defects in InP and GaAs is developed. Special attention is given to the definition of the virtual reactions, ~~from~~ which the real formation reactions can be formed. The available experimental and theoretical thermochemical data is reviewed and used for calculating the defect concentrations and the limitations of such an approach are discussed.

At low temperatures the main scattering mechanism limiting the mobility of electrons in doped semiconductors is caused by ionised impurities. The scattering by ionised impurities can be reduced by using modulation doped structures in which the free electrons are separated from the ionised donors [22]. The doped layer is in the wide band gap material (i.e. AlGaAs),

whereas the electrons are collected in the quantum well formed at the heterojunction.

It is an ubiquitous problem of the modulation doped GaAs/AlGaAs system that the so called inverted structure, in which the GaAs layer is grown on top of the AlGaAs, has much lower mobilities than the normal structure (AlGaAs on GaAs) [23]. A major reason for the inferiority of the inverted structure is the migration of silicon from the doped layer towards the quantum well [24]. It is not known whether the surface segregation or diffusion of silicon is causing the migration. In Chapter 6 low temperature Hall measurements are used for investigating the migration of Si towards the GaAs quantum well in AlGaAs/GaAs/AlGaAs modulation doped structures. Annealing experiments are used to show that silicon diffusion can degrade the 2 dimensional electron mobility.

## 1.2 References

- [1] S.Hiyamizu and Y.Mimura, J.Cryst.Growth 56 (1982) 455.
- [2] D.Delagebeaudeuf and N.T.Linh, IEEE Trans. on Electron.Dev. ED-29 (1982) 955.
- [3] M.I.Nathan and M.Heiblum, IEEE Spectrum 23 (1986) 45.
- [4] D.Ankri, W.Schaff, C.E.C.Wood, L.F.Eastman, D.W.Woodard and L.Rathburn, Inst.Phys.Conf.Ser. No 65 (1983) 431.
- [5] W.T.Tsang and R.L.Hartman, Appl.Phys.Lett. 38 (1981) 502.

- [6] F.Capasso, W.T.Tsang, A.L.Hutchinson and G.F.Williams, Appl.Phys.Lett. 40 (1982) 38.
- [7] S.Datta, M.R.Melloch, S.Bandyopadhyay, R.Noren, M.Vaziri, M.Miller and R.Reifenberger, Phys.Rev.Lett. 55 (1985) 2344.
- [8] W.I.Wang, Appl.Phys.Lett. 44 (1984) 1149.
- [9] W.T.Tsang, Proceedings of the 4th International Conference on MBE, York 1986. To be published in J.Cryst.Growth, February 1987.
- [10] M.B.Panish, Proceedings of the 4th International Conference on MBE, York 1986. To be published in J.Cryst.Growth, February 1987.
- [11] R.Heckingbottom, in "Molecular Beam Epitaxy and Heterostructures" Eds. L.L.Chang and K.Ploog (Nijhoff, Dordrecht, 1985), p.71.
- [12] T.Martin, C.R.Stanley, A.Iliadis, C.R.Whitehouse and D.Sykes, Appl.Phys.Lett. 46 (1985) 994.
- [13] D.A.Andrews, R.Heckingbottom and G.J.Davies, J.Appl.Phys. 54 (1983) 4421.
- [14] A.Iliadis, K.A.Prior, C.R.Stanley, T.Martin and G.J.Davies, J.Appl.Phys. 60 (1986) 213.
- [15] D.A.Andrews, R.Heckingbottom and G.J.Davies, J.Appl.Phys. 60 (1986) 1009.
- [16] C.E.C.Wood and B.A.Joyce, J.Appl.Phys. 49 (1978) 4854.
- [22] L.Esaki and R.Tsu, Internal Report RC 2418, IBM Research, March 1969.
- [23] T.J.Drummond, J.Klein, D.Arnold, R.Fischer, R.E.Thorne, W.G.Lyons and H.Morkoc, Appl.Phys.Lett. 42 (1983) 615.
- [24] K.Inoue, H.Sakaki, J.Yoshino and Y.Yoshioka, Appl.Phys.Lett. 46 (1985) 973.
- [17] R.M.Logan and D.T.J.Hurle, J.Phys.Chem.Solids 32 (1971) 1739.
- [18] D.T.J.Hurle, J.Phys.Chem.Solids 40 (1979) 613.
- [19] G.A.Baraff and M.Schlueter, Phys.Rev.Lett. 55 (1985) 1327.

[20] G.M.Blom, J.Cryst.Growth, 36 (1976) 125.

[21] R.L.S.Devine, PhD Thesis, University of Glasgow  
1985.

## CHAPTER 2

### SOME ASPECTS OF THE MBE GROWTH OF InP

#### 2.1 Introduction

A major incentive for the growth of InP and GaInAsP lattice matched to InP is their suitability as light sources and detectors in the 1.3-1.6 $\mu$ m wavelength range. However MBE has not been commonly used for the growth of InP. This is partly due to the reputation of phosphorus containing alloys as being "difficult" to grow because of the reactivity and high vapour pressure of phosphorus. A more serious obstacle to the growth of quaternary alloys is the difficulty of accurately controlling the composition of an alloy containing both As and P, which have sticking coefficients strongly dependent on the growth conditions [1]. Recently, however, the development of gas sources for MBE has shown considerable promise for solving these problems [2],[3].

The growth of undoped InP with the MBE system used also in this work has previously been studied by Martin et al. [4] who found sulphur to be the main unintentional impurity. The sulphur originates in the red phosphorus and sets a lower limit of the free electron concentration of  $1-2 \times 10^{15} \text{ cm}^{-3}$  in high quality InP [4],[5]. The highest reported electron mobility in InP grown using elemental sources is  $55000 \text{ cm}^2/\text{Vs}$  [5].

In this work InP was grown by using conventional solid sources, the main emphasis being on the properties of sulphur doped material. However, it was found necessary to characterise some aspects of the growth of undoped InP for the modelling of the dopant incorporation and desorption processes. Especially, the In and P<sub>2</sub> fluxes were calibrated to find the correct

pressures to use for the thermodynamic calculations. On the basis of the flux calibration experiments it is shown that the true flux equivalent pressure can differ from the beam equivalent pressure given by the ion gauge by over an order of magnitude. From the phosphorus stabilisation experiments the accommodation coefficient of  $P_2$  can be determined.

Also, the desorption of indium at elevated temperatures may decrease the growth rate of InP thus leading to erroneous conclusions about the effect of growth conditions on the dopant concentration. Hence the In desorption was studied both experimentally and on the basis of the equilibrium model of Heckingbottom [6].

An ubiquitous morphological problem on MBE grown InP are the so called oval defects [7]. There is evidence that similar defects on GaAs can affect the electrical [8] and optical [9] characteristics of the layer, therefore some experiments were done to check whether similar effects apply to InP.

## 2.2 Experimental

The MBE growth apparatus used in these studies has, apart from small modifications, been previously described by Martin et al. [4]. The growth chamber was evacuated by a liquid nitrogen ( $LN_2$ ) trapped diffusion pump and a water cooled titanium sublimation pump (TSP). Extensive  $LN_2$  cryopanelling surrounded the substrate heater assembly. Ultimate background pressures were less than  $5 \times 10^{-10}$  mbar after a bakeout at about  $180^\circ C$  for 24 hours and typically  $2 \times 10^{-9}$  mbar between growth runs. The system was equipped with a load lock/transfer chamber evacuated by an ion pump. Pentaphenylether was used as the pump fluid in the diffusion pump which was backed by a rotary pump. To prevent the backstreaming of the rotary pump

oil into the diffusion pump, the backing line was equipped with a molecular sieve trap and the outlet from the diffusion pump was connected to a ballast tank separated from the backing line by a magnetic valve which only opened when the pressure in the ballast tank exceeded a preset value of about  $10^{-3}$  mbar. To reduce the amount of volatile phosphorus compounds reaching the rotary pump the backing line contained an activated carbon filter. The boil off nitrogen gas from a  $\text{LN}_2$  was utilised for ballasting the rotary pump to prevent the condensation of any phosphorus compounds in the pump oil, which was also continuously filtered through an external oil filter.

The pressure in the growth chamber was monitored by a movable ion gauge which was also used for calibrating the In and  $\text{P}_2$  fluxes prior to each growth run.

The phosphorus source was made of graphite with two independently heated stages, the first  $28 \text{ cm}^3$  low temperature stage to produce tetramers  $\text{P}_4$  from red phosphorus and the second, high temperature stage, to crack the tetramers to dimers ( $\text{P}_2$ ). The  $\text{P}_4$  to  $\text{P}_2$  conversion efficiency of the cracker section at  $900^\circ\text{C}$  is estimated to be over 90% [10].

The indium source was a  $3 \text{ cm}^3$  pyrolytic boron nitride (pBN) crucible surrounded by a tantalum heater and heat shielding.

The sulphur flux was generated by a Pt/ $\text{Ag}_2\text{S}$ / $\text{AgI}$ / $\text{Ag}$ /Pt galvanic cell [11] to overcome the problems associated with the handling of elemental sulphur in vacuum. Each beam source was shuttered with a manually operated shutter. All the sources except the electrochemical cell were surrounded by watercooling jackets to prevent the heating of the stainless steel walls of the growth chamber. Prior to growth the In cell was outgassed for 15 minutes approximately  $30^\circ\text{C}$  above the intended operating temperature. The  $\text{P}_2$ -cracker was similarly outgassed at about  $950^\circ\text{C}$  for 1-2 hours.

Fe-, S- or Sn-doped (100)-InP substrates were cleaned with organic solvents and etched in a 10:1:1 solution of  $\text{H}_2\text{SO}_4:\text{H}_2\text{O}_2:\text{H}_2\text{O}$  for 15s. The substrates were either supplied polished by the manufacturers [12] or polished in a 1% bromine-methanol solution. The substrates were mounted on molybdenum plates with indium, introduced into the growth chamber through the load lock and heat cleaned in vacuo at about  $520^\circ\text{C}$  for 3 minutes in a stabilising  $\text{P}_2$  flux, usually about  $2-3 \times 10^{-6}$  mbar. The temperature of the Mo-plate was measured with a fixed thermocouple and calibrated by using the known eutectic transition temperature ( $577^\circ\text{C}$ ) of an Al-Si alloy as a reference point. During calibration measurements care was taken to keep the Mo-plate under a sufficient  $\text{P}_2$ -flux to prevent its emissivity from changing due to the depletion of phosphorus from the indium solder.

Hall mobilities and free electron concentrations were measured from square or clover-leaf samples with alloyed Sn-contacts with a computer controlled Hall apparatus. Photoluminescence measurements at 16K were used for characterising the optical properties of the grown layers. Free electron concentration profiles were measured with an electrochemical C-V profiler [13].

## 2.3 The calibration of the beam equivalent pressures

### 2.3.1 The calibration of the In-flux

The indium flux was calibrated by measuring the thickness of several layers grown with different In beam equivalent pressures (BEPs) as given by the ion gauge. At the low growth temperature of 480°C the possible desorption of In could be ignored (Section 2.5). The layers were either grown on substrates partially covered by a tantalum screen or they were etched with the electrochemical C-V profiler to provide a step structure for the electromechanical thickness measurement. The experimental data shows some scatter, probably caused by errors in the BEP measurements which were sensitive to the position of the ion gauge due to the collimation of the In beam. It was found that the growth rate varies linearly (within the error limits) with the indium BEP so that a BEP of  $4 \times 10^{-7}$  mbar is equivalent to a growth rate of 1.5  $\mu\text{m}/\text{h}$  (Figure 2-1).

For the thermodynamic calculations of Chapters 3 and 5 it is useful to convert the flux to pressure and to compare this to the measured beam equivalent pressure. Let us define the "true" pressure of indium as the the pressure  $p(\text{In})$  of an ideal gas which causes a flux  $F$ . Hence the relation between  $F$  and  $p(\text{In})$  is

$$F = p(\text{In}) / \{2\pi m k_B T\}^{1/2} \quad (2-1)$$

where  $m$  is the mass of the gas molecules,  $k_B$  is Boltzmann's constant and  $T$  is the temperature. By using equation (2-1) together with the growth rate calibration data the relation between the pressure  $p(\text{In})$  and the BEP can be calculated as

$$p(\text{In}) = 26 \cdot \text{In}(\text{BEP}) \quad (2-2)$$

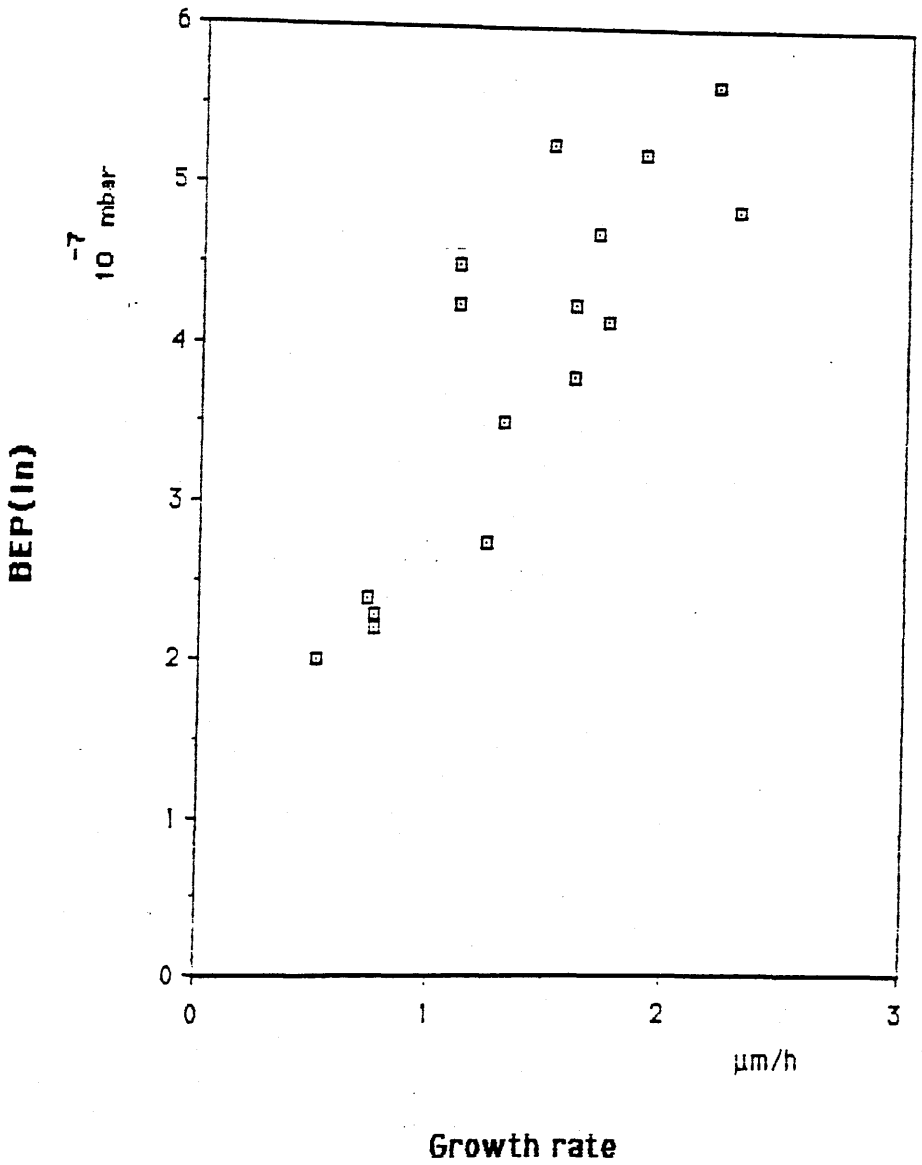


Figure (2-1). The growth rate of InP vs. the In-flux (BEP) measured by the flux monitoring ion gauge. Each data point corresponds to a different layer grown at  $T_s = 460-560^\circ\text{C}$ .

Ion gauges are usually calibrated for nitrogen at room temperature  $T_R=300K$ . The ionisation coefficient of molecules X can be estimated from (2-6):

$$C_X = \frac{0.4Z}{14} + 0.6 \quad (2-3)$$

where Z is the atomic number [14]. Essentially, the ion gauge measures the flux of the molecules striking the filament. By taking into account the temperature T of the molecules in the beam and the fact that the beam is collimated to some extent, on the basis of equation (2-1) the relation between the pressure and the BEP is given by

$$p(X) = \frac{A_c}{C_X} \sqrt{\frac{m(X)T}{m(N_2)T_R}} \cdot X(\text{BEP}) \quad (2-4)$$

where  $m(X)$ ,  $m(N_2)$  refer to the masses of the molecules X,  $N_2$ . The collimation factor  $A_c$  is 1 for an isotropic gas and 4 for a perfectly collimated beam. By taking the temperature of the indium beam as 1200K and the collimation factor  $A_c=4$ , the calculated correction factor between the pressure and the BEP of indium from (2-4) is  $C_f = 8$ , about a factor of 3 smaller than the experimental value. It is probable that most of the error is caused by an ionisation efficiency which is lower than predicted by equation (2-3).

### 2.3.2 The calibration of the P<sub>2</sub>-pressure

The P<sub>2</sub>-flux is difficult to calibrate directly due to the low sticking coefficient of phosphorus. An indirect method was used instead. The flux of P<sub>2</sub> molecules was estimated from the known weight M of the phosphorus charge and the geometry of the cracker section.

Assume a cylindrically symmetric beam emerging from a Knudsen type source. For a cosine law flux distribution the total number of molecules leaving the cell orifice (I) is related to the maximum flux at a distance r (here r = 0.1m) at the centre of the beam, F<sub>Max</sub>, by

$$I = \frac{2}{3}r^2 F_{Max} W \quad (2-5)$$

where W is the Clausing correction factor for the cracker orifice of finite length, in this case (diameter 8mm, length 22mm) W=0.72 [15].

After several growth runs i of duration t<sub>i</sub> the material in the cell has been consumed and the total evaporated mass can be written

$$M = m \sum_i I_i t_i \quad (2-6)$$

The gauge correction factor C<sub>f</sub> which relates the pressure to the BEP can be solved from equations (2-1,5 and 6) by using the experimental growth data to give

$$p(P_2) = 8P_2(\text{BEP}) \quad (2-7)$$

ie. C<sub>f</sub> = 8.

The theoretical value of C<sub>f</sub> for P<sub>2</sub> can be calculated as for indium in the preceding section. The collimation factor A<sub>c</sub> for P<sub>2</sub> is not known but it can be assumed to be smaller than 4 due to the scattering of P<sub>2</sub> or P<sub>4</sub>

molecules from the walls of the vacuum chamber and from the substrate heater assembly itself. (This could be demonstrated simply by rotating the ion gauge 180 degrees from the usual measuring position. Even though the direct flux from the phosphorus cell was zero due to the shielding behind the ion gauge, the measured BEP was typically about one half of the BEP in the direct flux.) As a compromise the value  $A_c = 3$  is used, giving with the temperature of the cracker (1200K) the pressure of  $P_2$  from equation (2-4):

$$p(P_2) = 7P_2(\text{BEP}), \quad (2-8)$$

therefore the calculated correction factor  $C_f = 7$ , in good agreement with the experimental result of equation (2-5). The agreement is probably somewhat fortuitous considering the inaccuracies in the assumptions made about the beam geometry.

#### 2.4 The $P_2$ -stabilisation of InP

Farrow [16] studied the evaporation of InP under both equilibrium (Knudsen) and free (Langmuir) evaporation conditions. He found that the evaporating phosphorus species was in both cases  $P_2$ . Under Langmuir conditions the evaporation rates of In and  $P_2$  are equal when the temperature is below the congruent limit  $T_c = 368^\circ\text{C}$ . Above  $T_c$  the evaporation rate of  $P_2$  exceeds that of In leaving an In-rich surface unless the surface of the crystal is stabilised. The stabilisation can be achieved by using a beam of phosphorus dimers or tetramers or even another group V species such as  $As_2$  [17]. In order to minimise sulphur contamination it is necessary to use an absolute minimum of phosphorus to keep the surface of InP stable during growth [4].

The stabilisation of InP by a  $P_2$ -beam was investigated by growing a number of layers at different  $P_2$ -overpressures. During the growth the temperature of the sample was gradually increased until the formation of In droplets on the growing surface was observed. The results are presented in Figure (2-2). It can be seen that at low temperatures the phosphorus flux needed to prevent the surface from going In-rich is roughly constant whereas it rises rapidly when the temperature is increased. To explain these results it was assumed [18] that the  $P_2$  flux needed for the stabilisation of the surface is simply the sum of the flux needed for growth ( $F_{In}/2$ ) and the flux of the desorbing phosphorus under equilibrium conditions as given by Farrow [16]. The solid lines in Figure (2-2) show that the experimental data fits the simple model well if  $p(P_2) = 1.5P_2(BEP)$ .

The proportionality constant 1.5 is smaller than the correction factor  $C_f = 7-8$  obtained from the flux calibration indicating that the accommodation coefficient for  $P_2$  under these conditions is about 0.2. This value is in reasonably good agreement with the accommodation coefficient 0.4 obtained by Panish et al. using thermally cracked phosphine as the  $P_2$  source [19].

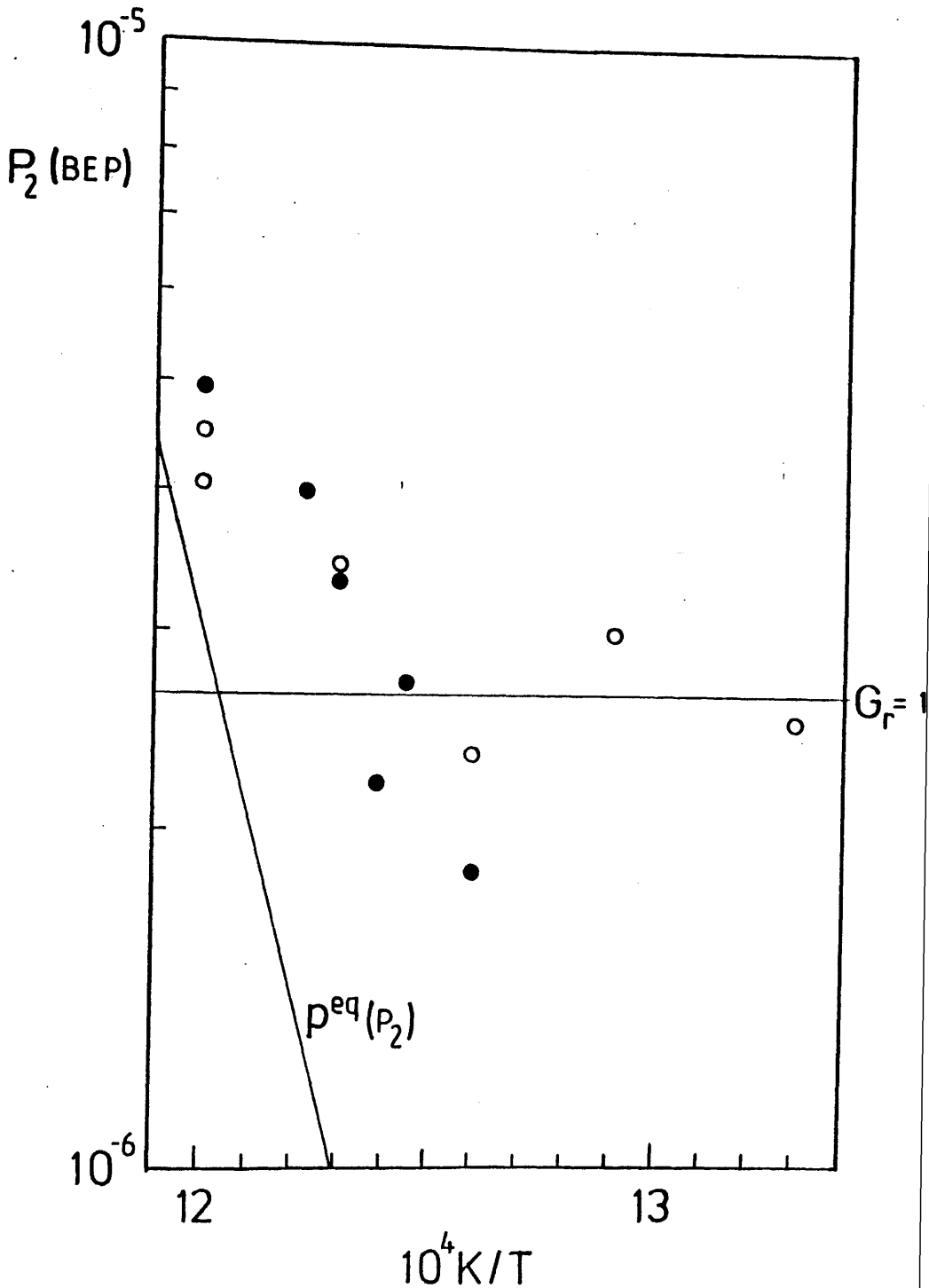


Figure (2-2). Experimental data of the In-rich transition of InP. Each data point was determined by increasing the temperature of the sample slowly ( $\sim 1^\circ\text{C}/\text{min}$ ) until the formation of In-droplets was observed. The phosphorus pressure was varied from sample to sample. The solid lines give the beam equivalent pressure (BEP) corresponding to the phosphorus flux needed for growth ( $G_r = 1.7\mu\text{m}/\text{h}$ ) and for stabilising the surface against  $P_2$  desorption ( $p^{\text{eq}}(P_2)$ , from [16]) calculated using the flux correction factor  $C_f=1.5$ .

$\bullet$   $G_r=1.1\mu\text{m}/\text{h}$

$\circ$   $G_r=1.7\mu\text{m}/\text{h}$ .

## 2.5 The desorption of In during the growth of InP

When III-V compounds are grown by MBE at high temperatures the desorption rate of the group III element may become significant leading to a reduction in the growth rate. No results on the possible evaporation of In from InP at the usual growth temperatures have been published. However, Fischer et al [20] have reported preferential desorption of Ga from GaAs and AlGaAs during MBE growth at temperatures above 640°C. The reduction of the growth rate caused by the desorption of Ga has been observed directly by monitoring RHEED intensity oscillations [21]. Indeed, layer-by-layer sublimation of GaAs can occur when the growth is stopped [22],[23],[24]. The evaporation rate of Ga has been shown to agree well with the mass action analysis of Heckingbottom [6]. By applying this model to InP the appropriate equilibrium dissociation reaction can be written as



and the equilibrium constant of (2-9),  $K_{\text{InP}}$ , is

$$K_{\text{InP}} = p(\text{In})\{p(\text{P}_2)\}^{1/2} \quad (2-10)$$

When reaction (2-9) is in equilibrium the forward and reverse rates are equal. From the principle of detailed balance it can be argued that the forward rate can be calculated using (2-10) even if the reaction is not in equilibrium. Equation (2-10) can be applied to the MBE growth of InP by taking  $p(\text{P}_2)$  as the P-beam pressure and assuming that  $p(\text{In})$  gives the pressure of the desorbing indium. The desorbing flux is obtained from the relation

$$F_{\text{des}} = \frac{p(\text{In})}{\sqrt{2\pi m k_B T}} \quad (2-11)$$

Because there are two phases, three components and one possible reaction in (2-9), the Phase Rule of chemical thermodynamics allows two degrees of freedom. Therefore both the temperature and the  $P_2$  flux can be changed independently to change the desorbing In-flux. The equilibrium constant  $K_{\text{InP}}$  inside the solidus is not known for InP (nor any other III-V compound) but it can be approximated by the equilibrium constant at the liquidus. This in turn can be calculated from the equilibrium vapour pressures, measured for GaAs by Pupp et al. [25] and for InP by Farrow [16]. From Farrow's data the equilibrium constant is found to be

$$K_{\text{InP}} = \exp\left(26.094 - \frac{48045}{T}\right) \quad (2-12)$$

The desorption rate of In from InP calculated from equations (2-10) and (2-12) has been plotted in Fig (2-3) for different phosphorus overpressures. For comparison the same data is shown for Ga-desorption from GaAs. The thick lines are the evaporation rates from an In-(Ga-) liquid in equilibrium with the compound and therefore give the In- (Ga-) rich boundaries of the phase diagram. It can be seen that for all growth conditions used in this work the predicted evaporation rate of In is negligible, being less than  $0.04\mu\text{m/h}$  at  $T_s=830\text{K}$ , which was the highest growth temperature.

For the sulphur doping studies of Chapter 3 several S-doped structures were grown in which the substrate temperature was increased in a stepwise fashion while keeping the phosphorus overpressure constant at about  $6 \times 10^{-5}$  mbar. Because of the temperature dependent desorption of sulphur the relative widths of the layers could be determined accurately from the electrochemical C-V profiles similar to Figure (3-1). The results confirmed that the desorption rate of In from InP at 830K is less than  $0.1\mu\text{m/h}$ .

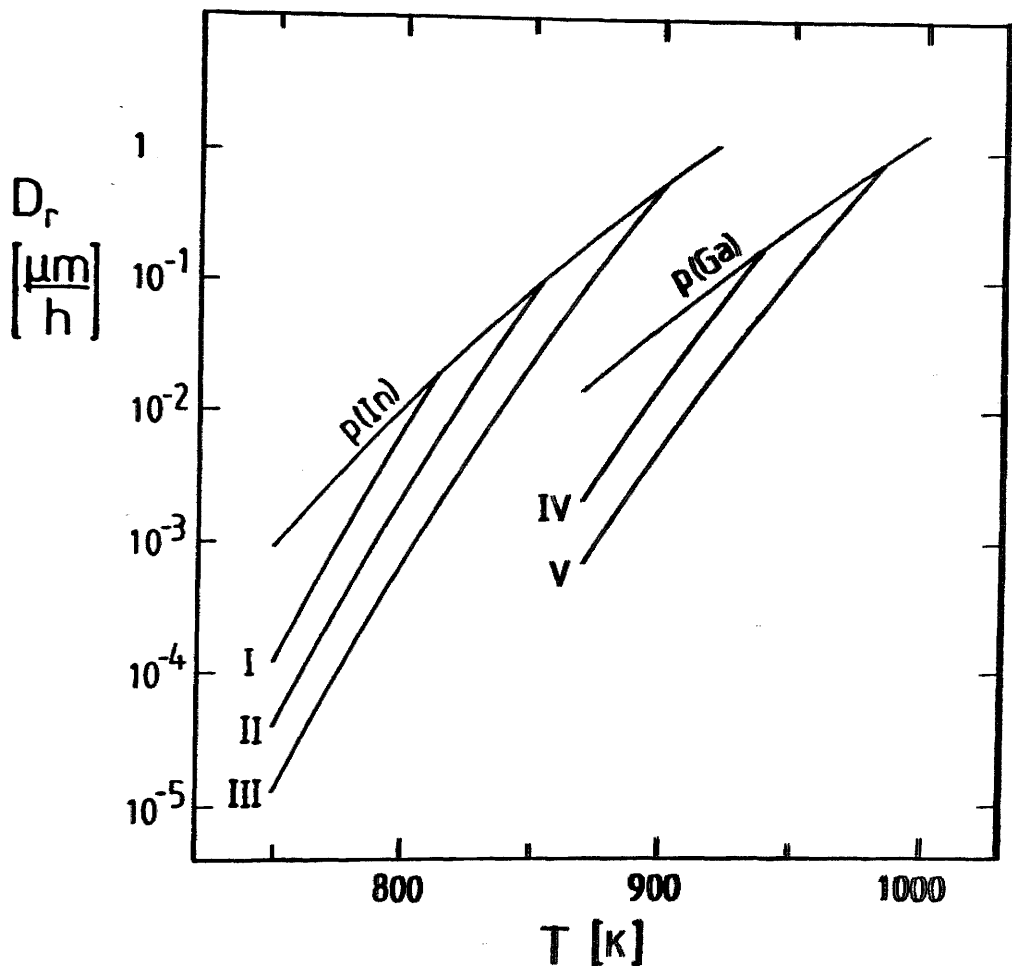


Figure (2-3). The desorption rate of In from InP under different  $P_2$  overpressures calculated using the mass action analysis proposed by Heckingbottom [6]. For comparison the same data for GaAs is also shown.

I:  $p(\text{P}_2) = 10^{-6}$  mbar      IV:  $p(\text{As}_2) = 10^{-6}$  mbar

II:  $p(\text{P}_2) = 10^{-5}$  mbar      V:  $p(\text{As}_2) = 10^{-5}$  mbar

III:  $p(\text{P}_2) = 10^{-4}$  mbar

$p(\text{In})$   $\{p(\text{Ga})\}$  gives the desorption rate corresponding to the equilibrium pressure of In  $\{\text{Ga}\}$  over InP  $\{\text{GaAs}\}$ .

## 2.6 Oval defects

### 2.6.1 Introduction

The most persistent morphological problem in MBE grown GaAs is the so called oval defects (ODs). Unsurprisingly, these defects are oval shaped, oriented with their long axis in a  $\langle 110 \rangle$  direction. They can have several possible origins, but mainly they seem to be due to contaminants on the substrate surface [26],[27],[28],[29],[30] or contamination, possibly  $\text{Ga}_2\text{O}$ , originating in the Ga cell during the growth [31],[32].

Oval defects are also always present on InP grown by MBE. In the undoped layers grown during the course of this work the OD densities were usually  $10^3$ - $10^4 \text{cm}^{-2}$  and occasionally as low as  $10^2 \text{cm}^{-2}$ . Not much is known about the origins of ODs in InP, but they can be assumed to be similar to GaAs. However, it is known that the OD density can be decreased by heavy S-doping [4]. In this section it will be shown that an external source can initiate oval defects on InP during the growth and that even highest OD densities seem to have no deleterious effects on the electrical or optical characteristics of the layers.

### 2.6.2 Results and discussion

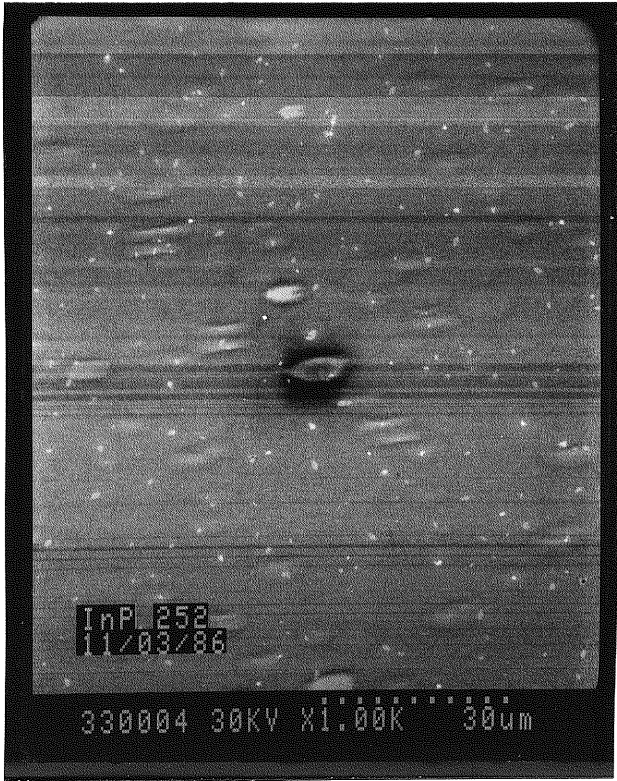
These experiments were originally meant for establishing the feasibility of magnesium doping of InP. Mg flakes were loaded into a PBN cell, similar to that used for In, and a total of 8 layers were grown at  $480^\circ\text{C}$ . During the growth the Mg cell was kept heated to a temperature which should have given an approximate doping level of  $10^{16}$ - $10^{19} \text{cm}^{-3}$ . However, the temperature could not be measured very accurately ( $\pm 50^\circ\text{C}$ ). The flux from the Mg cell was measured with the ion gauge to be

about  $1 \times 10^{-9}$  mbar when samples with the highest "doping level" were grown (260).

Figure (2-4) shows a photograph of the surface of a typical "Mg-doped" sample (252) taken with a scanning electron microscope (SEM). The oval defect density of this particular sample was about  $5 \times 10^5 \text{ cm}^{-2}$ . The OD densities of all the other "Mg-doped" layers were even higher, increasing up to  $1.5 \times 10^6 \text{ cm}^{-2}$  as the Mg cell temperature was increased to  $300^\circ\text{C}$  (Table 2-1). The ODs were of different sizes indicating that they were initiated continuously during the growth. Some layers contained pair defects (Figure 2-4), which are probably caused by sulphur contamination from the  $\text{H}_2\text{SO}_4:\text{H}_2\text{O}_2:\text{H}_2\text{O}$  etch [30].

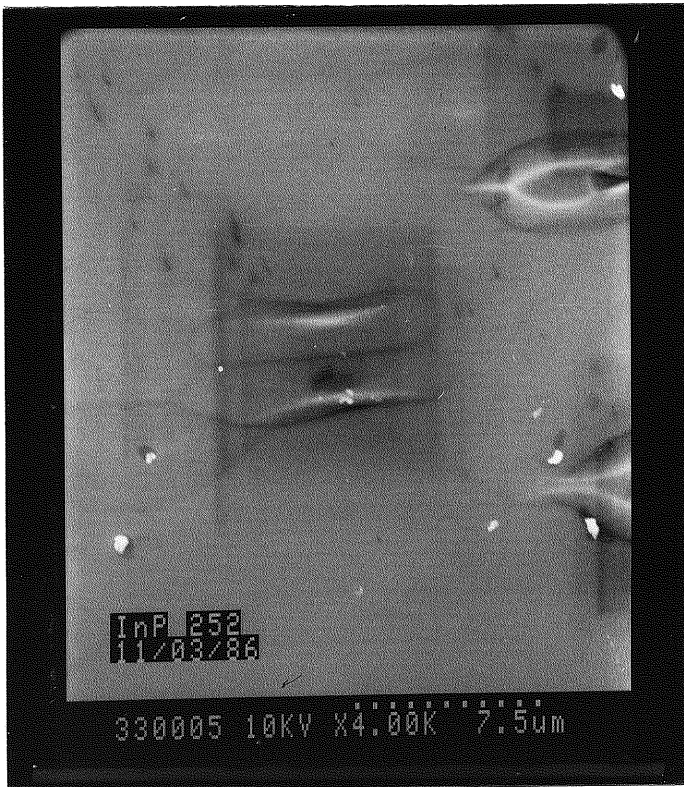
Remarkably, these extremely high defect densities did not lead to the degradation of either the electrical or the optical properties. The Hall mobilities of layers 252 and 255 were measured at 77K and 300K (Table 2-1). The mobilities of both layers were only slightly below the highest ever measured for a layer grown in the system (sample 203,  $\mu_{77\text{K}} = 42000 \text{ cm}^2/\text{Vs}$  [7]). This result should be contrasted with those of Shinohara et al. [8], according to whom the electrical properties of GaAs with a high oval defect density are significantly degraded.

The photoluminescence spectrum of a typical "Mg-doped" layer at 16K (sample 252) is shown in Figure 2-5 together with the spectrum of the benchmark sample 203. The PL spectra of all eight "Mg-doped" samples were very similar to that of layer 252 having main exciton peak half widths of 3.6-4.4meV, comparable to that of sample 203 (3.6meV). The intensities of the main peaks were about 50% to 110% of the intensity in layer 203, also indicating "good quality material". These findings are contrary to the results of Pettit et al. [33] and Bafleur et al. [9] that showed a reduction in the near



(a)

$T_{Mg} = 130^{\circ}C$   
Defect density:  
 $5 \times 10^5 \text{ cm}^{-2}$



(b)

Close-up of a pair defect on sample 252.

Figure (2-4). SEM micrographs of the "Mg-doped" InP sample 252.

band gap PL intensity in the vicinity of a single oval defect in GaAs and a dramatic decrease in the intensity over the wafer when the OD density was  $10^5$ - $10^6$ cm<sup>-2</sup>. However, the longitudinal phonon replicas at 9170-9900A of the 1.386eV acceptor peak were not as prominent as in sample 203.

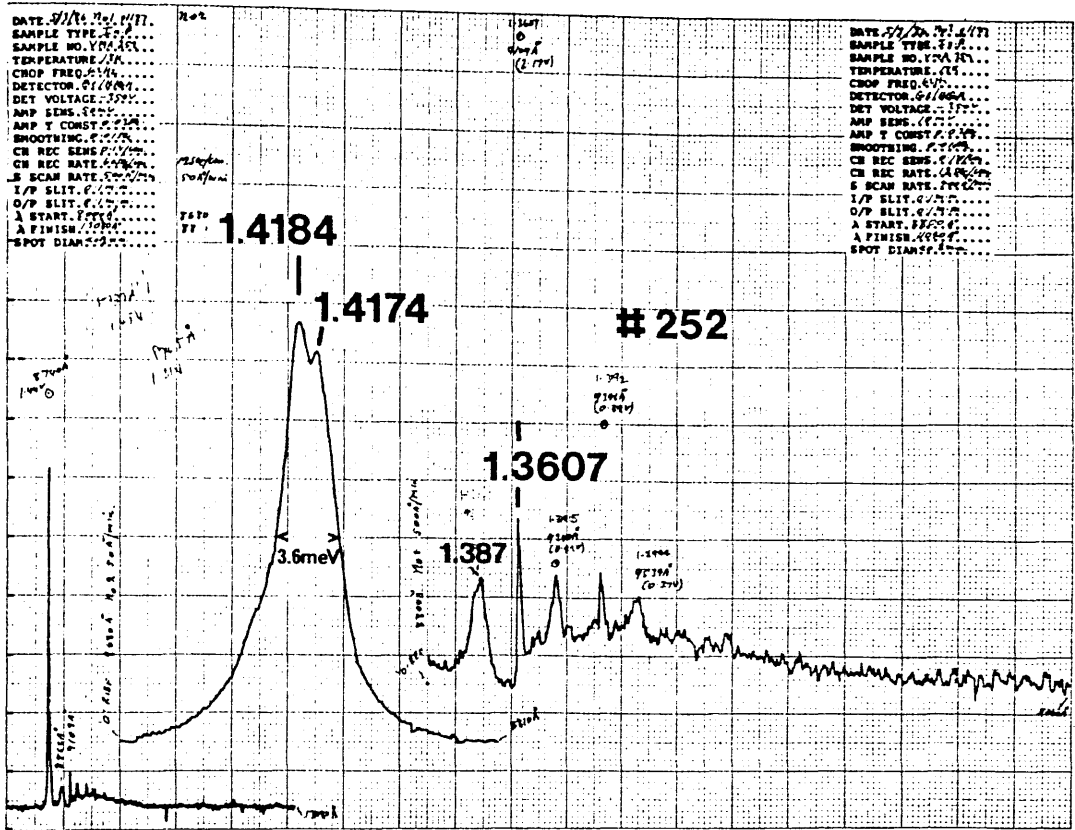
It is probable that the magnesium flakes used for the doping experiment were oxidised. This might explain why no sign of electrically active Mg in the layers could be detected. It is interesting to note that Pettit et al [33] obtained GaAs layers free of oval defects by doping with Mg up to a concentration of  $10^{19}$ cm<sup>-3</sup>. They assumed that Mg reduced gallium oxides on the surface, forming MgO, which would not act as a nucleation center for Ga droplets to initiate ODs. Hence it seems possible that the behaviour of MgO on InP is different, and it can in fact initiate the nucleation of indium droplets to start the formation of oval defects.

---

Sample	Mg-cell temp. [°C]	OD density [cm <sup>-2</sup> ]	n <sub>77K</sub> [cm <sup>-3</sup> ]	u <sub>77K</sub> [cm <sup>2</sup> /Vs]
252	130	$5 \times 10^5$	$2.4 \times 10^{15}$	28000
255	160	$7 \times 10^5$	$1.9 \times 10^{15}$	32000
259	260	$7 \times 10^5$		
260	300	$1.5 \times 10^6$		

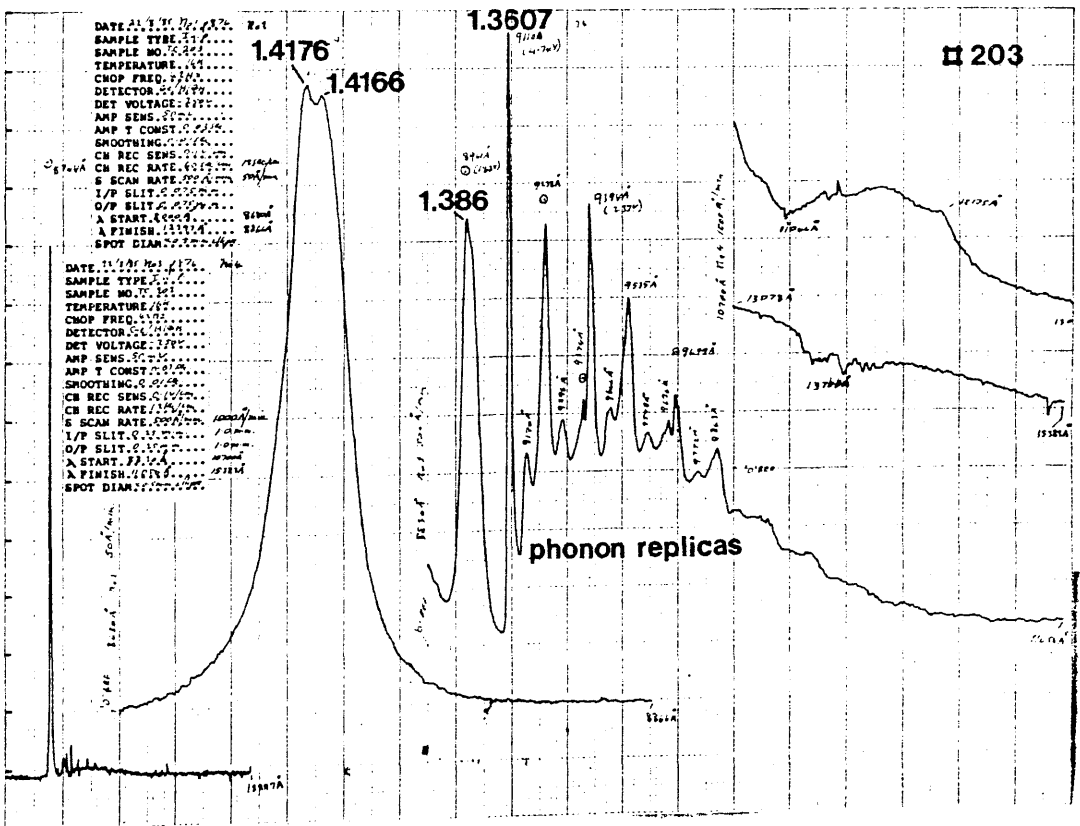
Table 2-1. Summary of the "Mg-doped" samples. Hall data was measured only for the two samples 252 and 255.

PL intensity (arbitrary units)



(a)

PL intensity (arbitrary units)



(b)

Figure (2-5). The photoluminescence spectra of the "Mg-doped" sample 252 (a) and the benchmark layer 203 (b). The intensity scale is the same in both graphs and the energies of some of the prominent peaks have been given (in eV).

## 2.7 Conclusions

The pressure of a molecular beam can be defined as the pressure of an ideal gas which causes a flux equal to that of the molecular beam. The pressure of the In beam is found to be 26 times of the beam equivalent pressure (BEP) given by the ion gauge.

The  $P_2$ -flux can be calibrated indirectly from the weight of the phosphorus charge and the geometry of the cracker-substrate system giving a correction factor  $C_f=8$  which is in good agreement with a calculation using an estimate for the ionisation coefficient of  $P_2$ .

The experimental phase diagram for the In-rich transition of InP under typical MBE conditions can be explained by assuming that the minimum  $P_2$ -flux necessary for preventing the surface from becoming In-rich is the sum of the flux needed for growth and of the flux needed to stabilise the surface against the desorption of  $P_2$ . The experimental data fits the model well if an accommodation coefficient of 0.2 is assumed for  $P_2$ .

The thermodynamic equilibrium model predicts that the desorption rate of In is negligible even at the highest growth temperatures ( $560^\circ$ ). Experimental results confirm that the upper limit of the desorption rate is less than  $0.1\mu\text{m/h}$  at  $560^\circ\text{C}$ .

Layers grown under a flux of oxidised magnesium have oval defect densities of up to  $1.5 \times 10^6 \text{cm}^{-2}$ . The high defect concentrations are not associated with any observable degradation of either the Hall mobility of electrons, the free electron concentration or the near band gap photoluminescence intensity.

## 2.8 References

- [1] C.T.Foxon and B.A.Joyce, Surf.Sci. 64 (1977) 293.
- [2] W.T.Tsang, "Chemical Beam Epitaxy of  $\text{Ga}_{0.47}\text{In}_{0.53}\text{As}/\text{InP}$  Quantum Wells and Heterostructure Devices", 4th International conference on MBE, York 1986, To be published in J.Cryst.Growth.
- [3] M.B.Panish, "Gas Source Molecular Beam Epitaxy of GaInAs(P): Gas Sources, Single Quantum Wells, Superlattice P-I-N's and Bipolar Transistors", 4th International conference on MBE, York 1986, To be published in J.Cryst.Growth.
- [4] T.Martin, C.R.Stanley, A.Iliadis, C.R.Whitehouse and D.E.Sykes, Appl.Phys.Lett. 46 (1985) 994.
- [5] J.S.Roberts, P.A.Claxton, J.P.R.David and J.H.Marsh, Electron.Lett. 22 (1986) 506.
- [6] R.Heckingbottom, J.Vac.Sci.Technol. B 3 (1985) 572.
- [7] T.S.Cheng, Private Communication.
- [8] M.Shinohara, T.Ito, K.Wada and Y.Imamura, Japan.J.Appl.Phys. 23 (1984) L371.
- [9] M.Bafleur and A.Munoz-Yague, J.Cryst.Growth 66 (1984) 472.
- [10] R.F.C.Farrow, P.W.Sullivan, G.M.Williams and C.R.Stanley, Collected Papers of 2nd International Symposium on Molecular Beam Epitaxy and Related Clean Surface Techniques, Tokyo 1982.
- [11] G.J.Davies, D.A.Andrews and R.Heckingbottom, J.Appl.Phys. 52 (1981) 7214.
- [12] Metals Research and MCP Electronic Materials.
- [13] Polaron electrochemical profiler (Bio Rad).
- [14] C.E.C.Wood, D.Desimone, K.Singer and G.W.Wicks, J.Appl.Phys. 53 (1982) 4230.
- [15] M.A.Herman in "Optoelectronic Materials and Devices", Proceedings of the Third International School, Cetniewo 1981 (ed. M.A.Herman) p.231.
- [16] R.F.C.Farrow, J.Phys.D 7 (1974) 2436.

- [17] G.J.Davies, R.Heckingbottom, H.Ohno, C.E.C.Wood and A.R.Calawa, Appl.Phys.Lett. 37 (1980) 290.
- [18] T.Martin, Private Communication.
- [19] M.B.Panish, H.Temkin and S.Sumski, J.Vac.Sci.Technol. B3 (1985) 657.
- [20] R.Fischer, J.Klem, T.J.Drummond, R.E.Thorne, W.Kopp, H.Morkoc and A.Y.Cho, J.Appl.Phys. 54 (1983) 2508.
- [21] J.Ralston, G.W.Wicks and L.F.Eastman, J.Vac.Sci.Technol. B 4 (1986) 594.
- [22] J.M.Van Hove, P.R.Pukite, G.J.Whaley, A.M.Wowchak and P.I.Cohen J.Vac.Sci.Technol. B 3 (1985) 1116.
- [23] J.M.Van Hove and P.I.Cohen, Appl.Phys.Lett. 47 (1985) 726.
- [24] Y.Imura, H.Takasugi and M.Kawabe, Japan.J.Appl. Phys. 25 (1986) 95.
- [25] C.Pupp, J.J.Murray and R.F.Pottie, J.Chem.Thermodynamics 6 (1974) 123.
- [26] M.Bafleur, A.Munoz-Yague and A.Rocher, J.Cryst.Growth 59 (1982) 531.
- [27] H.Kakibayashi, F.Nagata, Y.Katayama and Y.Shirakawa, Japan.J.Appl.Phys. 23 (1984) L846.
- [28] N.Watanabe, T.Fukunaga, K.L.I.Kobayashi and H.Nakashima, Japan.J.Appl.Phys. 24 (1985) L498-L500.
- [29] Shang-Lin Weng, C.Webb, Y.G.Chai and S.G.Bandy, Appl.Phys.Lett. 47 (1985) 391.
- [30] Y.G.Chai, Y-C.Pao and T.Hierl, Appl.Phys.Lett. 47 (1985) 1327.
- [31] Y.G.Chai and R.Chow, Appl.Phys.Lett. 38 (1981) 796.
- [32] K.Akimoto, M.Dohsen, M.Arai and N.Watanabe, J.Cryst.Growth 73 (1985) 117.
- [33] G.D.Pettit, J.M.Woodall, S.L.Wright, P.D.Kirchner and J.L.Freeouf, J.Vac.Sci.Technol. B2 (1984) 241.

## CHAPTER 3

### THE EFFECT OF GROWTH CONDITIONS ON THE INCORPORATION AND DESORPTION OF SULPHUR IN MBE GROWN InP

#### 3.1 Introduction

The choice of suitable dopants for MBE-grown GaAs and InP is quite limited, even for n-type material. Generally an ideal dopant should be non-amphoteric, should have a low electrical activation energy and show no compensation effects up to the solubility limit to facilitate doping at high concentrations. It should also not exhibit bulk diffusion, surface segregation or accumulation effects in order not to cause any smearing of abrupt interfaces.

The MBE process itself sets some additional constraints on the desirable properties of dopants. Ideally the sticking coefficient should be unity, and the desorption of the dopant should be negligible at any growth temperature to permit a reproducible control of the free electron concentration. Also the vapour pressure should be suitable for ultra high vacuum (UHV) use, i.e. it should not be too low to avoid excessively hot sources, and it should not be too high to make the evaporation rate controllable.

The n-type dopants used for MBE grown GaAs include tin, germanium, silicon and the chalcogens sulphur, selenium and tellurium.

Tin has a suitable vapour pressure range for UHV; it also allows high doping levels of  $> 10^{19} \text{ cm}^{-3}$  to be achieved [1] and it has a sticking coefficient of unity [2]. However, tin shows very strong surface segregation, which causes smearing of doping profiles [2].

Of the group IV elements germanium has had limited use due to its amphoteric nature. Silicon is the most commonly used n-type dopant in MBE grown GaAs. It has a unity sticking coefficient [3], does not segregate on the surface and yields excellent electrical characteristics up to  $5 \times 10^{18} \text{ cm}^{-3}$ . Above this concentration, however, silicon becomes compensated and the free electron concentration deviates from the Si atom concentration [4] and the maximum achievable  $N_D - N_A$  is about  $7 \times 10^{18} \text{ cm}^{-3}$  [5]. Also the vapour pressure of Si is very low necessitating the use of a hot source.

An alternative for the n-type doping of GaAs and InP is offered by the chalcogens S, Se and Te. Their disadvantage is a high vapour pressure which makes the control of a conventional Knudsen source difficult. This problem has been circumvented by the use of captive sources such as PbS, PbSe [6], SnTe [7], SnSe<sub>2</sub> [8] or H<sub>2</sub>S [9]. The source problem has been solved by the development of the galvanic Pt/Ag/AgI/Ag<sub>2</sub>S/Pt-cell by Davies et al [10] who have investigated both S and Se doping of GaAs and AlGaAs [11],[12],[13]. A similar source has also been used for the S doping of InP [14].

Chalcogens have several advantages as dopants. At least Te in GaAs [7] and S in InP [14] allow doping concentrations well above  $10^{19} \text{ cm}^{-3}$  to be achieved. They are non-amphoteric and no detectable surface segregation or bulk diffusion at the usual MBE growth temperatures has been observed. However it has been well established that the growth conditions affect the incorporation of Te [15] and Se [12] into GaAs and S into InP [14].

In particular, a thorough investigation of sulphur doped GaAs by Andrews et al. [11] has shown that sulphur desorbs at growth temperatures above  $580^{\circ}\text{C}$  with an activation energy of  $3\text{eV}$ , a value similar to the activation energies of desorption also measured for both Se and Te [12],[15]. On the basis of thermodynamic calculations the loss of S is attributed to the formation of  $\text{Ga}_2\text{S}$ . The desorption reaction can be fully suppressed by increasing the  $\text{As}_4:\text{Ga}$  flux ratio and thereby decreasing the population of free Ga on the surface available for the formation of the sub-sulphide.

It can be assumed that the behaviour of S in InP is analogous to S in GaAs [17] and it is incorporated solely on P sites in InP, even though this has not been definitely proved. Previous work by Iliadis et al. [14] has shown that sulphur is incorporated into MBE grown InP as a nearly ideal donor for substrate temperatures  $T_s < 500^{\circ}\text{C}$ . At higher temperatures, however, a loss of sulphur is observed.

Sulphur has also been identified by Martin et al. [16] as the major residual donor in nominally undoped InP grown by solid source MBE. Therefore a better understanding of the incorporation and desorption behaviour of sulphur is needed for both its use as an intentional dopant and to optimise the growth parameters for the growth of high quality inadvertently doped InP.

In this work free electron concentration ( $N_D - N_A$ ) profiles obtained by electrochemical C-V profiling of InP intentionally doped with sulphur have been used to provide data on the influence of the incident sulphur flux ( $F_S$ ), the phosphorus to indium flux ratio ( $R$ ), the substrate temperature ( $T_s$ ) and the growth rate ( $G_r$ ) on the incorporation and desorption of sulphur. A thermodynamic analysis of the probable desorption reactions is presented. The experimental results are analysed further on the basis of the kinetic model in Chapter 4.

### 3.2 Experimental

The MBE growth apparatus used in these studies was described in Chapter 2. To overcome the problems associated with the handling of elemental sulphur in vacuum the sulphur flux was generated by an electrochemical source, which is in many respects an ideal dopant source for MBE. It is bakeable up to 400°C, yet its temperature during the growth is low and constant. Moreover, the sulphur flux can be controlled accurately and fast - with a time constant of ~1s - allowing the growth of extremely abrupt interfaces. The electrochemical source is a combination of the solid state electrochemical cell and a conventional Knudsen source, consisting of a compressed pellet of Ag/AgI/Ag<sub>2</sub>S between platinum electrodes [10]. By changing the voltage E applied across the electrodes the chemical potential and the activity of the sulphur in Ag<sub>2</sub>S is changed. Therefore the equilibrium pressure of sulphur over the cell can be adjusted to give a flux of sulphur molecules S<sub>n</sub> (n=1,2,3,...) that is exponentially dependent on the voltage E:

$$F_S(n) = C(T)\exp(2nFE/RT) \quad (3-1)$$

where C(T) is a constant, dependent on the cell temperature T and system geometry, F is Faraday's constant and R is the gas constant.

The temperature of the electrochemical cell was monitored with a thermocouple and was kept constant at 200°C while E was always less than 180mV. Under these conditions the sulphur beam consists predominantly of sulphur dimers S<sub>2</sub> [11]. The flux of sulphur atoms which is twice the flux of the sulphur dimers will be referred to as F<sub>S</sub> throughout the following discussions.

The concentration of sulphur in the epitaxial layers was estimated from the free electron concentration obtained by electrochemical C-V profiling. Comparison with secondary ion mass spectrometry (SIMS) profiles has shown that  $N_D - N_A$  in the high purity InP layer agrees well with the concentration of sulphur atoms ( $C_B$ ) if  $C_B$  exceeds  $10^{16} \text{ cm}^{-3}$  [14],[18]. The influence of the growth parameters on  $C_B$  was investigated by adjusting one parameter during the growth of each layer while maintaining the other parameters constant.

### 3.3. Results and discussion

#### 3.3.1 The effect of the growth temperature on $C_B$

The concentration of incorporated sulphur atoms was measured as a function of the growth temperature ( $T_S$ ) by keeping the  $P_2$ - and In-fluxes constant while  $T_S$  was changed. Figure (3-1) shows the C-V profile of a typical layer from such an experiment. The dependence of  $C_B$  on the reciprocal substrate temperature  $1/T_S$  with a constant incident sulphur flux is shown in Figure (3-2). There are two distinct temperature regimes in the desorption behaviour of S. At substrate temperatures  $T_S > 500^\circ\text{C}$  the desorption rate is much higher than the incorporation rate while at  $T_S < 480^\circ\text{C}$  desorption is negligible. The slope of the high temperature part of the curve gives an activation energy of desorption of approximately 4.5eV, a value which is higher than 3.0eV measured for S, Se and Te in GaAs [11]. The explanation for the different activation energy is considered in Chapter 4.

In earlier work, Iliadis et al [18] obtained an activation energy of about 1eV for the desorption of sulphur from nominally undoped InP. It is possible that the desorption mechanism is different when sulphur is present in InP at low concentrations of  $< 10^{16}\text{cm}^{-3}$ . The experiment was repeated (Figure (3-3)) but the results were inconclusive mainly because the free electron concentration measured by the C-V profiling technique is lower than the sulphur concentration due to compensation effects at  $N_D - N_A < 10^{16}\text{cm}^{-3}$ .

Another explanation for the lower activation energy could be that the desorption mechanism is affected by the sulphur species used for doping. However, a thermodynamic calculation using tabulated thermochemical constants [19] confirms that the sulphur emerging from the high temperature cracker ( $900^\circ\text{C}$ ) zone of the

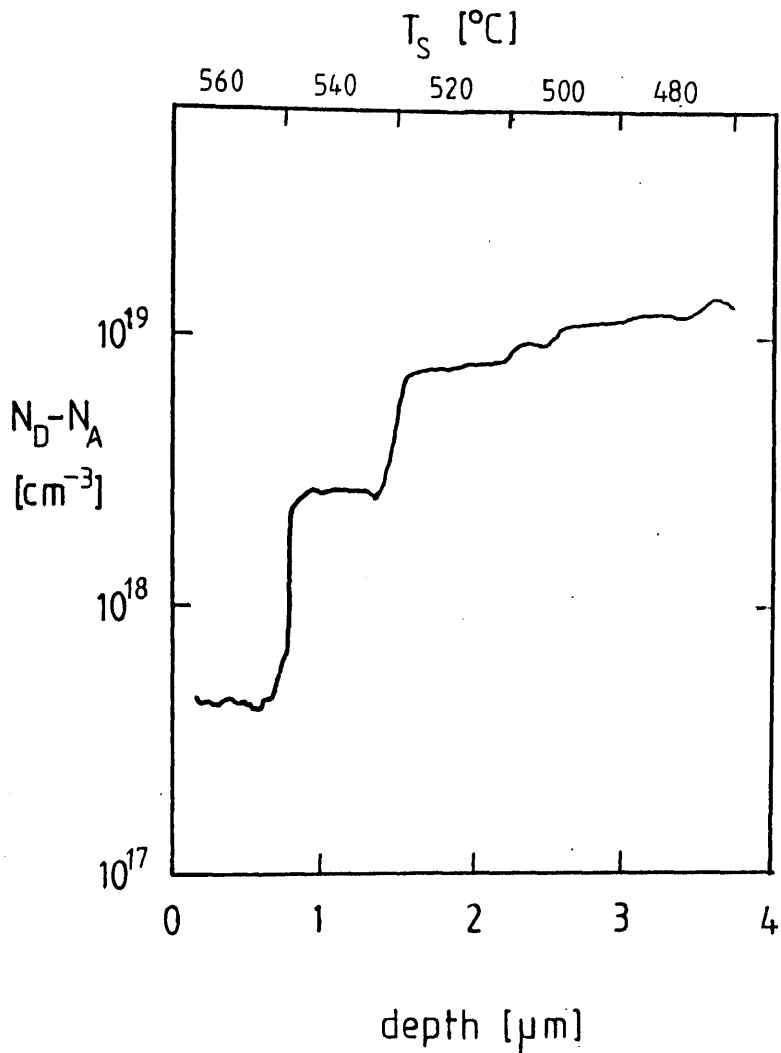


Figure (3-1). An electrochemical depth profile of a Si-doped sample used to test the  $C_B$  vs.  $T_S$  relation. The growth temperature was varied as shown in the diagram while other growth parameters were constant.

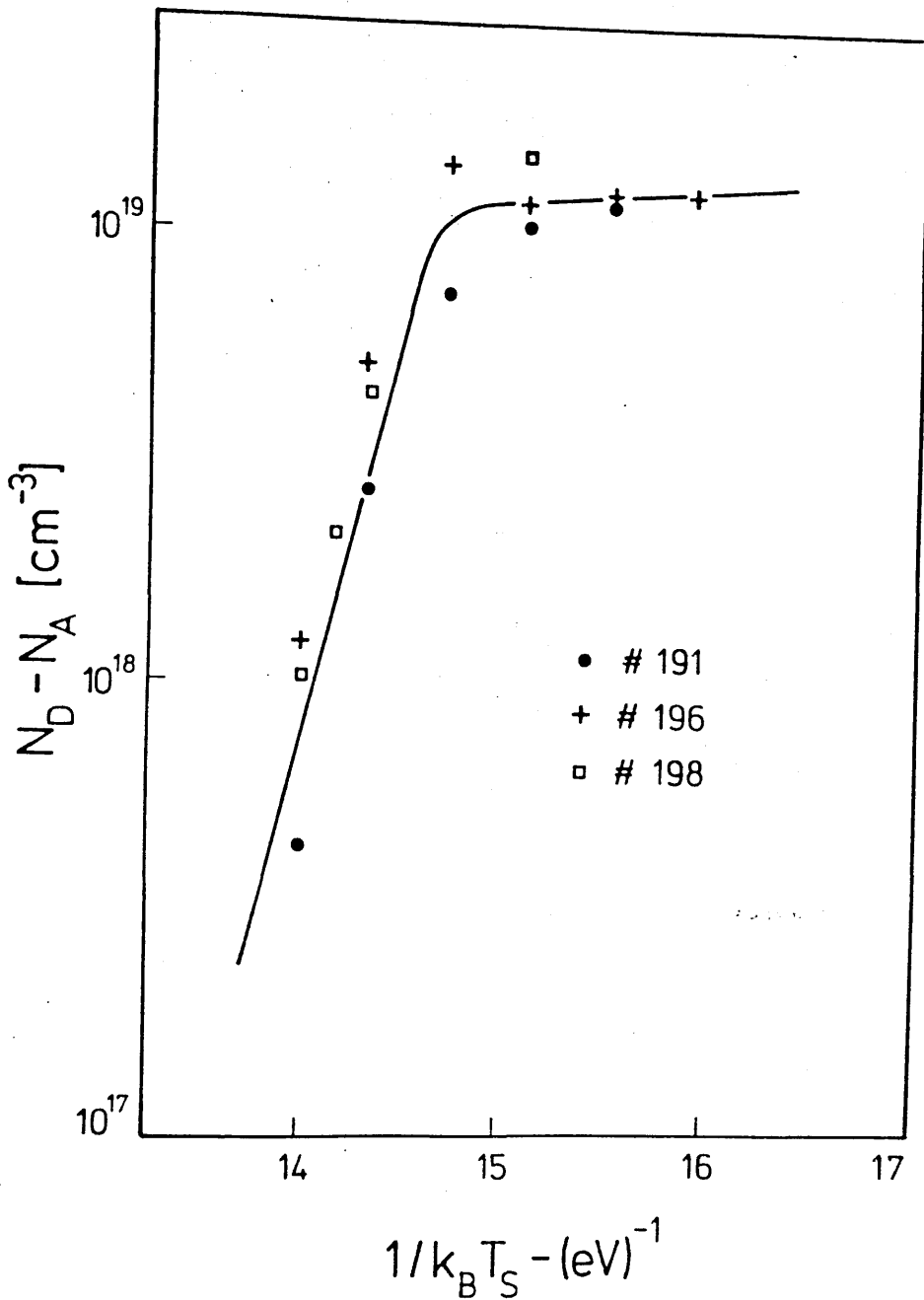


Figure (3-2). Free electron concentrations in S-doped layers plotted against reciprocal growth temperature.  $G_r = 1.5 \mu\text{m/h}$ ,  $p(P_2) = 6.5 \times 10^{-6} \text{mbar}$  (#196 and #198),  $p(P_2) = 4.7 \times 10^{-6} \text{mbar}$  (#191). The slope of the curve in the high temperature regime gives the activation energy of desorption  $H = 4.5 \text{eV}$ .

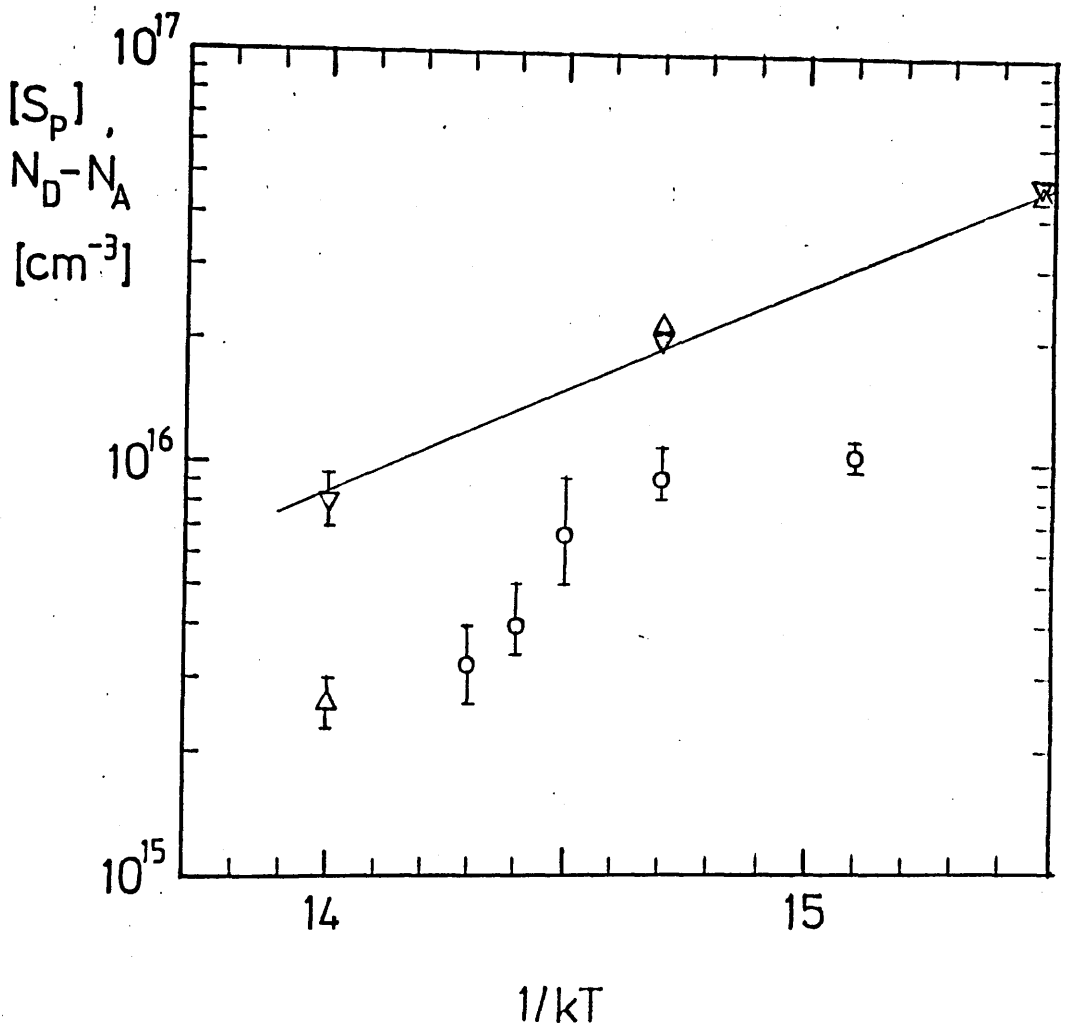


Figure (3-3). The sulphur concentration vs. substrate temperature for a nominally undoped sample obtained by Iliadis et al. [18] from SIMS measurements ( $\nabla$ ) indicates an activation energy of 1eV. At lowest concentrations the free electron concentration ( $\Delta$ ) deviates from the SIMS result, probably due to higher compensation.

$N_D - N_A$  ( $\circ$ ) for another sample grown under identical conditions ( $p(P_2) = 6.6 \times 10^{-6}$  mbar,  $p(In) = 4.8 \times 10^{-7}$  mbar) indicate less sulphur in the phosphorus charge. The activation energy of 1eV, however, cannot be confirmed solely by electrochemical profiling.

phosphorus source should also be predominantly dimers, hence differences in the incident sulphur species cannot explain the (possible) low activation energy of desorption at low sulphur concentrations.

### 3.3.2 $C_B$ as a function of the incident sulphur flux

If the concentration of the incorporated dopant atoms ( $C_B$ ) is measured as a function of the dopant cell temperature, the dependence of  $C_B$  on the flux can be deduced from the known relation between the flux and the temperature in an ideal Knudsen cell. This method has been used to show that  $C_B$  is - with the exception of Ge [3] - directly proportional to the dopant flux for most n-type dopants [3],[20],[11],[12],[21],[14]. All of these measurements have been made on samples grown at such low temperatures that the desorption of the dopant can be assumed negligible. As shown in Chapter 4 a similar experiment in the high desorption regime reveals some information on the kinetic order of the desorption reaction.

$C_B$  was measured as a function of the incident sulphur flux  $F_S$  both in the low desorption ( $T_S=480^\circ\text{C}$ ) and high desorption regimes ( $T_S=540^\circ\text{C}$ ).  $F_S$  was varied by adjusting the voltage  $E$  applied to the electrochemical cell. In Fig. 3-4  $\log(C_B)$  versus  $E$  has been plotted for two samples grown at 480 and  $540^\circ\text{C}$ . From the slope of these lines it can be seen that  $N_D - N_A$  is linearly proportional to the incident flux even in the high desorption regime. Hence a linear relation between  $C_B$  and the incident flux is not evidence of a unity sticking coefficient [3]. The correct interpretation (see Chapter 4) is that the kinetic order of the desorption reaction must be equal to that of the incorporation reaction.

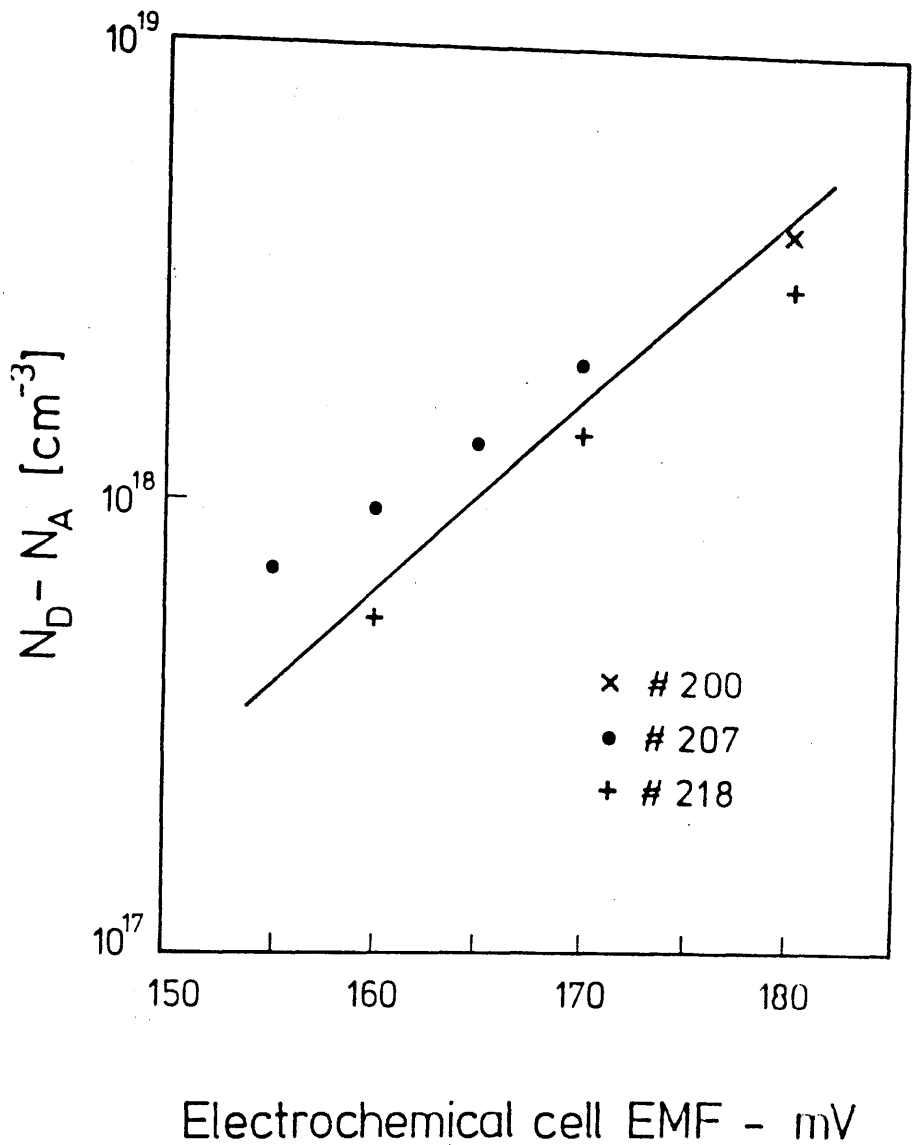


Figure (3-4). The measured free electron concentrations in S-doped epitaxial layers plotted as a function of the voltage  $E$  applied to the electrochemical cell. Samples grown at  $480^{\circ}\text{C}$  (#200 and #207) and  $540^{\circ}\text{C}$  (#218). The slope of the solid line gives the theoretical dependence of the  $S_2$  flux on  $E$ .

### 3.3.3 $C_B$ as a function of the growth rate

Figure (3-5) shows the C-V plots recorded for two layers, one grown at  $480^\circ\text{C}$  where the desorption rate of S is negligible and the other at  $520^\circ\text{C}$  where the desorption and incorporation rates are roughly equal (Figure (3-2)). In Fig. (3-6) the ratio  $F_S/C_B$  versus  $G_r$  has been plotted. The incident sulphur flux  $F_S$  was estimated from  $N_D - N_A$  for layers grown in the low desorption regime ( $T_S = 480^\circ$ ). The slope of the high temperature plot is unity indicating that the desorption rate is independent of the incident indium flux (see Chapter 4).

The free electron concentration was also measured as the function of the growth rate from a sample grown in the high desorption regime ( $T_S = 540^\circ\text{C}$ ) where the desorption rate is much higher than the incorporation rate.  $C_B$  is independent of  $G_r$  under the high desorption conditions (Figure (3-7)), corresponding to the results of Wood et al for Mg-doped GaAs [22]. These results are in agreement with the model that the incorporation rate is directly proportional to, and the desorption rate is independent of the growth rate (Chapter 4).

### 3.3.4 $C_B$ versus the $P_2$ :In flux ratio

The effect of the  $P_2$ :In flux ratio  $R$  on  $C_B$  in the high desorption regime was determined in the range  $R = 10-30$  by changing the  $P_2$  flux while the In flux was held constant. As shown in Figure (3-8), increasing  $R$  suppresses desorption slightly, but this effect is much weaker than that observed for GaAs [11]. Hence it seems that the use of sulphur as a dopant for MBE InP grown above  $500^\circ$  will be limited.

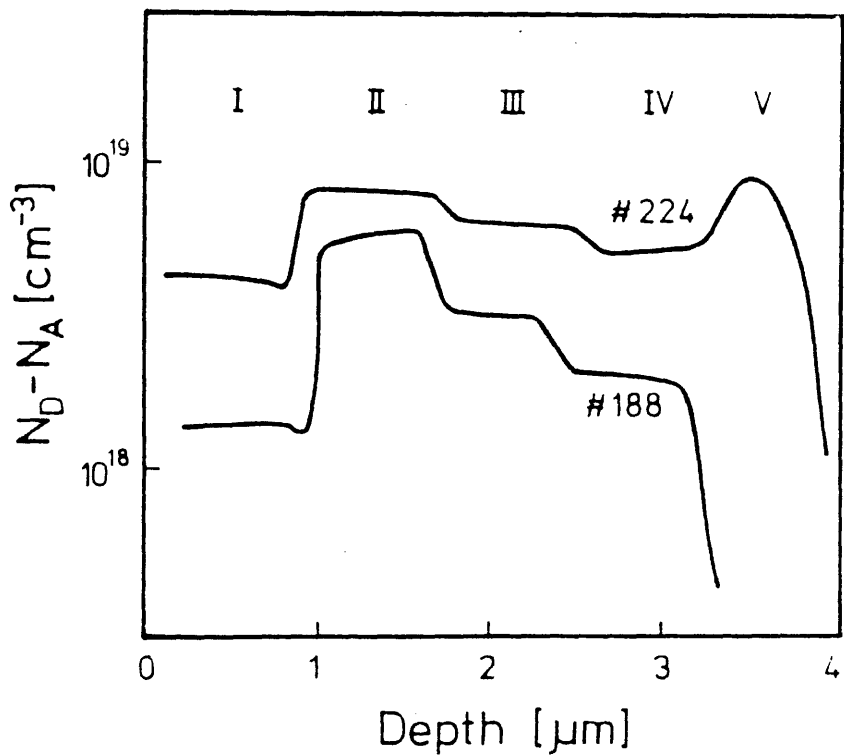


Figure (3-5). Electrochemical C-V plots of  $N_D - N_A$  for two layers with constant  $S_2$  flux but varied  $I_{in}$  flux.

(a)  $T_s = 520^\circ\text{C}$  (#224).

(b)  $T_s = 480^\circ\text{C}$  (#188).

(I)  $p_{In} = 5.6 \times 10^{-7}$  mbar,

(II)  $p_{In} = 1.5 \times 10^{-7}$  mbar,

(III)  $p_{In} = 2.8 \times 10^{-7}$  mbar,

(IV)  $p_{In} = 4.4 \times 10^{-7}$  mbar,

(V)  $p_{In} = 4.4 \times 10^{-7}$  mbar,  $T_s = 480^\circ\text{C}$ .

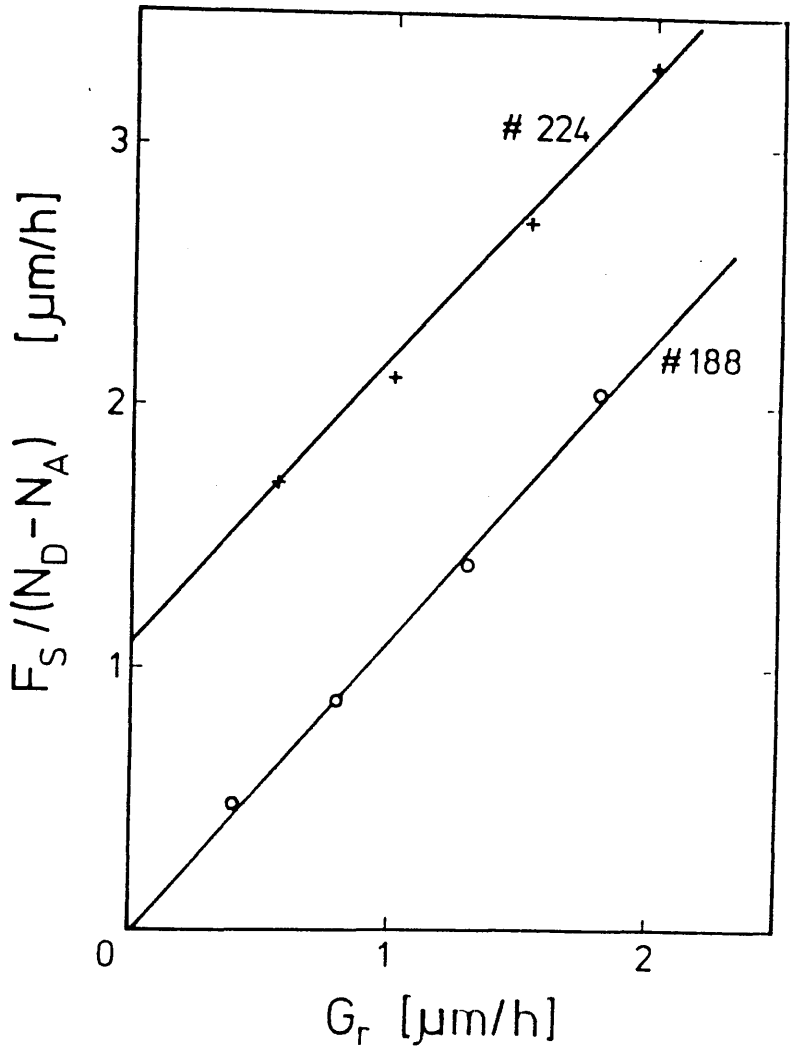


Figure (3-6). The ratio of the incident sulphur flux to the concentration of incorporated sulphur  $F_S / (N_D - N_A)$  plotted against the growth rate.  $T_S = 520^\circ\text{C}$  (#224),  $T_S = 480^\circ\text{C}$  (#188). Note the slope is unity as in equation (4-13).

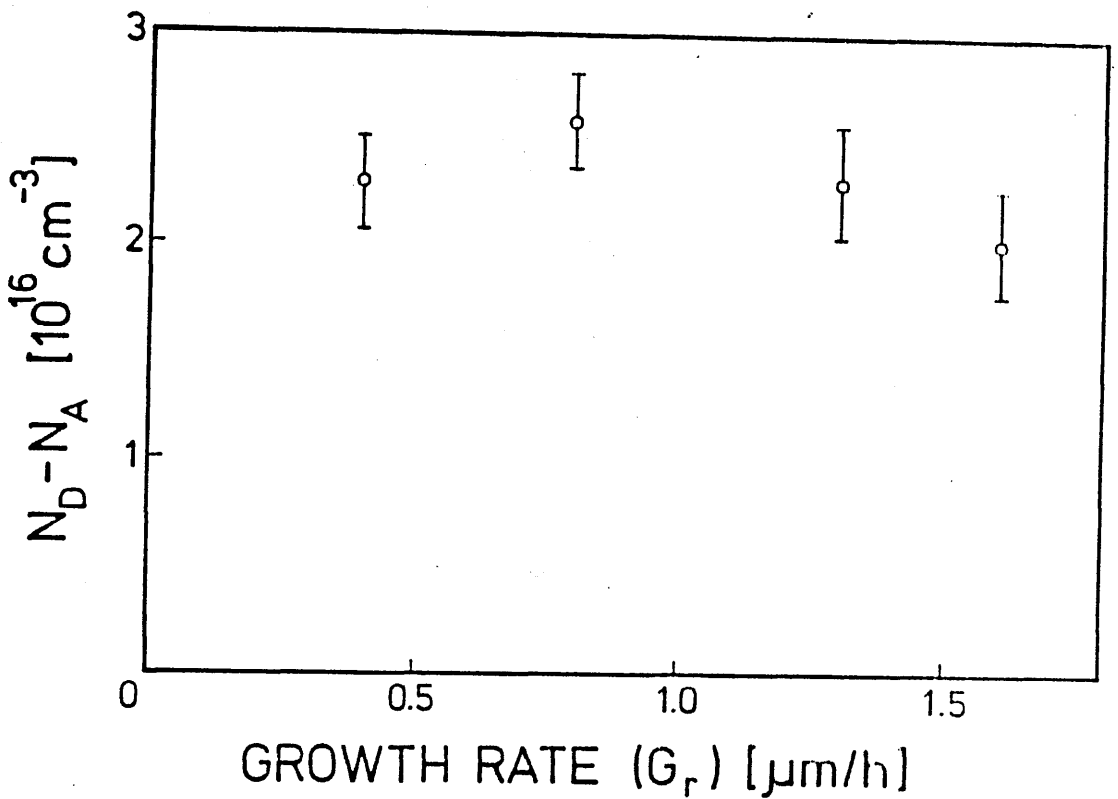


Figure (3-7).  $N_D - N_A$  as determined from an electrochemical C-V profile in S doped InP as a function of the growth rate ( $G_r$ ). Growth in the high desorption regime ( $T_s = 540^\circ\text{C}$ ).

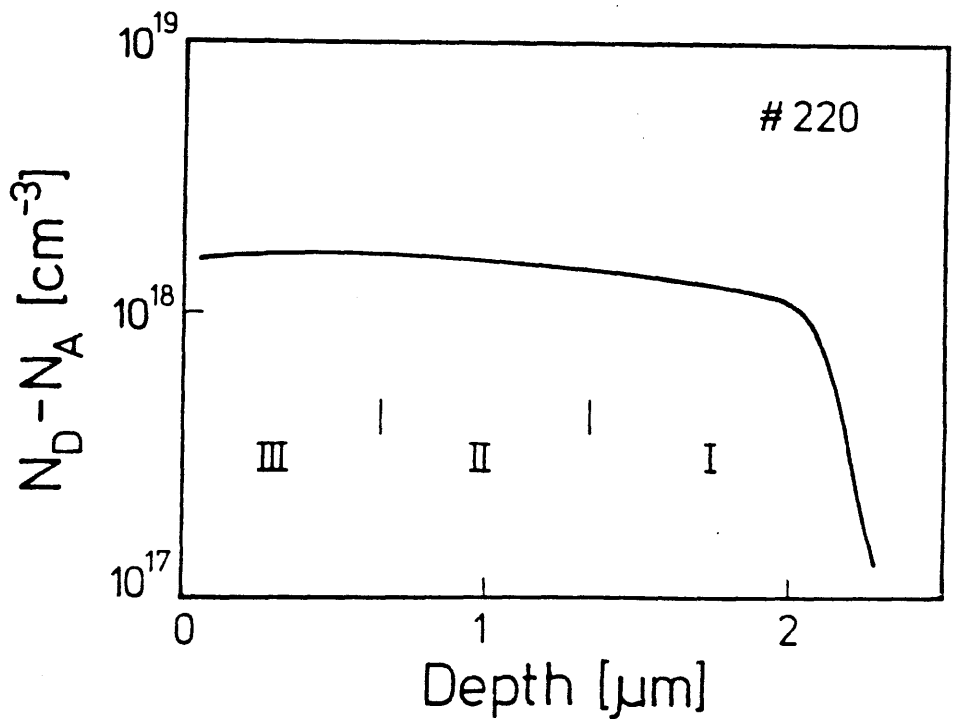


Figure (3-8). The electrochemical C-V plot of  $N_D - N_A$  for layer No. 220 grown under constant  $I_n$  and  $S_2$  fluxes at  $T_s = 540^\circ\text{C}$ . The  $P_2$  flux was increased during the growth so that the uncorrected flux ratio as given by the BEP gauge was (I)  $R = 10$ , (II)  $R = 20$ , (III)  $R = 30$ .

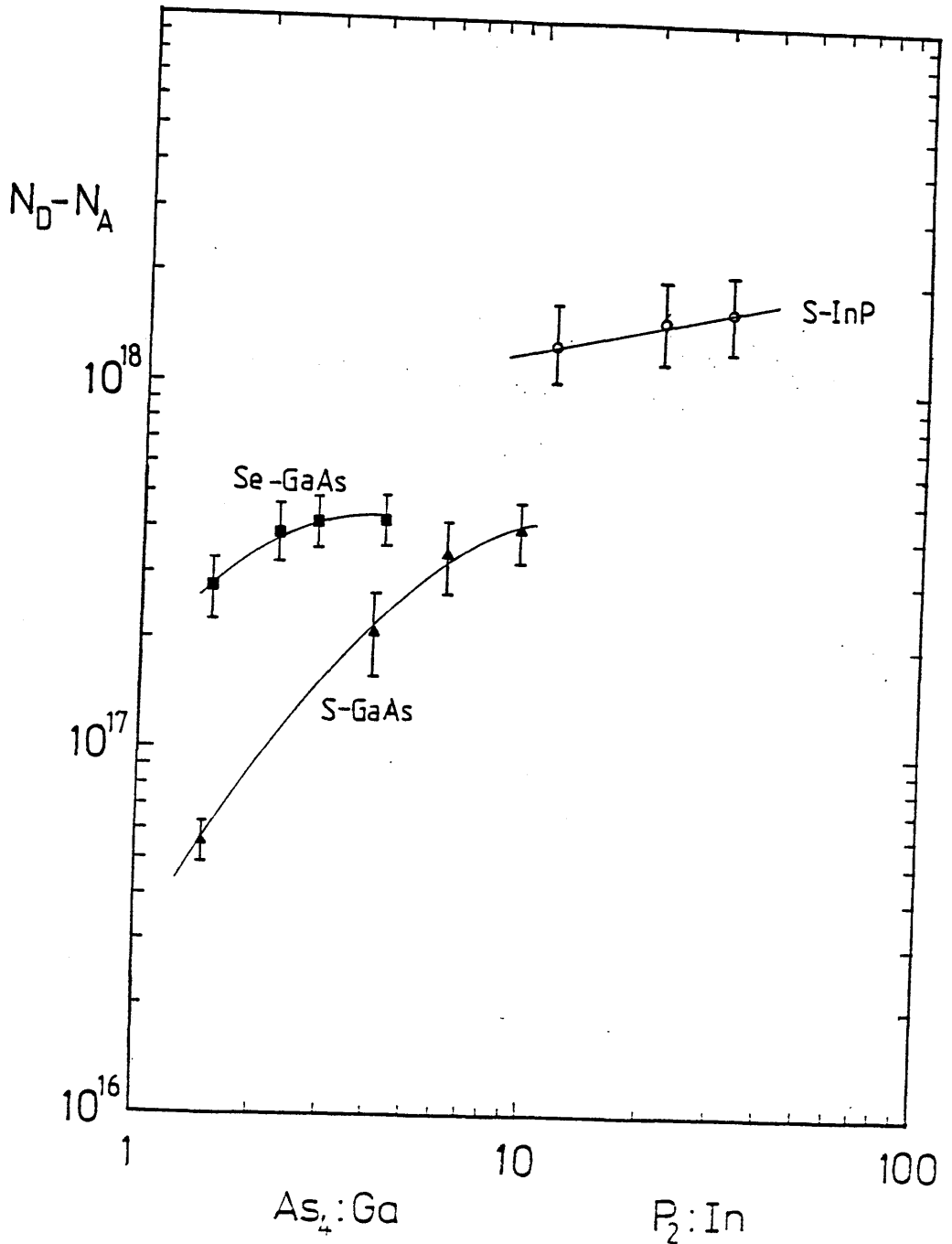


Figure (3-9). The free electron concentration as a function of the uncorrected  $P_2:In$  flux ratio in S doped InP grown in the high desorption regime ( $T_s = 540^\circ C$ ). For comparison  $N_D - N_A$  is shown as a function of the  $As_4:Ga$  flux ratio in S- and Se-doped GaAs [11,12]. Note that the desorption rate was low at the growth temperature used for Se-doped GaAs in Ref. [12].

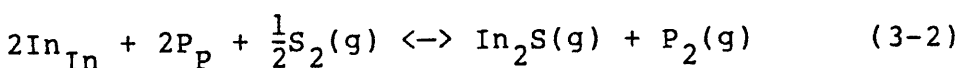
### 3.4 A thermodynamic analysis of sulphur incorporation and desorption

Heckingbottom et al. [23] have pointed out that before the arriving species in the MBE process are incorporated into the crystal they have a finite lifetime on the substrate surface and therefore time to acquire the substrate temperature. This temperature can be used in thermodynamic equilibrium calculations to predict which dopants are suitable for the MBE growth of GaAs [24].

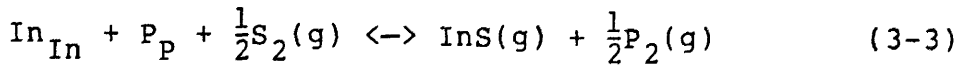
Reflection high energy electron diffraction (RHEED) oscillation measurements of GaAs [25] and AlGaAs [26] have confirmed that the desorption rate of Ga can be calculated from the mass action analysis of Heckingbottom [27]. Thermodynamic equilibrium calculations have also been used for identifying likely desorbing species and kinetic reaction barriers in S- and Se-doped GaAs [11],[12] and  $\text{Ga}_{1-x}\text{Al}_x\text{As}$  [13], and in S-doped InP [14].

In this work thermodynamic calculations are used to establish that the observed desorption rate of S from InP is near that predicted by an equilibrium reaction [28].

It is believed that chalcogens desorb from the III-V compounds as sulphides of the group III metal so that for S-doped InP the possible volatile species are  $\text{In}_2\text{S}$  and  $\text{InS}$ . By using standard thermochemical data Iliadis et al. [14] have shown that near chemical equilibrium a complete desorption of sulphur should occur through the reaction



In (3-2) the subscripts denote sites in the InP lattice and (g) refers to molecules in the vapour phase. Under typical MBE conditions the equilibrium pressure of  $\text{In}_2\text{S}$  would be of the order of  $10^{-6}$  to  $10^{-3}$  mbar implying that there must be a kinetic barrier preventing this reaction from proceeding. Iliadis et al. also showed that desorption through the formation of InS via reaction



is possible if the reaction (3-2) is prevented by a kinetic barrier.

By invoking Heckingbottoms argument that the arriving species acquire the substrate temperature very quickly, it can be argued that the sulphur taking part in the desorption reaction is in equilibrium with the crystal rather than with the vapour phase. Hence one should use sulphur in the P site ( $\text{S}_{\text{P}}$ ) rather than sulphur in the vapour phase ( $\text{S}_2(\text{g})$ ) in the equilibrium calculations. For instance instead of equation (3-3) one should write for the desorption reaction of InS:

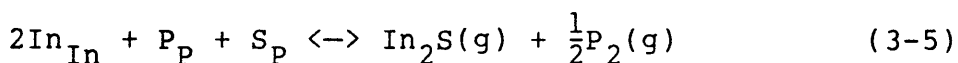


Reaction (3-4) would also explain the very weak dependence of  $C_{\text{B}}$  on  $p(\text{P}_2)$  since the desorption rate of InS would not be affected by changes in the  $\text{P}_2$  flux.

Heckingbottom [29] estimated thermochemical constants from VPE growth data for the calculation of the concentration of incorporated sulphur in MBE material in equilibrium with  $\text{S}_2$  vapour. By using VPE growth data for S-doped InP [30] the same method can be used for estimating the flux of InS desorbing via reaction (3-4) for a given  $C_{\text{B}}$ . Under typical high temperature conditions ( $T_{\text{S}}=560^{\circ}\text{C}$ ,  $G_{\text{r}}=1.7\mu\text{m}/\text{h}$ ,  $p(\text{S})=8\times 10^{-9}\text{mbar}$ ,  $C_{\text{B}}=10^{17}\text{cm}^{-3}$ ) the pressure of desorbing InS would be  $p(\text{InS}) = 10^{-17}\text{mbar}$

which is about 8 orders of magnitude smaller than the observed desorption rate. Even from the reaction (3-3) between  $S_2$  vapour and InP,  $p(\text{InS}) = 6 \cdot 10^{-11}$  mbar, about a factor of 100 smaller than the observed rate. Considering the approximate nature of the thermochemical data used for the calculation, this value must be considered within the error limits. However, the crucial point to note is that the enthalpy of reaction (3-3) is about 2.9eV which is over 1.5eV lower than the measured activation energy of desorption. Therefore the formation of InS does not appear to explain the high desorption rates.

If VPE data is again used for estimating the desorption rate of  $\text{In}_2\text{S}$  from the bulk through the reaction



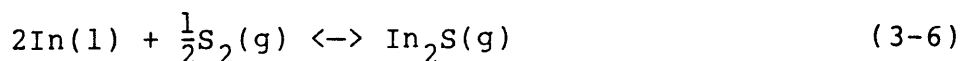
a value  $p(\text{In}_2\text{S}) = 4 \cdot 10^{-12}$  mbar is obtained.

Therefore it can be concluded that the desorption of sulphur from InP is not far from the equilibrium as given by the reaction (3-5).

The reason for the difference between the group V pressure dependence of S-doped InP and GaAs cannot be understood solely on the basis of the equilibrium reaction (3-5). The pressure effect is determined by a competition between the desorption and incorporation reactions. On the one hand for InP, a high  $\text{P}_2$  flux will decrease the incorporation rate of sulphur due to the competition between S and P for the available group V lattice sites. On the other hand, however, the desorption rate will also decrease due to a reduction in the population of surface indium. The experimental data of Section 3.3.4 suggests that the two effects must nearly cancel each other. It seems likely that one or both of these reactions must be kinetically different

for GaAs. In fact Andrews et al. [12],[11] have shown that the desorption of both Se and S from GaAs can be fully suppressed by increasing the  $As_4:Ga$  flux ratio. It is not known whether the use of tetramers ( $As_4$ ) in the GaAs experiments (as opposed to  $P_2$  dimers in the InP studies) had a significant effect on the desorption mechanism.

It may be noted that the growth temperatures were near or below the congruent evaporation limit of  $650^\circ C$  for GaAs contrary to the InP samples reported here which were grown  $160^\circ C$  above the congruent point of InP. At such high temperatures the vapour pressure of In probably follows the indium liquidus and thus the activity of indium can be expected to be a relatively weak function of the applied phosphorus pressure. Then the reaction producing  $In_2S$  can be written in a form not involving phosphorus assuming the indium activity is the same as that of pure indium,



The calculated equilibrium pressure of  $In_2S$  at 800K is  $10^{-4}$  mbar or over 5 orders of magnitude greater than the observed desorption rate. It therefore seems that the activity of sulphur in the desorption reaction is much nearer to that of sulphur incorporated into the crystal rather than  $S_2$  vapour, i.e. sulphur is nearer to equilibrium with the crystal rather than the vapour phase.

### 3.5 Conclusions

The incorporation and desorption of S in MBE grown InP has been studied in detail and its behaviour compared with S in GaAs.

The activation energy of desorption of S from InP is about 4.5eV in the high doping regime, compared with 3eV in GaAs. The result of Iliadis et al [18] giving an activation energy of 1eV in nominally undoped InP could not be confirmed.

The concentration of the incorporated S atoms is directly proportional to the incident sulphur flux in both the high and the low desorption regimes, indicating equal kinetic orders for the incorporation and desorption reactions.

The desorption rate of sulphur can be reduced only slightly by increasing the  $P_2$  overpressure, in contrast to S-doped GaAs in which the sulphur concentration is proportional to the  $As_4$  pressure. Hence the strong desorption limits the use of S as a dopant for MBE grown InP to temperatures below  $500^{\circ}C$ . Equilibrium calculations alone cannot explain the relative insensitivity of the desorption of sulphur to the  $P_2$  pressure; kinetics of the incorporation and desorption reactions must be considered instead as discussed in Chapter 4.

Thermodynamic calculations based on VPE growth data show that  $In_2S$  rather than  $InS$  is the most likely desorbing species, analogously to  $Ga_2S$  in S-GaAs [11]. From the calculated equilibrium desorption rates it is concluded that the sulphur taking part in the desorption reaction should be considered in equilibrium with the crystal rather than the vapour phase.

### 3.6 References

- [1] J.J.Harris, B.A.Joyce, J.P.Gowers and J.H.Neave, Appl.Phys. A 28 (1982) 63.
- [2] C.E.C.Wood and B.A.Joyce, J.Appl.Phys., 49 (1978) 4854.
- [3] Y.G.Chai, R.Chow and C.E.C.Wood, Appl.Phys.Lett. 39 (1981) 800
- [4] J.Maguire, R.Murray, R.C.Newman, R.B.Beall and J.J.Harris, To be published in J.Appl.Phys.
- [5] J.H.Neave, P.J.Dobson, J.J.Harris, P.Dawson and B.A.Joyce, Appl.Phys. A 32 (1983) 195.
- [6] C.E.C.Wood, Appl.Phys.Lett. 33 (1978) 770.
- [7] D.M.Collins, Appl.Phys.Lett. 35 (1979) 67.
- [8] R.S.Smith, P.M.Ganser and H.Ennen, J.Appl.Phys. 53 (1982) 9210.
- [9] F.Briones, D.Golmayo, L.Gonzalez and J.L. de Miguel, Appl.Phys. A 36 (1985) 147.
- [10] G.J.Davies, D.A.Andrews and R.Heckingbottom, J.Appl.Phys. 52 (1981) 7214.
- [11] D.A.Andrews, R.Heckingbottom and G.J.Davies, J.Appl.Phys. 54 (1983) 4421.
- [12] D.A.Andrews, M.Y.Kong, R.Heckingbottom and G.J.Davies, J.Appl.Phys. 55 (1984) 841.
- [13] D.A.Andrews, R.Heckingbottom and G.J.Davies, J.Appl. Phys. 60 (1986) 1009.
- [14] A.Iliadis, K.A.Prior, C.R.Stanley, T.Martin and G.J.Davies, J.Appl.Phys. 60 (1986) 213.
- [15] D.M.Collins, J.N.Miller, Y.G.Chai and R. Chow, J.Appl.Phys. 53 (1982) 3010.
- [16] T.Martin, C.R.Stanley, A.Iliadis, C.R.Whitehouse and D.E.Sykes, Appl.Phys.Lett. 46 (1985) 994.
- [17] F.Sette, S.J.Pearnton, J.M.Poate and J.E.Rowe, Phys.Rev.Lett. 56 (1986) 2637.
- [18] A.Iliadis, T.M.Martin and C.R.Stanley, unpublished data 1985.

- [19] K.C.Mills, Thermodynamic Data for Inorganic Sulphides, Selenides and Tellurides (Butterworths, London 1974)
- [20] R.Fischer, T.J.Drummond, R.E.Thorne, W.G.Lyons and H.Morkoc, Thin Solid Films 99 (1983) 391.
- [21] Y.Kawamura and H.Asahi, Appl.Phys.Lett. 43 (1983) 780.
- [22] C.E.C. Wood, D.Desimone, K.Singer and G.W.Wicks, J.Appl.Phys. 53 (1982) 4230.
- [23] R.Heckingbottom, G.J.Davies and K.A.Prior, Surf.Sci. 132 (1983) 375.
- [24] R.Heckingbottom, C.J.Todd and G.J.Davies, J. Electrochem.Soc. 127 (1980) 444.
- [25] J.M.Van Hove and P.I.Cohen, Appl.Phys.Lett. 47 (1985) 726.
- [26] J.Ralston, G.W.Wicks and L.F.Eastman, J.Vac.Sci. Technol. B4 (1986) 594.
- [27] R.Heckingbottom, J.Vac.Sci.Technol. B3 (1985) 572.
- [28] V.M.Airaksinen, T.S.Cheng and C.R.Stanley, Proc. 4th International Conference on MBE, York 1986. To be published in J.Cryst.Growth.
- [29] R.Heckingbottom, in: Molecular Beam Epitaxy and Heterostructures, Eds. L.L.Chang and K.Ploog (Nijhoff, Dordrecht, 1985) p71.
- [30] R.C.Clarke, J.Crystal Growth 54 (1981) 88.

## CHAPTER 4

### A KINETIC MODEL FOR DOPANT INCORPORATION AND DESORPTION IN MBE GROWN InP AND GaAs

#### 4.1 Introduction

Several important dopants used in the molecular beam epitaxy (MBE) of III-V compounds desorb at elevated growth temperatures leading to sticking coefficients below unity. Kinetic details of the desorption and incorporation reactions for dopants exhibiting surface accumulation have been deduced from the transients in the dopant concentration profiles caused by step changes in the growth conditions [1,2,3]. The basic kinetic model used as the starting point for our analysis is that proposed by Wood and Joyce [4] for Sn-doped GaAs according to which the incorporation occurs from a surface layer. The rate equation for the surface population  $C_s$  of the dopant atoms can be written:

$$dC_s/dt = F - J_{des}(C_s) - J_{inc}(C_s) \quad (4-1)$$

$F$  is the incident dopant flux and both the net incorporation ( $J_{inc}$ ) and desorption ( $J_{des}$ ) rates are functions of  $C_s$ . This paper is mainly concerned with sulphur doped InP, but both sulphur and selenium doped GaAs are considered to illustrate salient points.

Existing experimental data is used to show how on the basis of the model (4-1) some details of the desorption and incorporation reactions for the chalcogens can be deduced even though these dopants are not known to accumulate on the crystal surface under the usual growth conditions.

As already discussed in Section 3.4, the arriving species in the MBE process have a finite lifetime on the substrate surface and therefore time to acquire the substrate temperature [5]. In this work, as a further application of thermodynamics, the activation energies of desorption are compared to the enthalpies of equilibrium reactions between the bulk crystal and the vapour phase calculated from standard thermochemical data.

#### 4.2 The concentration of incorporated dopant atoms vs. incident flux

The starting point for our analysis is the model of Wood and Joyce described by equation (4-1). Let the kinetic orders of incorporation and desorption reactions be  $m$  and  $n$ . In the steady state  $dC_s/dt = 0$  and equation (4-1) reduces to the trivial form

$$F = J_{inc} + J_{des} = K' C_s^m + D C_s^n \quad (4-2)$$

where  $K'$  and  $D$  are the rate constants of incorporation and desorption.

Information about the kinetic orders of the desorption and incorporation reactions can be obtained by measuring the concentration of incorporated dopant atoms in the bulk ( $C_B$ ) as a function of the incident flux at a temperature ( $T_s$ ) where desorption rate is high  $J_{des} \gg J_{inc}$ . Let us assume that as the result of such an experiment  $C_B$  is known to be proportional to some power  $k$  of the incident flux

$$C_B = N \cdot F^k \quad (4-3)$$

The constant of proportionality  $N$  is a function of  $T_s$ ,

the group V flux and the growth rate. The relation between the net incorporation rate and the growth rate ( $G_r$ ) is

$$J_{inc} = C_B \cdot G_r \quad (4-4)$$

In the high desorption regime equation (4-2) can be simplified since the desorption rate nearly equals the incident flux:

$$J_{des} = F \quad (4-5)$$

By solving  $F$  from the experimental result of equation (4-3) and using  $C_B$  given by (4-4) we obtain from (4-5):

$$J_{des} = (J_{inc}/N \cdot G_r)^{1/k} \quad (4-6)$$

The kinetic order of the desorption reaction is  $1/k$  times the kinetic order of the incorporation reaction. As shown in Chapter 3 for S-doped InP,  $C_B$  is directly proportional to the incident sulphur flux even in the high desorption regime [6]:

$$C_B = N \cdot F \quad (4-7)$$

Therefore,  $k = 1$  and the desorption and incorporation reactions are of equal kinetic orders relative to  $C_S$ . The simplest assumption to explain this is that both rates of reaction are of the first order ( $m=n=1$ ) and therefore proportional to  $C_S$ , in analogy to Sn in MBE grown GaAs, which has been shown by Harris et al. [3] to have first order incorporation kinetics.

### 4.3 Growth rate dependence of $C_B$

In the high desorption regime the surface concentration can be solved from (4-2) and (4-4):

$$C_S^n = C_B \cdot G_r / K' \quad (4-8)$$

Then (4-5) and (4-8) yield

$$C_B = K' F / D \cdot G_r \quad (4-9)$$

Wood et al. [7] have shown for Mg-doped GaAs that  $C_B$  is independent of the growth rate. The same is true for S-doped InP grown at 540°C (Figure (3-7)). Then from equation (4-9) the ratio of the rate constants must be proportional to the growth rate:

$$K' / D = G_r \quad (4-10)$$

Whereas sulphur is believed to desorb from InP as  $In_2S$  [8], the most likely desorbing species in Mg-doped GaAs is either elemental Mg or some compound of As and Mg. Different desorption mechanisms would mean a different dependence on the growth rate and a compensating difference in the incorporation mechanism. While this is not impossible, a simpler assumption is that used by Wood et al. for their model of Mg-doped GaAs: the incorporation rate constant  $K'$  is directly proportional to the growth rate. Then the desorption rate constant is not a function of  $G_r$  and

$$K' = K \cdot G_r \quad (4-11)$$

For values of the growth temperature  $T_s$  between 500°C-530°C the incorporation and desorption rates of S in InP are roughly equal and eq. (4-2) can be written

$$F = J_{\text{inc}} + J_{\text{des}} = (K \cdot G_r + D) C_s^n \quad (4-12)$$

Equations (4-8) and (4-12) can then be used to deduce the ratio of the incident flux to the concentration of incorporated dopant atoms

$$F/C_B = D/K + G_r \quad (4-13).$$

$F/C_B$  vs.  $G_r$  has been measured for S in InP (see Figure (3-6)) and found to confirm equation (4-13) and the relationship expressed in equation (4-10). The desorption rate of sulphur is independent of the incident indium flux  $F_{\text{In}}$  (which equals the growth rate) whereas the incorporation rate is directly proportional to  $F_{\text{In}}$ .

#### 4.4 The dependence of $C_B$ on the group V pressure

If dopant desorption is significant a change in the flux of the group V element usually affects the incorporation and desorption rates due to a change in the surface stoichiometry of the growing crystal. Let the rate constants be proportional to some powers  $t$  and  $u$  of the group V pressure  $p(V)$ , i.e.

$$D = D_0 p(V)^t \quad (4-14) \text{ and}$$

$$K' = K_0 G_r p(V)^u \quad (4-15)$$

$C_B$  can be solved by using equations (4-9), (4-14) and (4-15).

$$C_B = K_0 F p(V)^{u-t} / D_0 \quad (4-16)$$

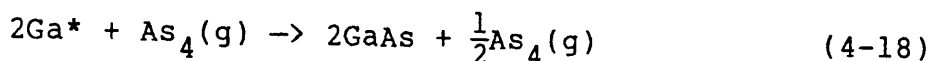
Akimoto et al. [9] have shown by secondary ion mass spectroscopy (SIMS) that the concentration of incorporated Si atoms [Si] in GaAs grown at 540°C is dependent on the As<sub>4</sub>:Ga flux ratio R. When 0.7 < R < 8 [Si] ~ R<sup>1/2</sup> and when R > 8 [Si] ~ R<sup>1</sup>. These results were explained by proposing two different incorporation mechanisms. However, as can be seen from eq. (4-16) the pressure dependence is affected by both the desorption and incorporation reactions. If details of the incorporation kinetics are deduced on this basis, the desorption mechanism must also be taken into account, i.e. a change in the C<sub>B</sub> vs. flux ratio R relation can be caused by a change either in the desorption reaction or the incorporation reaction. In the simplest case the dopant desorbs as elemental molecules and the desorption rate is expected to be independent of p(V). For Si this may not be true because elemental Si is not very volatile at typical growth temperatures. Chalcogens in GaAs or InP tend to form chalcogenides of the group III metals. The stoichiometry of the desorbing species can be assumed to determine t in a simple way. As an example we consider S desorption from GaAs and InP. In Figure (3-9), C<sub>B</sub> in layers of GaAs and InP grown in the high desorption regime has been plotted as a function of the applied As<sub>4</sub> and P<sub>2</sub> pressures.

In GaAs C<sub>B</sub> is directly proportional to p(As<sub>4</sub>) whereas in InP C<sub>B</sub> is nearly independent of p(P<sub>2</sub>). In the case of GaAs, if the desorbing species is Ga<sub>2</sub>S, the appropriate reaction between the surface atoms \* is



To determine the effect of the As<sub>4</sub> pressure the kinetic model of As<sub>4</sub> incorporation into GaAs as given by Foxon and Joyce [10] is used. According to this model from any two As<sub>4</sub> molecules four As atoms are incorporated in the GaAs lattice and the other four desorb as

an  $As_4$  molecule:



If a mass action relationship is assumed the following inverse relationship is obtained

$$[Ga^*]^2 \sim p(As_4)^{-1}$$

Therefore,  $t=-1$  and  $u=0$  and the incorporation rate of S can be considered independent of the applied  $As_4$  pressure. If the model is correct the  $[S_{As}]$  vs.  $p(As_4)$  data should not be affected if As dimers are used instead of tetramers. This can be seen by considering the mass action relation analogous to (4-18):



Consequently  $[Ga^*] \sim p(As_2)^{-1}$  and  $t = -1$  as before. Therefore, as far as the surface gallium is concerned an incident  $As_4$  molecule is equivalent to an  $As_2$  molecule. This model is in agreement with the results of Van Hove and Cohen [11] who observed no difference between the effects of incident  $As_4$  and  $As_2$  fluxes on the evaporation rate of Ga from GaAs above 850K.

S doped InP differs slightly from GaAs. According to Fig 3,  $[S_p]$  is nearly independent of the applied  $P_2$  pressure. Using the notation of equation (4-16) this means  $u-t = 0$ , or  $u = t$ . As shown above for  $As_2$ ,  $t = -1$  if  $In_2S$  is the desorbing species. Therefore, also  $u = -1$ :

$$K' \sim p(P_2)^{-1}.$$

It can be concluded that the observed  $[S_V]$  vs.  $p(V)$  dependence in the high desorption temperature regime can be explained by assuming an incorporation rate which is independent of  $p(As_4)$  in the case of GaAs and inversely

proportional to  $p(P_2)$  in InP. Since the growth temperatures were near or below the congruent evaporation limit of  $650^\circ\text{C}$  for GaAs, it is possible that the number of available As sites is relatively independent of the  $\text{As}_4$  flux due to the low evaporation rate of  $\text{As}_2$  through the decomposition of the crystal. In contrast, the growth of InP occurred  $160^\circ\text{C}$  above the congruent point at which temperature the desorption rate of  $P_2$  is quite high [12].

#### 4.5 The activation energy of desorption

Rate constants  $K$  and  $D$  are expected to be temperature dependent:

$$K = K_1 \exp(E_{\text{inc}}/k_B T) \quad (4-20a)$$

$$D = D_1 \exp(E_{\text{des}}/k_B T) \quad (4-20b)$$

Then from (4-11) the temperature dependence of  $C_B$  in the high desorption regime can be written

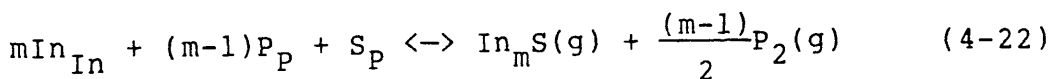
$$C_B = K_1 F / D_1 \cdot \exp((E_{\text{inc}} - E_{\text{des}})/k_B T) \quad (4-21)$$

Equation (4-21) shows that the activation energy of desorption  $E_A$  measured from the slope of the  $\ln C_B$  vs.  $1/T$  plot is in fact the difference of the activation energies of incorporation and desorption from the surface phase.  $E_{\text{des}}$  can be measured for high surface concentrations  $C_s$  directly from the surface lifetime of the dopant as has been done for Mg-doped GaAs by Wood et al. [7].  $E_{\text{inc}}$  for Sn in GaAs has been measured from the exponential concentration transients caused by surface accumulation [3,5].  $E_{\text{inc}}$  can also be inferred from  $E_A$  and  $E_{\text{des}}$  as shown for Sb and Ga doped silicon by Iyer et al. [2].

It has already been noted that the concentration of

incorporated dopant atoms is independent of the growth rate in the high desorption regime. Also the incorporation rate is directly proportional to the growth rate, which means that at a given temperature and group V pressure  $C_B$  is proportional to the surface population of dopant atoms  $C_S$ .

Both observations are in fact in agreement with the expected behaviour of an equilibrium reaction. Therefore, kinetic effects are relatively unimportant and it may be possible to calculate the activation energy of desorption from thermochemical data. It will be shown that in a thermodynamic equilibrium between the vapour and solid phases the  $C_B$  vs.  $1/T$  plot yields the enthalpy of the desorption reaction. As an example we consider the desorption of sulphur from InP. The desorbing species is believed to be the volatile indium sulphide  $In_mS$  ( $m$  is either 1 or 2) and in principle there is a wide choice of possible desorption reactions. The prime requirement for a proper reaction is that it conserves the relative numbers of the group III and V lattice sites [13]. As discussed in Section 3 the desorption rate can be considered independent of the incident indium flux, therefore the correct desorption reaction is taken to be the simplest one which does not involve In atoms in the vapour phase:

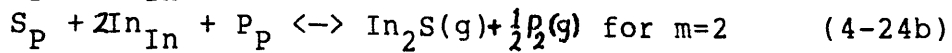


where  $m=1$  or  $2$ . From (4-22) the concentration of the incorporated chalcogen  $[S_P]$  is calculated by using the corresponding enthalpy and entropy  $H_{22}$  and  $S_{22}$  in the equilibrium constant of (4-22):

$$[S_P] = p(In_mS) \cdot p(P_2) \exp(H_{22}/k_B T - S_{22}/k_B) \quad (4-23)$$

The pressure of the desorbing sulphide  $p(In_mS)$  is nearly constant in the high desorption regime so that if

the pressure of the group V element  $p(P_2)$  is also kept constant, the slope of the  $\ln[S_p]$  vs.  $1/k_B T$  plot is the enthalpy  $H_{22}$ . For the two values of  $m$  reactions (4-22) can be written




---

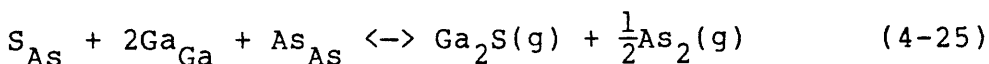
Reaction	Enthalpy	Ref.
$S_p + P(\text{g}) \leftrightarrow S(\text{g}) + P_p$	$H_a = 0.37\text{eV}$	[14]
$\text{In}(\text{s}) + S(\text{s}) \leftrightarrow \text{InS}(\text{g})$	$H_b = 2.5\text{eV}$	[15]
$S(\text{g}) \leftrightarrow S(\text{s})$	$H_c = -3.0\text{eV}$	[15]
$\frac{1}{2}P_2(\text{g}) \leftrightarrow P(\text{g})$	$H_d = 2.6\text{eV}$	[16]
$\text{In}_{\text{In}} + P_p \leftrightarrow \text{In}(\text{s}) + \frac{1}{2}P_2(\text{g})$	$H_e = 1.63\text{eV}$	[12]
$2\text{In}(\text{s}) + S(\text{s}) \leftrightarrow \text{In}_2\text{S}(\text{g})$	$H_f = 1.6\text{eV}$	[15]

Table 4-1. Experimental values of enthalpies for relevant reactions

The enthalpy of (4-24a) can be calculated from the enthalpies summarised in Table 4-1. These values are from experimental results except for  $H_a$  which is estimated from the substitution energy of S in InP calculated by Kraut and Harrison [4]. The result is  $H_{24a} = H_a + H_b + H_c + H_d + H_e = 4.0\text{eV}$ .

In a similar fashion we can write for reaction (4-24b)  $H_{24b} = H_a + H_c + H_d + 2H_e + H_f = 4.8\text{eV}$ .

The measured activation energy of desorption for InP [6] is about 4.5eV, a value intermediate between  $H_{24a}$  and  $H_{24b}$ . For GaAs the activation energies of desorption for Te [17], S [18] and Se [19] are all about 3eV. Consider the case of S desorption from GaAs; Andrews et al. [18] have shown that  $\text{Ga}_2\text{S}$  is the most likely desorbing compound. The desorption reaction would be similar to (4-24b):



The substitution energy of S in GaAs is not available. However, it is expected to be comparable to the substitution energy of Te [20], i.e.  $H_a = -0.44\text{eV}$ . For the other enthalpies the following values are found:  $H_d = 2.0\text{eV}$  [21],  $H_e = 1.9\text{eV}$  [22],  $H_f = 0.2\text{eV}$  [15]. The enthalpy of reaction (4-25) becomes  $H_{25} = H_a + H_c + H_d + 2H_e + H_f = 2.6\text{eV}$ , which is also in good agreement with the experimental results. The same calculation for Se and Te can be expected to produce similar results, i.e. enthalpies near 3eV.

## 4.6 Conclusions

A theoretical analysis of the effect of growth conditions on the incorporation of sulphur in MBE grown InP is found to provide information on the kinetics of the dopant incorporation and desorption reactions. On the basis of the kinetic model by Wood and Joyce [4] the linear dependence of the concentration of incorporated dopant atoms on the incident dopant flux in the high desorption regime is found to imply equal kinetic orders of the incorporation and desorption reactions. From the growth rate dependence of sulphur in InP grown at a high substrate temperature, the ratio of the rate constants of incorporation and desorption is shown to be proportional to the growth rate. It is assumed that the incorporation rate is directly proportional to and the desorption rate is independent of the growth rate. The observed difference in the effect of the group V element overpressure on the incorporation behaviour of S in GaAs and InP can be explained by an incorporation rate constant which is not a function of the applied  $As_4$  pressure in the case of GaAs and an incorporation rate which is inversely proportional to the applied  $P_2$  pressure in InP.

The calculated enthalpies of equilibrium desorption reactions between the bulk crystal and the vapour phase in good agreement with the activation energies of desorption of S in InP and S, Se and Te in GaAs.

## 4.7 References

- [1] C.E.C.Wood, D.DeSimone and S.Judaprawira, J.Appl.Phys. 51 (1980) 2074.
- [2] S.S.Iyer, R.A.Metzger, F.G.Allen, VLSI Sci.&Technol. 1984, Proc. of the 2nd International Symposium on very large scale integration science and technology (Electrochemical Society, 1984), p473.
- [3] J.J.Harris, D.E.Ashenford, C.T.Foxon, P.J.Dobson and B.A.Joyce, Appl.Phys. A33 (1984) 87.
- [4] C.E.C.Wood and B.A.Joyce, J.Appl.Phys. 49 (1978) 4854.
- [5] R.Heckingbottom, G.J.Davies and K.A.Prior, Surf.Sci. 132 (1983) 375.
- [6] V.M.Airaksinen, T.S.Cheng and C.R.Stanley, Proc. 4th International Conference on MBE, York 1986. To be published in J.Cryst.Growth.
- [7] C.E.C.Wood, D.Desimone, K.Singer and G.W.Wicks, J.Appl.Phys. 53 (1982) 4230.
- [8] A.Iliadis, K.A.Prior, C.R.Stanley, T.Martin, and G.J.Davies, J.Appl.Phys. 60 (1986) 213.
- [9] K.Akimoto, M.Dohsen, M.Arai and N.Watanabe, Appl.Phys.Lett 43 (1983) 1062.
- [10] C.T.Foxon and B.A.Joyce, Surf.Sci. 50 (1975) 434.
- [11] J.M.Van Hove and P.I.Cohen, Appl.Phys.Lett. 47(1985) 726.
- [12] R.F.C.Farrow, J.Phys.D 7(1974) 2436.
- [13] F.A.Kroger, F.H.Stieltjes and H.J.Vink, Philips Res. Repts 14 (1959) 557.
- [14] E.A.Kraut and W.A.Harrison, J.Vac.Sci.Technol. B2(1984)409.
- [15] K.C.Mills, Thermodynamic Data for Inorganic Sulphides, Selenides and Tellurides (Butterworths, London 1974).
- [16] O.Kubaschewski and C.B.Alcock, Metallurgical Thermochemistry, 5.ed. (Pergamon, Oxford 1975).

- [17] D.M.Collins, J.N.Miller, Y.G.Chai and K.Chow, J.Appl.Phys. 53 (1982) 3010.
- [18] D.A.Andrews, R.Heckingbottom and G.J.Davies, J.Appl.Phys. 54 (1983) 4421.
- [19] D.A.Andrews, M.Y.Kong, R.Heckingbottom and G.J.Davies, J.Appl.Phys. 55 (1984) 841.
- [20] E.A.Kraut Private communication.
- [21] Thermodynamic properties of the elements, No 18 of the Advances in Chemistry Series (American Chemical Society, Washington D.C. 1956).
- [22] C.Pupp, J.J.Murray and R.F.Pottie, J.Chem.Thermodynamics 6 (1974) 123.

## CHAPTER 5

### A THERMODYNAMIC MODEL FOR THE CALCULATION OF NATIVE DEFECT CONCENTRATIONS IN InP AND GaAs

#### 5.1 Introduction

The concentrations of native point defects, i.e. vacancies, antisite defects and self-interstitials and their various complexes can in principle be calculated for any III-V compound grown under equilibrium conditions. Such a calculation starts with the definition of the appropriate formation reactions from the vapour or liquid phases and the various reactions between different defect species. For the calculation of defect concentrations the law of mass action is used. The equilibrium constant  $K$  of a chemical reaction can be calculated from the standard free energy change ( $\Delta G^{\circ}$ ) or equivalently from the difference of the standard entropies ( $\Delta S^{\circ}$ ) and enthalpies ( $\Delta H^{\circ}$ ) of the reaction products and reactants:

$$K = \exp(\Delta S^{\circ}/k_B - \Delta H^{\circ}/k_B T) \quad (5-1)$$

where  $k_B$  is Boltzmann's constant. Mass action laws can provide enough independent equations for solving all neutral defect concentrations. If ionised defects are considered, another relation is needed to determine the number of free carriers. This is provided by the charge neutrality condition. Then of course all ionised defects must be taken into account in the model, whether native or otherwise.

As an example consider a simple model for GaAs where the only charged defects are assumed to be As vacancies. If the crystal is in equilibrium with the vapour phase, the formation reaction for a neutral As vacancy  $V_{As}$  can be written:



The ionisation reaction of  $V_{As}$  is



And the Schottky relation for free carriers:



Finally the charge neutrality condition can be written

$$[V_{As}^+] + p = n \quad (5-2d)$$

where  $n$  is the free electron concentration and  $p$  the free hole concentration. Equations (5-2a-d) allow all four unknown concentrations  $[V_{As}]$ ,  $[V_{As}^+]$ ,  $p$  and  $n$  to be simultaneously solved from the corresponding laws of mass action:

$$K_{2a} = (p(As_2))^{-1/2} [V_{As}]^{-1} \quad (5-3a)$$

$$K_{2b} = [V_{As}^+]n/[V_{As}] \quad (5-3b)$$

$$K_{2c} = [e^-][h^+] = np/N_c N_v \quad (5-3c)$$

Strictly speaking one should use activities instead of concentrations in the mass action laws (5-3a and b). This kind of model can be constructed as complicated as desired. Any defects can be included by just adding the appropriate formation and ionisation reactions. The formation reactions can be either similar to (5-2a), reactions between the vapour or liquid phase and the bulk, or reactions between defects, for instance Schottky relations (5-2c).

Models similar to that given in equations (5-2) have been used for calculating concentrations of point defects in GaAs by Logan and Hurle [1], Hurle [2] and Baraff and Schlueter [3], in AlGaAs by Blom [4] and in both GaAs and AlGaAs by Devine [5]. Hurle has also used the point defect model to construct solubility curves of dopants in GaAs [11,12,13]. The use of such a possibly quite complicated model rests on several assumptions.

Firstly, because the activities of different chemical species are usually not known they are taken as unity. This is not necessarily correct. Since defect concentrations are low it can be assumed that Raoult's law is obeyed and activities are in fact unity but there is no experimental evidence to support this choice. The only species for which activity data is available are free carriers [6] and the group III and V elements themselves.

Secondly, the crystal growth is assumed to occur so close to thermodynamic equilibrium that the use of thermodynamic equilibrium calculations is justified. This is indeed true for liquid phase epitaxy (LPE) where very small values of supercooling of only a few degrees K are generally used. In the MBE of InP the typical overpotential for growth is 20-40°C, ie. the growth temperature is 20-40°C below the value which would cause the growing crystal surface to become In-rich.

Support for the idea that thermodynamic equilibrium is applicable to MBE is provided by the work of Heckingbottom et al. who have shown that equilibrium calculations can successfully be used for explaining doping behaviour in MBE-grown GaAs [7,8,9,10].

Thirdly it is assumed that thermochemical data, i.e. standard entropies and enthalpies are in fact available for all the relevant defects. This assumption is quite false. As shown in Section 5.3, apart from some recent experimental data on the ionisation energies of some probable antisite defects, only simple theoretical estimates of the enthalpies and Schottky constants of vacancies and antisite defects exist. Further, the knowledge of enthalpies and entropies of formation is not in itself sufficient. For donors and acceptors the ionisation energies are also required. A great amount of published data, both experimental and theoretical, on the ionisation energies of point defects is available. Unfortunately, there is currently no consensus about the correct values for even the most common defects in GaAs. For InP the situation is more unfavourable since this material is less completely characterised than GaAs.

Fourthly the point defects are assumed to have insufficient time to react during the cooling down of the crystal and are therefore frozen in at concentrations comparable to the equilibrium growth temperature, or that the cool down occurs slowly enough for the point defects to maintain their equilibrium concentrations down to room temperature.

It is clear that given the unsatisfactory state of our knowledge of the relevant thermodynamic quantities, the results obtained from thermodynamic calculations are not very accurate. For instance, a modest error of 0.5eV in the standard free energy of the formation reaction of a defect at 750K can lead to the concentration of the defect being over- or underestimated by

over three orders of magnitude. Of course the thermodynamic constants can be used as adjustable parameters to fit the thermodynamic model to experimental data. Given the multitude of defects and their possible complexes a model can be made to fit any data. It should also be noted that errors in the concentration of one ionised defect can affect the concentrations of all the other ionised defects through the charge neutrality condition. It must be concluded that the goal of calculating the defect concentrations self-consistently is at present overambitious.

A slightly easier task has been undertaken in this work. The purpose has been partly to develop the calculation method itself, especially the correct partitioning of the virtual free energies. Also the model has been simplified by taking the Fermi-level as an adjustable parameter, therefore there is no need for self-consistency in regard of the charge neutrality condition. Also the model has been written in a form which allows the concentrations of different defects be calculated independently of each other. Consequently defects of which little is known, such as interstitials and various complexes of defects can be ignored. Finally, even though the results are inevitably in error by several orders of magnitude, some general trends of the defect concentrations can be obtained from the data.

The usual approach to calculate the enthalpy (or entropy) of a defect formation reaction is to divide the reaction into simpler virtual reactions. The enthalpy of the real reaction is obtained from the virtual enthalpies by addition [14],[16],[11]. However, since the virtual reactions are not real, physically realisable reactions, their thermochemical constants cannot be determined unambiguously [14]. In Section 5.2 the "virtual" reactions are defined as such physically realisable reactions, which correspond to the ideal

virtual reactions as closely as possible. Consequently, the "virtual" reactions have unambiguous thermochemical constants. It is also shown in Section 5.2 how the virtual free energy of the incorporation reaction of the group V element from the vapour phase is calculated from the vapour pressure.

In Sections 5.3 and 5.4 estimates of the virtual enthalpies and entropies of formation of neutral vacancies, divacancies, antisite defects and antistructure defects are obtained from published theoretical data. Estimates of the enthalpies and entropies of ionisation are given in Section 5.5.

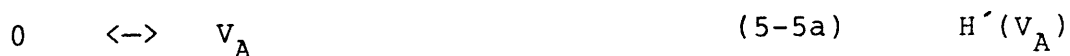
The thermodynamic model is described in Section 5.6. and the defect concentrations are calculated by using the thermodynamic data of the previous Sections. The implications of the results are discussed.

## 5.2 The partitioning of the virtual free energies

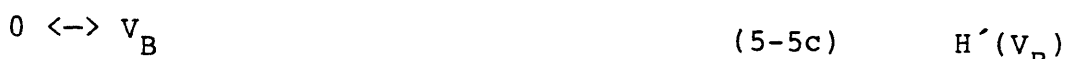
Consider the formation reaction of a cation vacancy:



where B denotes the group V element and the subscripts A, B the cation and anion sites in the lattice. The formation reaction (5-4) can be written as the sum of the two virtual reactions (5-5a and b):



Virtual quantities are distinguished from the real ones by a dash. Similarly one can write the formation reaction for the anion vacancy  $V_B$  as the sum of the two reactions (5-5c,d):



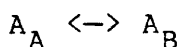
The problem with the partitioning of the virtual standard free energies is that the structural elements of the crystal (for instance  $P_P$ ,  $In_{In}$ ,  $P_{In}$  etc. for InP) are not independent variables due to the conservation of lattice sites rule. (For an excellent discussion of the structural and building units see Ref. [14].) Therefore, they do not have true chemical potentials, i.e. the chemical potential of a structural element cannot be determined by adding a single structural element to the crystal because such a process does not conserve the relative numbers of lattice sites. Hence, if a reaction is to have a true chemical potential, it must either conserve the number of lattice sites or a whole building unit consisting of equal numbers of the group III and V lattice sites must be added to or removed from the crystal. Assume that the real crystal can be built from  $b$  different, independent building units. Then it can be shown that the virtual free energies of all but  $b$  structural elements can be chosen freely [14]. The  $b$  remaining virtual free energies must be assigned so that the free energies of real chemical reactions involving building units are correct. In other words the number of virtual chemical potentials that can be assigned freely is  $s-b =$  (the number of structural elements) - (the number of independent building units). For instance in our model of Section 5.4  $s-b = 6-5 = 1$ . Therefore, one virtual free energy can be chosen arbitrarily.

Because of this arbitrariness the virtual quantities cannot be used for tabulating thermochemical data. It is necessary to define "virtual" reactions as such physically realisable reactions which correspond to the ideal virtual reactions as closely as possible. According to Van Vechten [16], the virtual formation

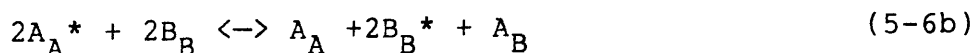
reactions of vacancies (5-5a and b) are defined so as to conserve the number of atoms in the crystal. To create a vacancy  $V_A$  an atom A is removed from its site in the bulk to a site on the surface of the crystal. For an elemental semiconductor like Si or Ge, this definition of the virtual reaction does not cause any difficulties of interpretation. In a compound semiconductor, however, the relative number of the lattice sites inside the crystal is not conserved. For instance, the virtual reaction (5-5a) should be written



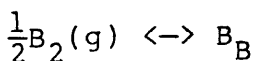
where \* denotes surface atoms. It can be seen that a new lattice site B is created inside the crystal. Similarly the virtual formation reaction of an antisite



actually denotes a reaction in which an atom B is removed from its site to the surface of the crystal and an atom A from the surface is moved into the resulting vacancy:



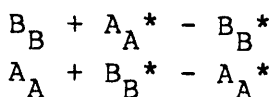
Finally the virtual reaction for the incorporation of the group V element from the vapour



should be written

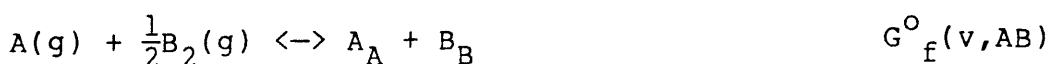


These "virtual" reactions are actually physically realisable reactions because surface atoms have been taken explicitly into account. Formally this means that two new independent variables have been introduced into the system:



It should be noted that the additional degree of freedom which allows the surface stoichiometry of the crystal to vary relaxes the strict original requirement of the conservation of the relative numbers of lattice sites: an isolated lattice site may be added to the crystal if a corresponding change is made in the numbers of the surface atoms on different sites.

The virtual free energies of formation for vacancies and antisites have been calculated by Van Vechten [16]. The remaining problem is to determine the virtual free energy or equivalently the free enthalpy and entropy of equations (5-5b) and (5-5d). In other words we must decide how the free energy of formation  $G_f^{\circ}(v,AB)$  of the compound AB from the vapour phase through the reaction



is divided between reactions (5-5b) and (5-5d). Van Vechten considered the problem in Ref [15]. He determined the virtual enthalpies and entropies for formation reactions from the pure elemental liquids:



and postulated that the enthalpies and entropies should be apportioned as in the stoichiometric liquid. As shown

by Hurle [2] this choice leads to equal partitioning in GaAs, i.e. the virtual enthalpies of (5-7a) and (5-7b) are both one half of the heat of formation of GaAs from the elemental liquids.

Devine [5] took a different approach. He assumed that the enthalpies of vacancy formation reactions from the monoatomic vapour are equal in GaAs, i.e. the enthalpies of reactions (5-8) are equal:



This was justified by the equal covalent radii of As and Ga atoms and the fact that for PbS the formation enthalpies are known to be nearly the same. Because according to Van Vechten [16] the virtual enthalpies for the Ga and As vacancies are equal, the virtual enthalpies of As and Ga incorporation from the monoatomic vapour should also be equal.

The partitioning suggested by Van Vechten leads to a different result from that obtained by Devine. By using equation (5-6c) the partitioning problem can be solved formally. The equilibrium constant of (5-6c) is

$$K = \exp\left(-\frac{G'(v, B_B)}{k_B T}\right)$$

From the law of mass action the standard free energy change can be solved:

$$G'(v, B_B) = -k_B T \ln\left(\frac{[B_B^*]}{[A_A^*] p(B_2)}\right) \quad (5-9)$$

Therefore, the virtual free energy of formation (for B) can be calculated by measuring the vapour pressure of  $B_2(g)$  over the crystal as a function of the temperature

while the surface stoichiometry is kept constant. It should be noted that the value of the virtual free energy of equation (5-9) will probably depend on the point in the phase diagram where it is measured.

The virtual free energies of formation can also be calculated without taking the surface explicitly into account. Consider a  $\text{In}(g) + \text{P}_2(g)$  vapour in equilibrium with the  $\text{InP}$  crystal. As shown in Figure (5-1), the formation of  $\text{InP}$  from the elemental liquids  $\text{In}(l)$  and  $\text{P}(l)$  requires three processes:

I) The evaporation of  $\text{In}$  and  $\text{P}$  under equilibrium conditions. The equilibrium pressures are  $p^*(\text{In})$  and  $p^*(\text{P}_2)$ .

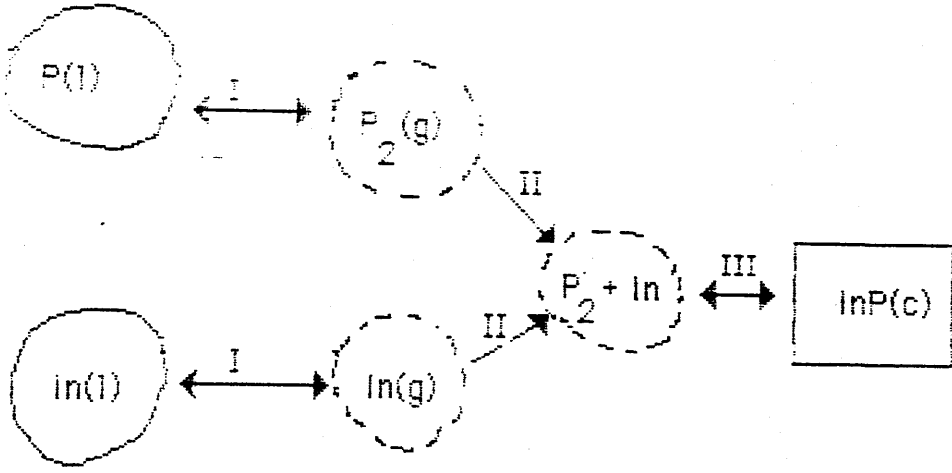
II) Compression and mixing of the  $\text{In}$  and  $\text{P}_2$  vapours so that they are in equilibrium with the  $\text{InP}$  crystal at pressures  $p(\text{In})$  and  $p(\text{P}_2)$ .

III) Growth from the vapour phase under equilibrium conditions.

The free energy changes of each process are straightforward to calculate. For the equilibrium processes I and III  $G=0$ . Process II consists of an isothermal compression and mixing. For ideal gases the mixing process is equivalent to an isothermal expansion. Therefore, the net effect of II is an isothermal expansion (or compression) from the equilibrium pressure  $p^*(i)$  to  $p(i)$  ( $i = \text{In}$  or  $\text{P}_2$ ), and the free energy changes are simply

$$G_f'(l, \text{In}) = k_B T \ln\left(\frac{p(\text{In})}{p^*(\text{In})}\right) \quad (5-10a)$$

$$G_f'(l, \text{P}) = \frac{kT}{2} \ln\left(\frac{p(\text{P}_2)}{p^*(\text{In})}\right) \quad (5-10b)$$



Pure,  
elemental  
liquids

Equilibrium  
evaporation

Compression  
and mixing

Equilibrium growth

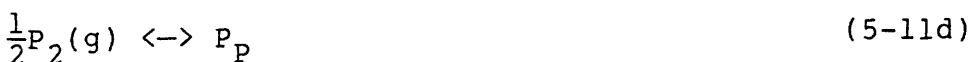
Figure (5-1). A schematic diagram of the processes for growing InP from the elemental reference liquids.

Since the initial and final states of the processes shown in Fig. 5-1 are standard states, the free energy changes given in equations (5-10) are in fact the virtual standard free energies of formation. Their sum is the standard free energy of formation of InP  $G_f^0(l, \text{InP})$ . It should be pointed out that the virtual free energies depend on the equilibrium partial pressures during the growth. According to (5-10b), a doubling of the phosphorus pressure during the growth at a typical temperature of 750K will lead to an increase of 22.4meV in the virtual free energy of phosphorus incorporation. Instead of using equations (5-10) it will be more useful to calculate the virtual free energies of reactions (5-5b) and (5-5d) from the vapour phase. To start the process we have vapours at the standard state of 1bar. Through an isothermal expansion they acquire the equilibrium pressures with the solid and the growth occurs at equilibrium as before. Therefore, we get the following virtual standard free energies:

$$G'(v, \text{In}) = k_B T \ln( p(\text{In}) ) \quad (5-11a)$$

$$G'(v, P_P) = \frac{k_B T}{2} \ln( p(P_2) ) \quad (5-11b)$$

for the virtual reactions



Equation (5-11b) is in fact equivalent to equation (5-9), even though the requirement that the surface stoichiometry must be conserved is not explicitly stated. The equilibrium pressures  $p^*$  of each species over the elemental reference liquid, and the pressures of the group III and V species ( $p^0$ ) over InP and GaAs in

the Knudsen equilibrium are given in Table 5-1. The equilibrium pressure of the group III element is very nearly the same over the pure liquid as over the compound in these conditions. Therefore the Knudsen equilibrium represents the group III rich part of the phase diagram and gives the vapour pressures along the liquidus.

The epitaxial growth occurs near the liquidus both in the high temperature MBE growth of InP and GaAs and in LPE. Therefore, it is interesting to calculate the virtual free energies at the liquidus. This can be done by replacing the pressures in eq. (5-10) by the Knudsen equilibrium pressures in Table 5-1 giving

$$G'(v, \text{In}) = k_B T \ln(p^0(\text{In})) = 12.84k_B T - 2.50\text{eV} \quad (5-12a)$$

$$G'(v, P_2) = \frac{k_B T}{2} \ln(p^0(P_2)) = 13.25k_B T - 1.64\text{eV} \quad (5-12b)$$

for InP. From Table 5-1 virtual enthalpies and entropies for GaAs can also be obtained. When the group V pressure is increased and the growth moves away from the liquidus, the virtual enthalpies can be expected to remain unchanged. The change in the virtual free energies is mainly due to changes in the entropy term. However, the effect of any reasonable pressure change is small compared to the absolute value of the virtual free energy.

$$p = \exp(A - B/k_B T)$$

	A	B/eV	Reference
$p^*(P_2)$	14.29	1.42	[17]
$p^*(As_2)$	16.33	1.83	[17]
$p^*(In)$	12.33	2.46	[18]
$p^o(In)$	12.84	2.50	[18]
$p^o(Ga)$	12.78	2.69	[19]
$p^o(P_2)$	26.50	3.28	[18]
$p^o(As_2)$	26.55	3.84	[19]

Table 5-1. Experimental values for the equilibrium pressures ( $p^*$ ) of  $P_2$ ,  $As_2$  and In over the elemental reference liquids and In, Ga,  $P_2$  and  $As_2$  over InP and GaAs ( $p^o$ ).

### 5.3 The enthalpies of formation of neutral defects

#### 5.3.1 Vacancies and divacancies

Experimental data on the enthalpies of formation of vacancies in III-V compounds does not exist. Virtual enthalpies of single vacancy formation in zinc-blende type semiconductors have been estimated by Van Vechten [16]. He treated vacancies as macroscopic cavities and calculated the enthalpies  $H'(V_x)$  from the surface energy of the cavity. His theory predicts that  $H'(V_x)$  will be larger for the component with the larger tetrahedral covalent radius  $r_c$ . Van Vechten used the same method for calculating the virtual enthalpies of divacancies  $H'(V_A V_B)$ . The virtual reactions are:



The values of the virtual enthalpies are given in Table 5-2.

---

	$r_c(A)$	$r_c(B)$	$H'(V_A)$	$H'(V_B)$	$H'(V_A V_B)$
GaAs	1.755A	1.755A	2.31eV	2.31eV	3.64eV
InP	2.013A	1.616A	2.74eV	1.87eV	3.84eV

Table 5-2. Covalent radii of anions and cations and virtual enthalpies of neutral mono- and divacancies in GaAs and InP [16].

### 5.3.2 Antisite and antistructure defects

Van Vechten has calculated the virtual enthalpies of antisite defect formation [15],[16] for the virtual reactions



where Z can be 0,1 or 2 depending on the charge state of the defects. These enthalpies consist of two contributions, one ( $H'_0$ ) from the reduction of the band gaps due to the disorder in the crystal potential, and the other ( $H'_e$ ) from the excess or deficit of electrons and the separation of the Fermi level from the top of the valence band and the bottom of the conduction band (where the extra electrons are added or subtracted). Van Vechten also estimated the virtual enthalpies of neutral antistructure defects for the reaction



They turn out to be simply the sums of the neutral parts of the enthalpies ( $H'_0$ ) because the antistructure defects are neutral and the electronic contributions to the enthalpy ( $H'_e$ ) cancel out. The values of the enthalpies are given in Table 5-3. Kraut and Harrison (K&H) [21] have used the universal parameter tight binding method to calculate cohesive energies, antisite and neutral antistructure defect energies for zinc-blende structure semiconductors (Table 5-3).

	$H_{O'}(B_A)$	$H_{O'}(A_B)$	$H_{e'}(B_A^{+Z})$	$H_{e'}(A_B^{-Z})$	$H(B_A A_B)$
VV:					
GaAs	0.35eV	0.35eV	$Z(E_F - H_V)$	$Z(H_C - E_F)$	0.70eV
InP	0.42eV	0.89eV	"-	"-	1.30eV
K&H:					
GaAs	-1.36eV	2.12eV	$Z(E_F - H_V)$	$Z(H_V - E_F)$	0.57eV
InP	-1.56eV	3.25eV	"-	"-	1.27eV

Table 5-3. The virtual enthalpies of antisite- and antistructure defects in GaAs and InP according to Van Vechten [16] (VV) and Kraut and Harrison [21] (K&H).

---

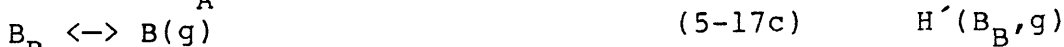
	$H_{O'}(B_A^{2+})$	$H_{O'}(A_B^{2-})$	$H(B_A A_B)$
GaAs:			
K&H	2.53eV	3.63eV	2.60eV
VV	3.05eV	3.05eV	2.55eV
InP:			
K&H	2.72eV	4.17eV	3.22eV
VV	3.02eV	3.49eV	2.93eV
Averages:			
GaAs	2.79eV	3.34eV	2.57eV
InP	2.87eV	3.84eV	3.08eV

Table 5-4. The virtual enthalpies of formation for ionised antisite defects by Kraut and Harrison [21] and Van Vechten [16] (corrected values).

It can be seen from Table 5-3 that the antistructure enthalpies of VV agree well with those of K&H but the antisite defect enthalpies are completely different. (K&H mentioned in their paper that their values were "per bond" but this is probably not correct because the values per defect would be unrealistically high. However, K&H were unable to explain this discrepancy [22].) This is due to the fact that K&H values were calculated for real substitution reactions between the vapour and bulk:



whereas VV's virtual enthalpies are for virtual reactions (5-14). The contributions of the subtracted electrons are different in the two models. In K&H's model electrons are always added and subtracted at the valence band maximum whereas in VV's model they are added at the valence band maximum but subtracted at the conduction band minimum. K&H's results can be converted to virtual enthalpies corresponding to VV's virtual enthalpies. Consider only the formation reaction of the neutral antisite defect  $A_B$ . It can be written as the sum of the virtual reactions (5-17):



Therefore, the conversion is completed by subtracting the appropriate virtual enthalpies:

$$H_O'(A_B) = H_O(A_B) - H(B_2, B) - H'(B_B, g) - H'(g, A_A)$$

$H(B_2, B)$  can be found in Ref. [20],  $H'(B_B, g)$  and  $H'(g, A_A)$  are obtained from the equilibrium vapour pressure data for InP [18] and GaAs [19]. In an analogous way the formation enthalpy  $H_O(B_A)$  can be converted into  $H_O'(B_A)$ .

As Kroger [6] has pointed out, Van Vechten uses a floating standard state for electrons and holes, extra electrons being supplied and removed at the Fermi-level. In this work the normal convention of using the perfect crystal as the fixed standard state is adopted for electrons and holes. Then the virtual enthalpies of formation for fully ionised antisites are obtained by adding  $2xH_{cv}$  to VV's (and K&H's) values  $H_O'$ .

The formation enthalpies of neutral antistructures by reaction (5-15) are estimated from the values for ionised antisites:

$$H(B_A A_B) = \frac{3}{4} ( H'(B_A^{2+}) + H'(A_B^{2-}) - 2H_{cv} )$$

where  $2H_{cv}$  is subtracted because two  $e^-h^+$  pairs are annihilated. The factor  $3/4$  is due to the A-B bond of the antistructure pair. The results of these corrections are presented in Table 5-4. The values from both models agree well. The enthalpies of formation of neutral antisites can be obtained by simply subtracting the enthalpies of ionisation from the enthalpies of ionised antisites. The ionisation enthalpies are estimated on the basis of experimental and theoretical data in Section 5.3.4 giving the following values for the neutral anion antisites:

$$H'(P_{In}^0) = 2.87\text{eV} - 0.9\text{eV} - 1.2\text{eV} = 0.9\text{eV}$$

$$H'(As_{Ga}^0) = 2.79\text{eV} - 0.75\text{eV} - 1.0\text{eV} = 1.0\text{eV}.$$

## 5.4 The entropies of formation of neutral defects

The virtual entropies of formation for native defects in III-V compounds are not known and reliable methods of calculating the entropies have not been developed, therefore all estimates for the pre-exponential factors of the equilibrium constants are unreliable. However, the experimental data for point defects in ionic compounds indicate that the entropies are usually on the order of  $1k_B$  and generally less than about  $8k_B$  (Ref. [23] p.268).

Van Vechten [15] used the best estimates of the virtual entropies of vacancies in silicon and germanium,  $S'(V) = 1.1k_B$ , for GaAs vacancies. Here a broader range of values is adopted:

$$S'(V) = 2 \pm 2 k_B$$

The same values are used for the virtual entropies of divacancies and antisite defects.

The anion antisites are probably deep donors, therefore the entropy of ionisation can be assumed equal to the entropy of the band gap [15]:  $S_I'(B_A^{Z+}) = S_I'(A_B^{Z-}) = Z S_{cv}$  (see Section 5.5.3). The entropy of association of ionised antisites, i.e. for the reaction



can be separated into a configurational and vibrational part [23]:

$$S_{\text{assoc}} = S_{\text{conf}} + S_{\text{vibr}} = k_B \ln(Z/s) + k_B \ln f \quad (5-19)$$

In the configurational part  $Z$  is the number of equivalent configurations for the associate ( $Z=4$ ) and  $s$  the symmetry factor ( $s=1$ ).  $f$  is caused by the change in the vibration spectrum of the crystal and its magnitude is unknown. However, if the association of the two ionised antisites has no effect on the vibrational spectrum,  $f = 1$ . The other extreme occurs when the associate is equivalent to two neutral antisites, and  $f = \exp\{-2S'_I/k_B\}$ . Hence the value of  $f$  is taken as

$$k_B \ln f = -S'_I \pm -S'_I$$

and the total entropy of formation of an antistructure pair can be estimated as

$$\begin{aligned} S(B_A A_B) &= S'(B_A^0) + S'(A_B^0) + S_I(B_A) + S_I(A_B) + S_{\text{assoc}} \\ &\quad - 2 S_{\text{cv}} = \\ &= 5.4k_B + S_{\text{cv}})k_B \pm (4k_B + S'_I). \end{aligned}$$

where  $2 S_{\text{cv}}$  is subtracted because two e-h pairs are annihilated. By using the values given in Section 5.4.3 the following entropies are obtained:

$$\begin{aligned} S(P_{\text{In}} \text{In}_P) &= 10.3k_B \pm 8.9k_B \\ S(\text{As}_{\text{Ga}} \text{Ga}_{\text{As}}) &= 11.7k_B \pm 10.3k_B \end{aligned} \quad (5-20)$$

## 5.5 Enthalpies and entropies of ionisation

### 5.5.1 Ionisation energies of vacancies

A number of calculations of the electronic energy levels of vacancies in III-V semiconductors have been published recently. The computational complexity of first principles calculations has prevented their widespread use. Semiempirical methods based mainly on tight binding approximation are more common. The accuracy of the electronic states predicted with these methods is less than 0.5eV even for ideal nondistorted vacancies. For a real vacancy with significant distortion, the error in the energy levels is even greater [24]. Loualiche et al. [26] have developed a method of estimating the ionisation energies of undistorted defects from deep level transient spectroscopy (DLTS) and deep level optical spectroscopy (DLOS) allowing direct comparison with the results of calculations for ideal vacancies. The general chemical trends of the calculated energy levels are expected to be qualitatively correct. For the cation vacancies in both GaAs and InP the level of  $A_1$  symmetry is deep in the valence band whilst the  $T_2$  level is slightly above the valence band maximum. The  $A_1$  level of the anion vacancies is somewhere in the forbidden gap and  $T_2$  is located in the upper half of the gap [26,27,28,29,30,31]. Cation vacancies are expected to be acceptors whereas the anion vacancies are donors.

Monovacancies in GaAs have been observed from positron annihilation measurements [32], but the only vacancy to have been identified from EPR is  $V_p$  in InP [33]. Because experimental data is unavailable, the first ionisation enthalpy of both anion and cation vacancies is assumed to be  $\frac{1}{4}E_{CV}(0)$  in both GaAs and InP.

¶

### 5.5.2 Ionisation energies of antisite defects

The anion antisite defects are expected to be donors in both InP and GaAs [27],[25]. Strong experimental evidence is available to suggest that the EL2 deep level in GaAs is related to the  $\text{As}_{\text{Ga}}$  antisite defect. The situation is complicated by the fact that there are probably several different defects having similar activation energies but different electron capture cross sections, the so called EL2 family [35],[34]. Kaminska et al. defined EL2 as the defect present alone in typical Bridgeman grown GaAs [36] and used uniaxial stress and magnetic field experiments to show that it has tetrahedral symmetry and is therefore an isolated point defect, most probably  $\text{As}_{\text{Ga}}$ . EL2 has also been identified as the neutral  $\text{As}_{\text{Ga}}$  defect [37],[38]. More commonly, however, the energy levels 0.75eV and 1.0eV below the conduction band minimum have been attributed to the single and double ionised donor levels of  $\text{As}_{\text{Ga}}$  [39],[40],[41]. These values are used as the ionisation energies of the  $\text{As}_{\text{Ga}}$  double donor in this work even though the identification of EL2 as the isolated  $\text{As}_{\text{Ga}}$  is by no means undisputed [42],[43]

Experimental data for the anion antisite defect  $\text{P}_{\text{In}}$  in InP is not very extensive. Calculations suggest it is a shallow donor [27],[44]. Optically detected magnetic resonance (ODMR) investigations however give the first ionised level of the donor near the valence band maximum [45]. Also by ODMR Cavenett et al. [46] obtained the values  $\text{D}^0$  at  $E_{\text{c}}-0.89\text{eV}$  and  $\text{D}^+$  at  $E_{\text{v}}+0.09\text{eV}$  for the neutral and singly ionised levels of the donor. Therefore values of 0.9eV and 1.2eV are used for the enthalpies of ionisation.

Cation antisite defects are double acceptors in both GaAs and InP. Photoluminescence emissions at 77meV and 230 meV have been assigned to  $\text{Ga}_{\text{As}}$  [47,48,49,50,51].

This assignation is still controversial [56]. Wang et al. [52] showed that the A and B deep levels at 0.4eV and 0.7eV above valence band maximum are coupled and proposed they are in fact the two ionisation levels  $E_1$  and  $E_2$  of  $Ga_{As}$ . Theoretical calculations also predict energy levels near the maximum of the valence band [25]. A semiempirical model by Poetz and Ferry [53] gave values of 0.4eV and 0.6eV for  $E_1$  and  $E_2$ , in good agreement with results of Wang et al. It therefore seems probable that neutral  $Ga_{As}$  does not exist in n-type GaAs. As a compromise values  $E_1=0.2eV$  and  $E_2=0.4eV$  are adopted in this work.

Experimental results for the ionisation levels of the cation antisite  $In_p$  in InP do not exist. The values from the semiempirical model by Poetz and Ferry are used instead:  $E_1=1.6eV$ ,  $E_2=1.7eV$ . Therefore, it can be assumed that  $In_p$  exists only in the neutral state in InP.

### 5.5.3 The entropy of ionisation

Consider the ionisation reaction of the donor D:



The equilibrium constant of (5-21) is

$$K_{19} = \frac{[D^+]n}{[D]} \quad (5-22)$$

The concentration of ionised donors  $[D^+]$  can be calculated from

$$[D^+] = \frac{g_+}{g_o} [D] \exp\left(\frac{E_d - E_F}{k_B T}\right) \quad (5-23)$$

where  $g_+$  and  $g_0$  are the degeneracies of the ionised and neutral levels, respectively ( $g_+=1$ ,  $g_0=2$ ). and  $E_d$  is the donor energy level. For a nondegenerate semiconductor the free electron concentration is given by

$$n = N_c \exp\left(\frac{E_F - E_c}{k_B T}\right) \quad (5-24)$$

where  $N_c$  is the effective density of states in the conduction band. From equations (5-22 to 24) the equilibrium constant can be solved

$$K_{19} = \frac{1}{2} N_c \exp\left(\frac{E_d - E_c}{k_B T}\right) \quad (5-25)$$

By definition, the argument of the exponential in the mass action law gives the standard chemical potential of the reaction. At a constant temperature and pressure, the change in the standard chemical potential is equal to that of the free energy. Therefore, the ionisation energy  $E_I$  is the standard free energy of the ionisation reaction:

$$E_I = E_c - E_d = G_I^0$$

In principle the experimental ionisation energies give the standard free energies of ionisation. Unfortunately the free energies are functions of the temperature, the temperature dependent term in the free energy being mainly caused by the entropy change. The entropy of ionisation  $S_I$  itself is temperature dependent, approaching zero at low temperatures. Since the ionisation energies are usually measured at low temperatures, they equal the enthalpies of ionisation. The entropy of ionisation is due to the change in the lattice modes of the crystal caused by the change in the distribution of electronic charge within the crystal.

According to Van Vechten [16], for isoelectronic impurities, vacancies and interstitials,  $S_I$  equals the entropy of ionisation of an electron-hole pair across the energy gap ( $S_{cv}$ ). For hydrogenic impurities  $S_I$  varies depending on the binding energy of the electron. In impurities with tightly bound electrons  $S_I$  is nearly equal to  $S_{cv}$ , but for shallow impurities  $S_I$  is very small.

Hence, in most cases,  $S_I$  is easily obtained if  $S_{cv}$  is known.  $S_{cv}$  can be estimated from the temperature dependence of the band gap  $E_{cv}$ , which can be expressed as [54]

$$E_{cv}(T) = E_{cv}(0) - \frac{AT^2}{B+T} \quad (5-26)$$

where A and B are empirical constants. Since  $E_{cv}$  is a free energy change, the entropy is obtained by taking the derivative

$$S_{cv} = -\frac{dE_{cv}}{dT} = \frac{AT(2B+T)}{(B+T)^2} \quad (5-27)$$

At high temperatures  $S_{cv} \rightarrow A$ , and we can use values [55], [54]:

$$\begin{aligned} S_{cv} &= 6.27k_B && (\text{GaAs}) \\ S_{cv} &= 4.9k_B && (\text{InP}). \end{aligned} \quad (5-28)$$

The following values for the ionisation entropies of vacancies and antisites are used:

$$S_I(V_{Ga}), S_I(V_{As}), S_I(As_{Ga}) \text{ and } S_I(Ga_{As}) \ 6.3k_B, \text{ and } S_I(P_{In}) \text{ and } S_I(In_P) \ 4.9k_B.$$

## 5.6 The calculation of defect concentrations

### 5.6.1 The thermodynamic model

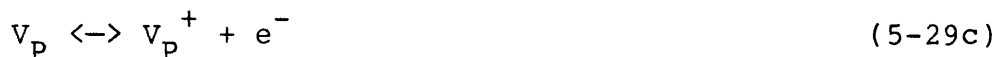
The definition and calculation of the virtual enthalpies and entropies of the defect formation reactions, together with a review of the best available (mainly theoretical) data was discussed in the preceding Sections. These results are used in Section 5.6 to calculate the concentrations of ionised defects. If the calculation is to be performed self-consistently, the charge neutrality condition is needed to determine the relative concentrations of positively and negatively charged defects. The disadvantage of such an ambitious model is that all charged defects, both extrinsic and intrinsic, must be included. The neutrality condition also couples ionised defects, so that an error in the concentration of one type of defect will produce errors in the concentrations of other defects.

In this work, a more modest approach is used. The Fermi-level of the crystal is taken as a parameter and the concentrations of defects are simply calculated for fixed values of the free electron concentration  $n$ . It should be noted that in principle  $n$  can be measured during the growth and adjusted within certain limits by simply introducing controlled amounts of a suitable dopant.

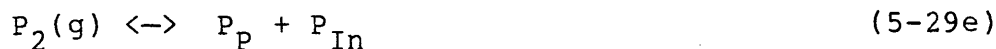
The formation reactions of neutral defects are written in a form which only utilises the group V dimer in the vapour phase and the majority species in their proper sites to preserve the correct number of lattice sites in each reaction, ie. each reaction can only create or annihilate an entire unit cell. The concentrations of the ionised defects are calculated by applying the enthalpies and entropies of ionisation to the neutral defects. The validity of the model is not affected by the number of defects included. New defects

can be introduced and their concentrations calculated in a similar manner, if their virtual enthalpies and entropies are known.

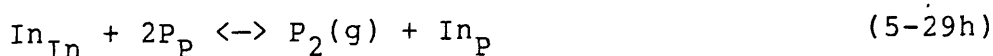
The reactions (5-29) used in the thermodynamic model for InP include the formation reactions of neutral and ionised vacancies (assumed singly ionised):



For neutral and ionised antisites, the formation reactions are



The cation antisite is assumed to be present only in the neutral state in InP:



Finally the formation reactions of divacancies and antistructures are



For GaAs an analogous set of reactions apply except that neutral  $\text{Ga}_{\text{As}}$  is assumed not to exist in n-type GaAs. The formation reaction for the ionised cation antisite is



The virtual reactions and their enthalpies and entropies are listed in Tables 5-5 and 5-6. From these virtual values the enthalpies and entropies of the real reactions (5-29) are calculated in Table 5-7.

### 5.6.2 Defect concentrations in InP and GaAs

The calculated concentrations of defects in n-type material ( $n = 10^{18} \text{cm}^{-3}$ ) at a constant group V pressure ( $10^{-5} \text{mbar}$ ) at temperatures suitable for MBE are shown in Figures 5-2,3,4 and 5. The results indicate that the most common native point defects in both n-InP and n-GaAs grown at typical MBE conditions are anion antisites  $\text{P}_{\text{In}}$  and  $\text{As}_{\text{Ga}}$ . However, the calculated concentrations of these antisites at low temperatures are unrealistically high indicating that the enthalpies of formation for these defects calculated by Van Vechten and Kraut & Harrison are too low, at least at the low temperatures used for MBE.

The density of neutral vacancies is seen to be very low, but in contrast, ionised cation vacancies should be present at relatively high concentrations. Neutral antistructures should not occur in InP but they may be present in GaAs.

The defect concentrations were also calculated along the liquidus up to the melting point in intrinsic material (Figures 5-6,7,8). The most common defects would appear to be antisites in the various charge

states, except  $\text{Ga}_{\text{As}}^{2-}$ , which is present in only very low concentrations. Because of the large difference in the covalent radii of In and P the concentration of  $\text{In}_\text{P}$  antisites can be expected to be very low. The calculated concentration of  $\text{In}_\text{P}$  is high, probably due to an underestimate for the enthalpy of formation, caused either by an error in the enthalpies calculated by Van Vechten, and Kraut and Harrison, or more likely incorrect values of ionisation enthalpies used for calculating the formation enthalpy of neutral antisites.

## 5.7 Conclusions

The virtual formation reactions of defects in a binary III-V compound can be written as physically realisable reactions if the surface atoms are taken explicitly into account. Such a formulation allows the "virtual" enthalpies and entropies of formation to be determined unequivocally to form a self-consistent system. The virtual free energy of incorporation of the group V element from the vapour phase is calculated correctly from the vapour pressure of the element over the compound during the growth.

A review of the available literature reveals that little experimental data of the virtual enthalpies and entropies of formation exists. However, good theoretical calculations for the enthalpies of formation of vacancies and antisites have been published. In particular, the enthalpies of formation of antisites and neutral antistructures from the two completely different model by Van Vechten [20], and Kraut and Harrison [21] are in good agreement.

For the entropies of formation neither experimental nor theoretical data is available and their assumed

values are almost pure speculation. The entropies of ionisation can be estimated as shown by Van Vechten [20].

A larger body of both experimental and theoretical data for the ionisation levels of native defects exists. The theoretical models are not sufficiently accurate to provide exact values of the ionisation enthalpies, whereas the utility of the experimental data is limited by the fact that it is difficult to identify the defects correctly, and that most native defects are in fact complexes rather than isolated point defects.

Considering the sparsity of reliable thermodynamic data, the self-consistent calculation of defect concentrations in III-V compounds is an overambitious goal. However, by taking the Fermi-level of the crystal as an adjustable parameter, the thermodynamic model for the calculation of the defect concentrations can be formulated without any need for self-consistency in regard of the charge neutrality condition. Moreover, by choosing the defect formation reactions so that only the group V element in the vapour phase, and the group III and V elements on their proper sites in the crystal are involved in the reaction, the concentrations of all isolated point defects can be calculated independently of each other, i.e. only those defects need to be included which are of interest or for which the thermodynamic data exists.

The best available data suggests that anion antisites are the most common native defects in InP and GaAs grown at typical MBE temperatures whilst ionised cation vacancies should also occur at relatively high concentrations.

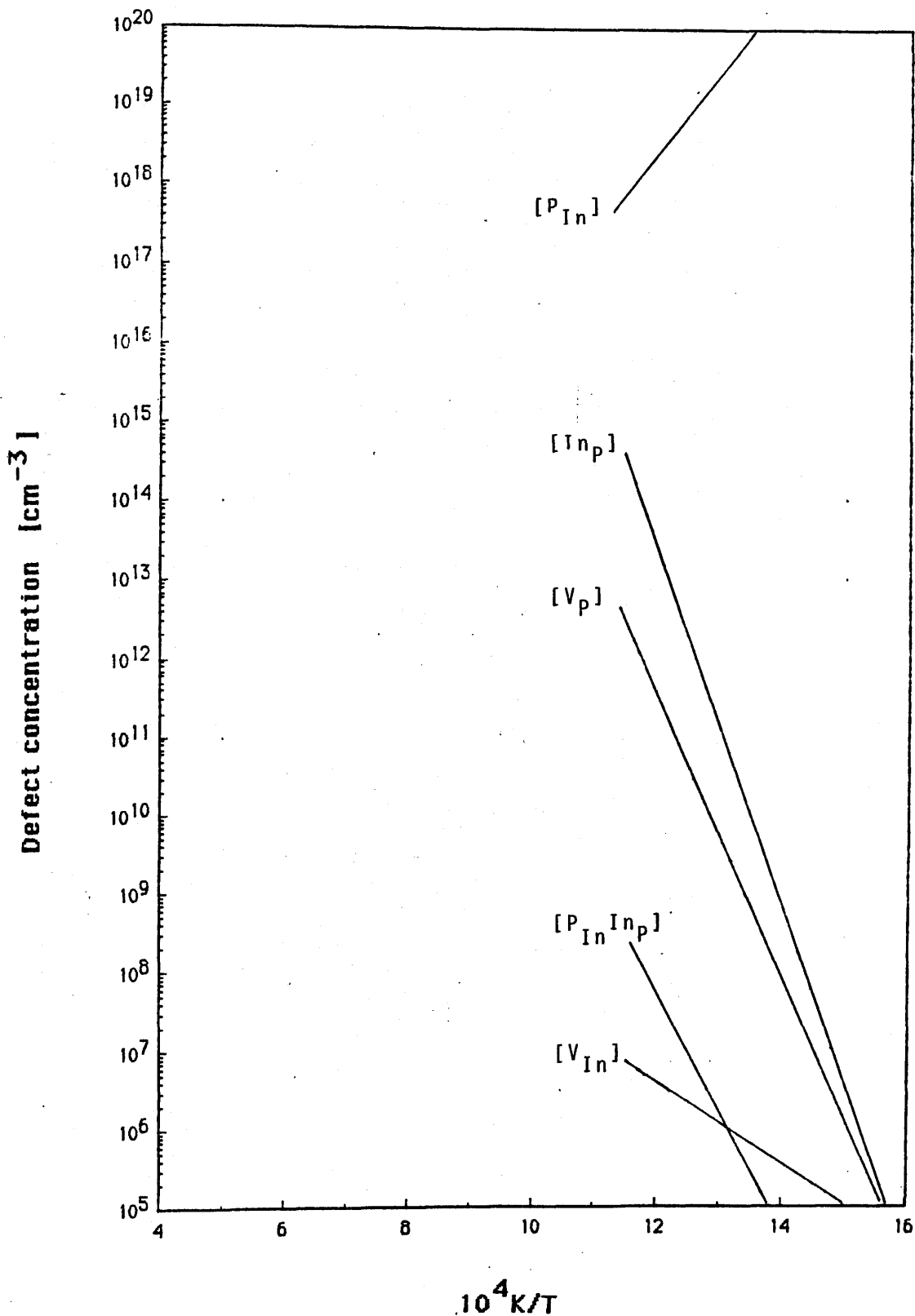


Figure (5-2). Calculated concentrations of neutral defects in InP plotted against the inverse of the temperature.  $p(P_2) = 10^{-8}$  bar.

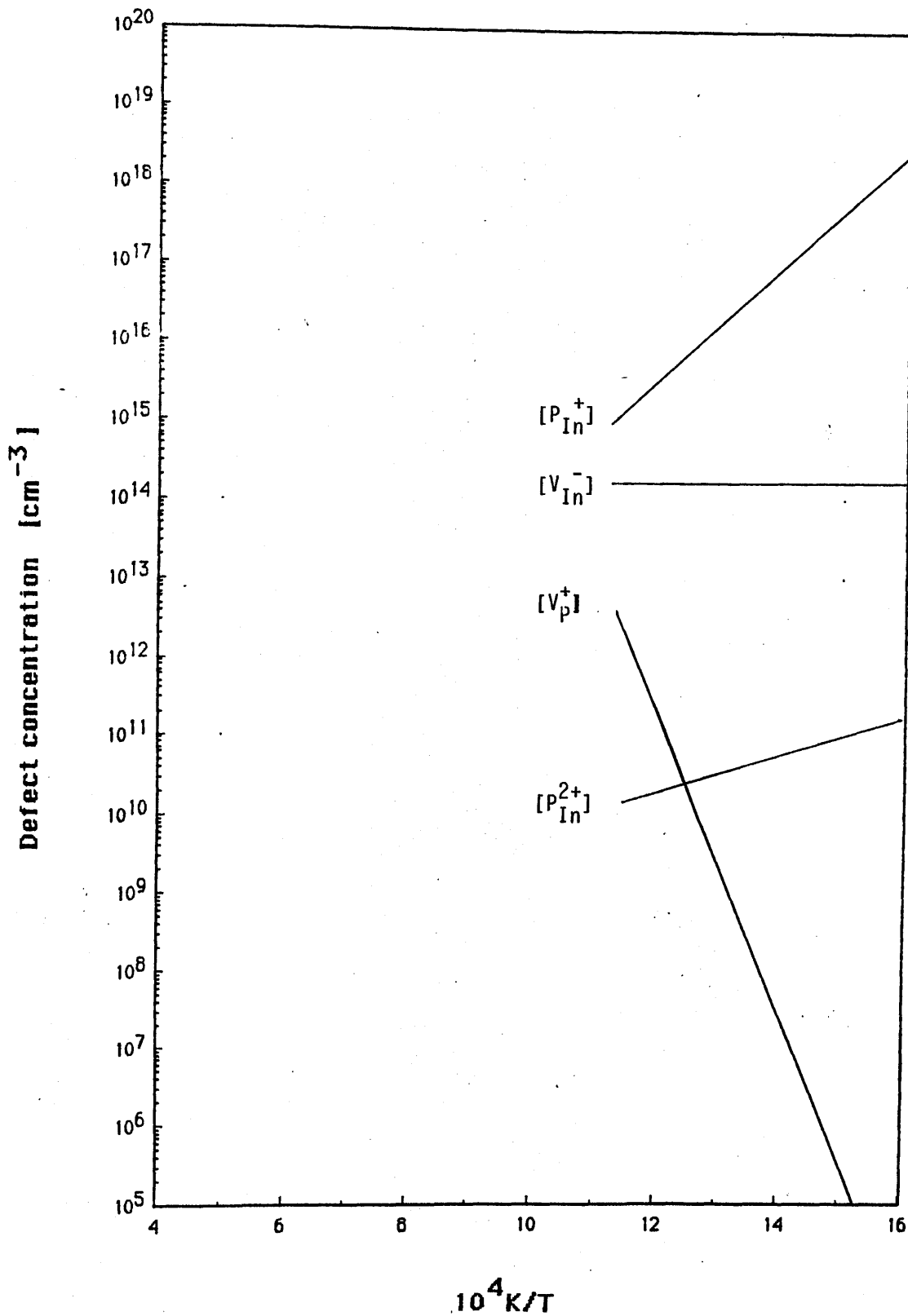


Figure (5-3). Calculated concentrations of ionised defects in InP plotted against the inverse of the temperature.  $p(P_2) = 10^{-8}$  bar,  $n = 10^{18}$  cm<sup>-3</sup>.

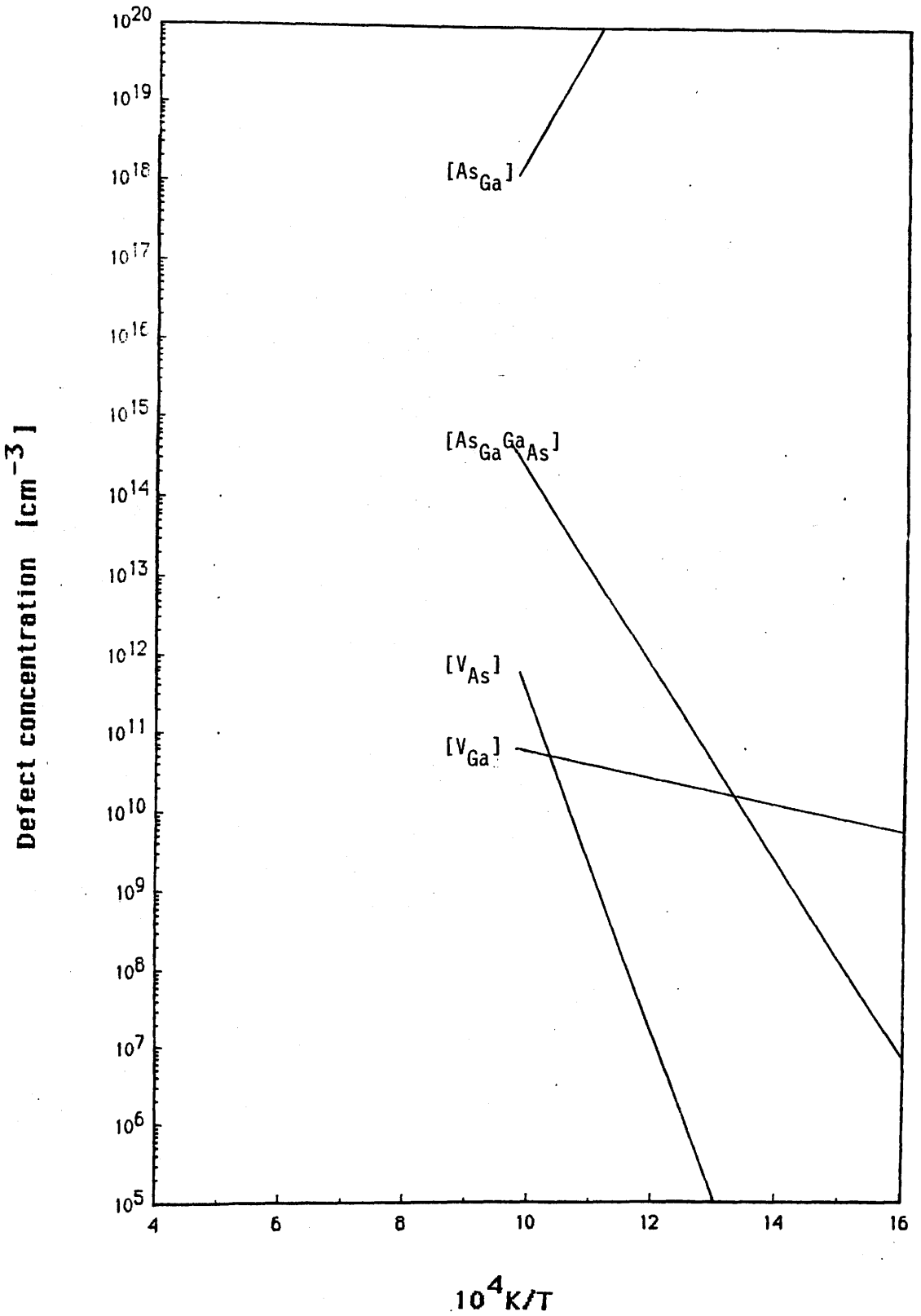


Figure (5-4). Calculated concentrations of neutral defects in GaAs plotted against the inverse of the temperature.  $p(\text{As}_2) = 10^{-8}$  bar.

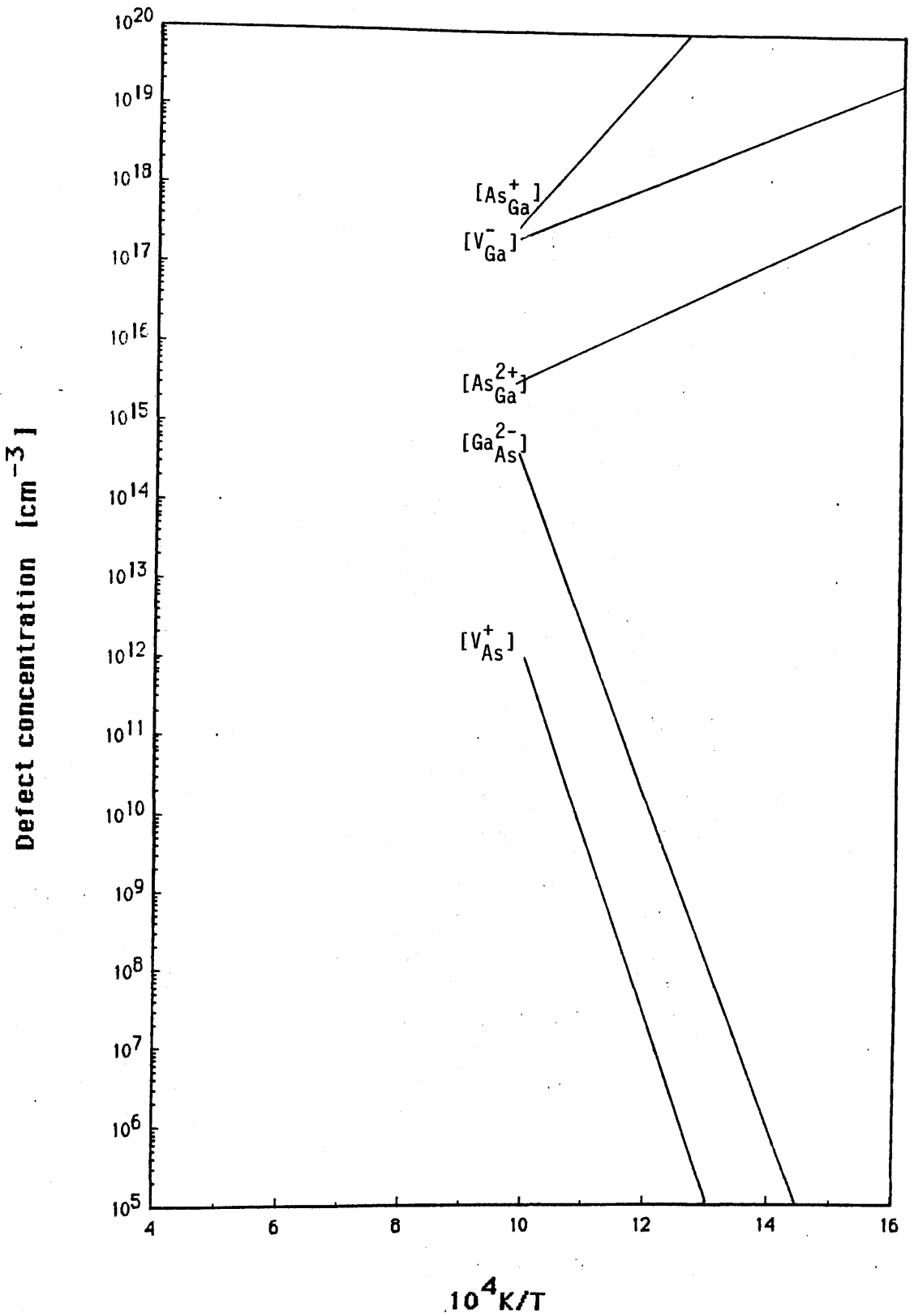


Figure (5-5). Calculated concentrations of ionised defects in GaAs plotted against the inverse of the temperature.  $p(\text{As}_2) = 10^{-8}$  bar,  $n = 10^{18} \text{ cm}^{-3}$ .

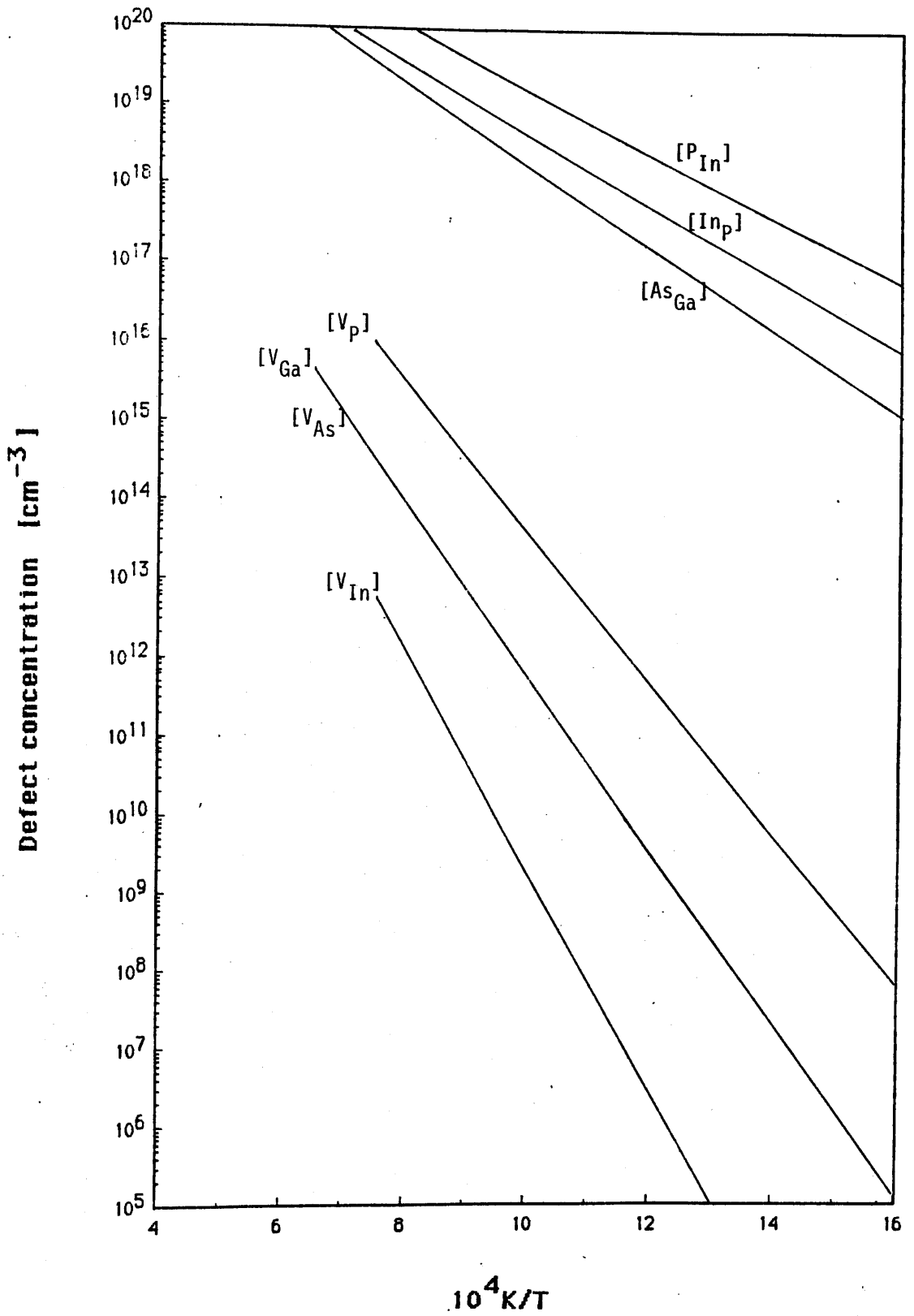


Figure (5-6). Calculated concentrations of neutral defects in InP and GaAs along the liquidus.

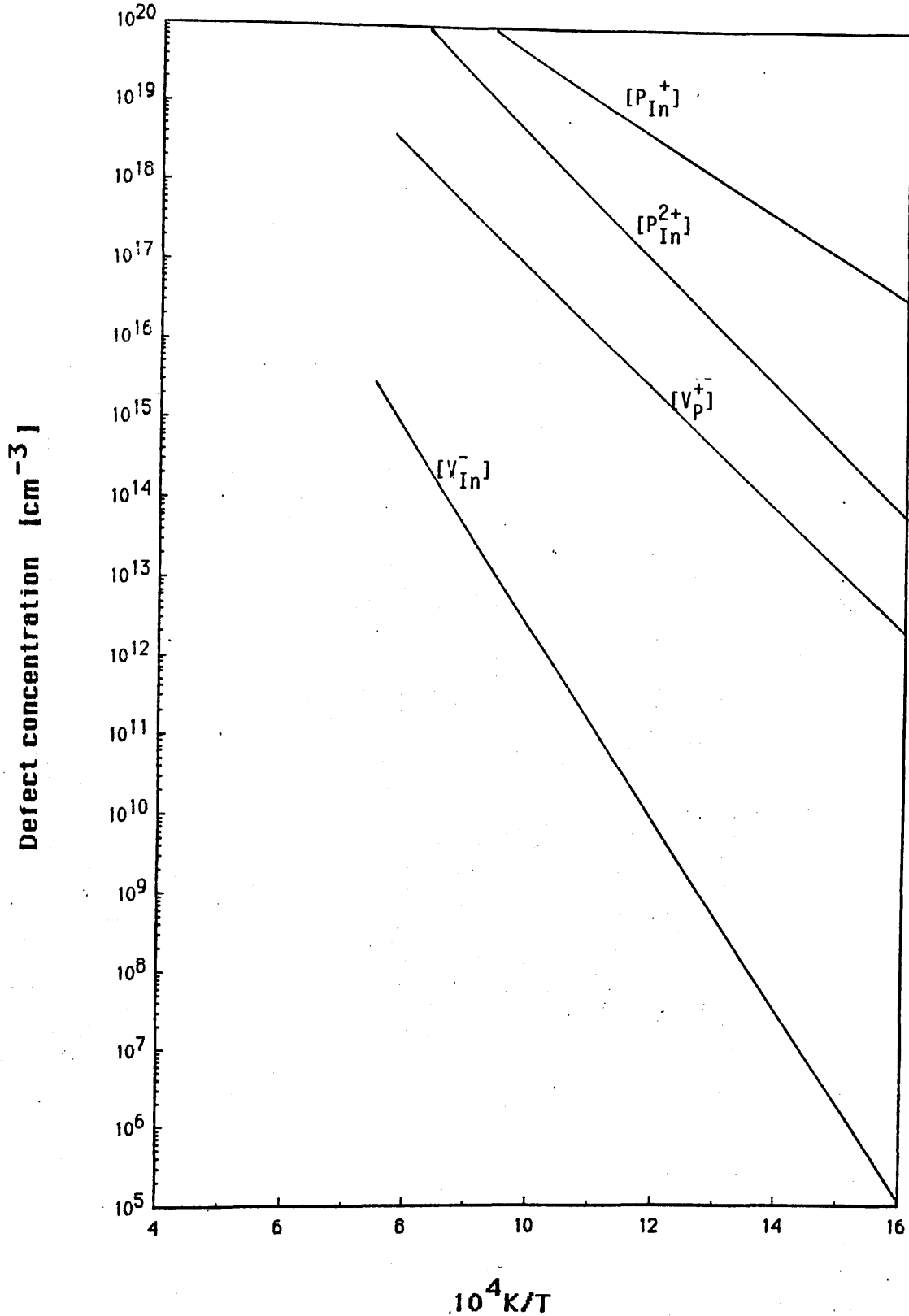


Figure (5-7). Calculated concentrations of ionised defects in InP along the liquidus (intrinsic material).

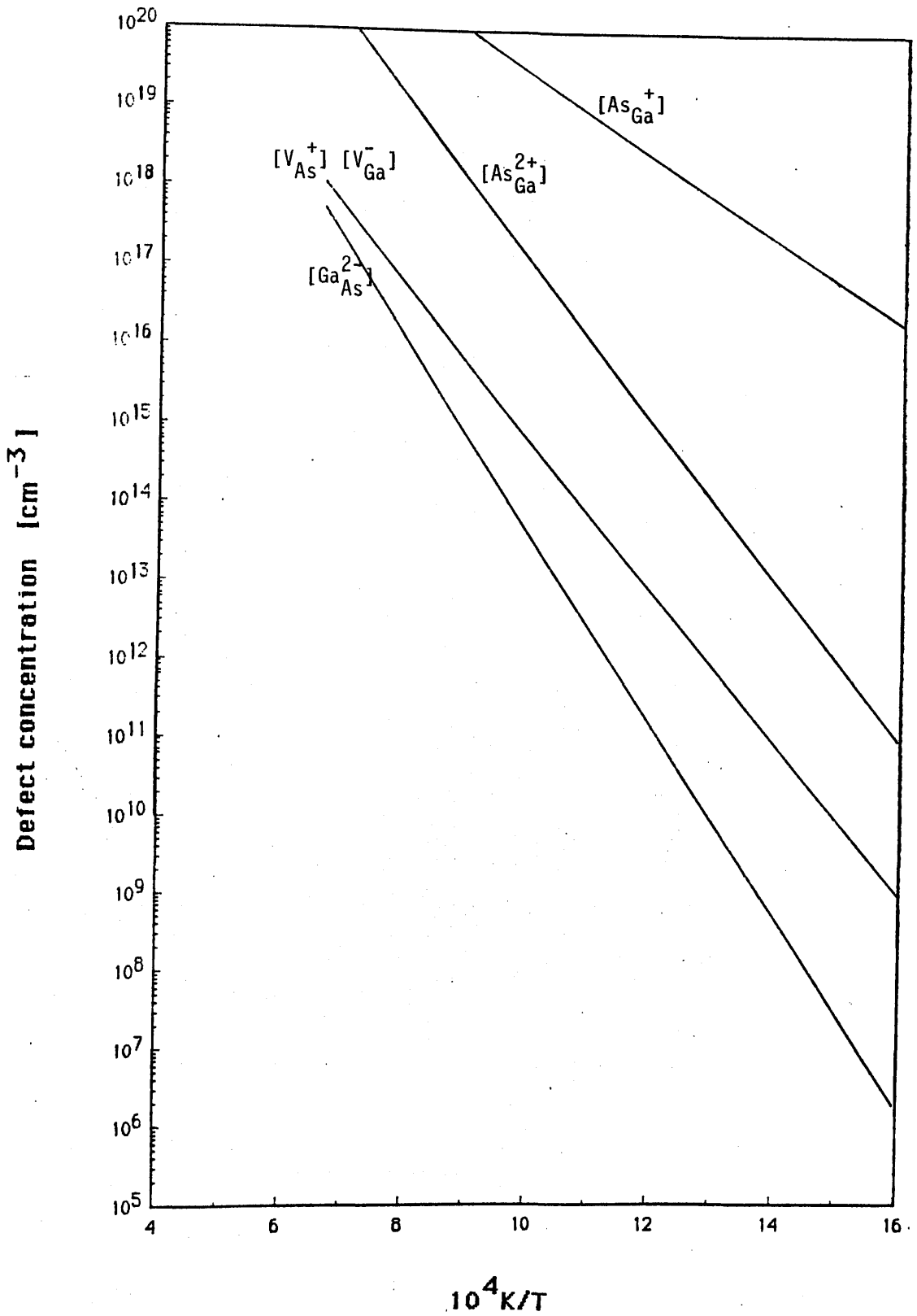


Figure (5-8). Calculated concentrations of ionised defects in GaAs along the liquidus (intrinsic material).

		H/eV	S/k <sub>B</sub>
$\frac{1}{2}P_2(g) \leftrightarrow P_P$	(a)	-1.64	-13.25
$0 \leftrightarrow V_{In}$	(b)	2.74	$2 \pm 2$
$0 \leftrightarrow V_P$	(c)	1.87	$2 \pm 2$
$0 \leftrightarrow V_{In}V_P$	(d)	3.84	$2 \pm 2$
$V_P \leftrightarrow V_P^+ + e^-$	(e)	0.34	4.9
$V_{In} \leftrightarrow V_{In}^- + h^+$	(f)	0.34	4.9
$P_P \leftrightarrow P_{In}$	(g)	0.8	$2 \pm 2$
$P_{In} \leftrightarrow P_{In}^+ + e^-$	(h)	0.9	4.9
$P_{In}^+ \leftrightarrow P_{In}^{2+} + e^-$	(i)	1.2	4.9
$In_{In} \leftrightarrow In_P$	(j)	0.9	$2 \pm 2$
$In_{In} + P_P \leftrightarrow P_{In}In_P$	(k)	3.08	$10.3 \pm 8.9$

Table 5-5. The enthalpies and entropies of the virtual formation reactions and ionisation reactions in InP.

		H/eV	S/k <sub>B</sub>
$\frac{1}{2}\text{As}_2(\text{g}) \leftrightarrow \text{As}_{\text{As}}$	(a)	-1.92	-13.27
$0 \leftrightarrow V_{\text{Ga}}$	(b)	2.31	$2 \pm 2$
$0 \leftrightarrow V_{\text{As}}$	(c)	2.31	$2 \pm 2$
$0 \leftrightarrow V_{\text{Ga}}V_{\text{As}}$	(d)	3.64	$2 \pm 2$
$V_{\text{As}} \leftrightarrow V_{\text{As}}^+ + e^-$	(e)	0.36	6.3
$V_{\text{Ga}} \leftrightarrow V_{\text{Ga}}^- + h^+$	(f)	0.36	6.3
$\text{As}_{\text{As}} \leftrightarrow \text{As}_{\text{Ga}}$	(g)	1.0	$2 \pm 2$
$\text{As}_{\text{Ga}} \leftrightarrow \text{As}_{\text{Ga}}^+ + e^-$	(h)	0.75	6.3
$\text{As}_{\text{Ga}}^+ \leftrightarrow \text{As}_{\text{Ga}}^{2+} + e^-$	(i)	1.0	6.3
$\text{Ga}_{\text{Ga}} \leftrightarrow \text{Ga}_{\text{As}}^{2-} + 2h^+$	(j)	3.34	$14.6 \pm 2$
$\text{Ga}_{\text{Ga}} + \text{As}_{\text{As}} \leftrightarrow \text{As}_{\text{Ga}}\text{Ga}_{\text{As}}$	(k)	2.57	$11.7 \pm 10.3$

Table 5-6. The enthalpies and entropies of the virtual formation reactions and ionisation reactions in GaAs.

InP:

$$\begin{aligned}K_{25a} &= K_a K_b = \exp(-11.25 - 1.1\text{eV}/k_B T) \\K_{25b} &= K_c / K_a = \exp(15.25 - 3.51\text{eV}/k_B T) \\K_{25c} &= K_e = \exp(4.9 - 0.34\text{eV}/k_B T) \\K_{25d} &= K_f^2 = \exp(4.9 - 0.34\text{eV}/k_B T) \\K_{25e} &= K_a^2 K_g = \exp(-24.5 + 2.45\text{eV}/k_B T) \\K_{25f} &= K_h = \exp(4.9 - 0.9\text{eV}/k_B T) \\K_{25g} &= K_i = \exp(4.9 - 1.2\text{eV}/k_B T) \\K_{25h} &= K_j / K_a^2 = \exp(28.5 - 4.18\text{eV}/k_B T) \\K_{25i} &= K_d = \exp(2 - 3.84\text{eV}/k_B T) \\K_{25j} &= K_k = \exp(10.3 - 3.05\text{eV}/k_B T)\end{aligned}$$

GaAs:

$$\begin{aligned}K_{25a} &= K_a K_b = \exp(-11.3 - 0.39\text{eV}/k_B T) \\K_{25b} &= K_c / K_a = \exp(15.3 - 4.21\text{eV}/k_B T) \\K_{25c} &= K_e = \exp(6.3 - 0.36\text{eV}/k_B T) \\K_{25d} &= K_f^2 = \exp(6.3 - 0.36\text{eV}/k_B T) \\K_{25e} &= K_a^2 K_g = \exp(-24.5 + 2.84\text{eV}/k_B T) \\K_{25f} &= K_h = \exp(6.3 - 0.75\text{eV}/k_B T) \\K_{25g} &= K_i = \exp(6.3 - 1.0\text{eV}/k_B T) \\K_{25i} &= K_d = \exp(2 - 3.64\text{eV}/k_B T) \\K_{25j} &= K_k = \exp(11.7 - 2.57\text{eV}/k_B T) \\K_{25k} &= K_j / K_a^2 = \exp(41.1 - 7.2\text{eV}/k_B T)\end{aligned}$$

Table 5-7. The equilibrium constants of the defect formation reactions (5-25) for InP and GaAs.

## 5.8 References

- [1] R.M.Logan and D.T.J. Hurle, *J.Phys.Chem.Solids* 32 (1971) 1739.
- [2] D.T.J. Hurle, *J.Phys.Chem.Solids* 40 (1979) 613.
- [3] G.A.Baraff and M.Schlueter, *Phys.Rev.Lett.* 55 (1985) 1327.
- [4] G.M.Blom, *J.Cryst.Growth* 36 (1976) 125.
- [5] R.L.S.Devine, PhD Thesis, University of Glasgow 1985.
- [6] F.A.Kroeger, *Ann.Rev.Mater.Sci.* 7 (1977) 449.
- [7] R.Heckingbottom, "The Application of Thermodynamics to Molecular Beam Epitaxy" in "Molecular Beam Epitaxy and Heterostructures", ed.s L.L.Chang and K.Ploog, Martinus Nijhoff Publishers (Dordrecht, 1985), p 71.
- [8] R.Heckingbottom and G.J.Davies, *J.Cryst.Growth* 50 (1980) 644.
- [9] D.A.Andrews, R.Heckingbottom and G.J.Davies, *J.Appl.Phys.* 54 (1983) 4421.
- [10] D.A.Andrews, M.Y.Kong, R.Heckingbottom and G.J.Davies, *J.Appl.Phys.* 55 (1984) 841.
- [11] D.T.J.Hurle, *J.Phys.Chem.Solids* 40 (1979) 627.
- [12] D.T.J.Hurle, *J.Phys.Chem.Solids* 40 (1979) 639.
- [13] D.T.J.Hurle, *J.Phys.Chem.Solids* 40 (1979) 647.
- [14] F.A.Kroger, F.H.Stieltjes and H.J.Vink, *Philips Res. Repts.* 14 (1959) 557.
- [15] J.A.Van Vechten, *J.Electrochem.Soc.* 122 (1975) 423.
- [16] J.A.Van Vechten, Chapter 1 in "Handbook on Semiconductors, vol 3", ed. S.P.Keller, North Holland, Amsterdam 1980.
- [17] M.B.Panish, *J.Cryst.Growth* 27 (1974) 6.
- [18] R.F.C.Farrow, *J.Phys.D* 7 (1974) 2436.

- [19] C.Pupp, J.J.Murray and R.F.Pottie, J.Chem. Thermodynamics 6 (1974) 123.
- [20] Thermodynamic Properties of the Elements, Advances in Chemistry Series 18 (American Chemical Society, Washington DC 1956).
- [21] E.A.Kraut and W.A.Harrison, J.Vac.Sci.Technol. B2 (1984) 409.
- [22] E.A.Kraut and W.A.Harrison, Private communication.
- [23] F.A.Kroger, "The Chemistry of Imperfect Crystals", vol. 2, 2nd ed., North Holland New York 1974, p.83.
- [24] M.Lannoo, J.Phys.C 17 (1984) 3137.
- [25] J.Van Der Rest and P.Pecheur, Physica 116B (1983) 121.
- [26] S.Loualiche, A.Nouailhat, G.Guillot and M.Lannoo, Proc. of the 13th International Conference on Defects in Semiconductors, Coronado 1984, ed.s L.C.Kimerling and J.M.Parsey,Jr (The Metallurgical Society of AIME, 1984) p.967.
- [27] L.A.Hemstreet, Physica 116B (1983) 116.
- [28] P.J.Lin-Chung and T.L.Reinecke, J.Vac.Sci.Technol. 19 (1981) 443.
- [29] D.N.Talwar and C.S.Ting, Phys.Rev.B 25 (1982) 2660.
- [30] J.Beyer, P.Kruger, A.Mazur and J.Pollman, J.Vac.Sci.Technol. 21 (1982) 358.
- [31] J.Bernholc and S.T.Pantelides, Phys.Rev. B 18 (1978) 1780.
- [32] G.Dlubek, O.Bruenner, F.Plazaola and P.Hautojaervi, J.Phys.C 19 (1986) 331.
- [33] H.J.von Bardeleben, Solid State Commun. 57 (1986) 137.
- [34] H.J.von Bardeleben, D.Stievenard and J.C.Bourgoin, Appl.Phys.Lett 47 (1985) 970.
- [35] J.Lagowski, Proc. of the 13th International Conference on Defects in Semiconductors, Coronado 1984, ed.s L.C.Kimerling and J.M.Parsey,Jr (The Metallurgical Society of AIME, 1984) p.73.

- [36] M.Kaminska, M.Skowronski and W.Kuszeko,  
Phys.Rev.Lett. 55 (1985) 2204.
- [37] K.Elliott, R.T.Chen, S.G.Greenbaum and R.J.Wagner,  
Appl.Phys.Lett. 44 (1984) 907.
- [38] M.Deiri, K.P.Homewood and B.C.Cavenett, J.Phys.C  
17 (1984) L627.
- [39] E.R.Weber and J.Schneider, Physica 116B (1983)  
398.
- [40] M.Baeumler, U.Kaufmann and J.Windscheif,  
Appl.Phys.Lett. 46 (1985) 781.
- [41] J.Lagowski, D.G.Lin, T.-P.Chen, M.Skowronski and  
H.C.Gatos, Appl.Phys.Lett. 47 (1985) 929.
- [42] B.K.Meyer and J.M.Spaeth, J.Phys.C 18 (1985) L99.
- [43] T.Figielski, E.Kaczmarek and T.Wosinski, Appl.Phys.  
A38 (1985) 253.
- [44] J.D.Dow and R.E.Allen, J.Vac.Sci.Technol. 20 (1982)  
659.
- [45] M.Deiri, A.Kana-ah, B.C.Cavenett, T.A.Kennedy and  
N.D.Wilsey, J.Phys.C 17 (1984) L793.
- [46] B.C.Cavenett, A.Kana-ah, M.Deiri, T.A.Kennedy and  
N.D.Wilsey, J.Phys.C 18 (1985) L473.
- [47] P.W.Yu, W.C.Mithcel, M.G.Mier, S.S.Li and  
W.L.Wang, Appl.Phys.Lett. 41 (1982) 532.
- [48] P.W.Yu and D.C.Reynolds, J.Appl.Phys. 53 (1982)  
1263.
- [49] T.Hiramoto, Y.Mochizuki, T.Saito and T.Ikoma,  
Japan.J.Appl.Phys. 24 (1985) L921.
- [50] S.G.Bishop, B.V.Shanabrook and W.J.Moore,  
J.Appl.Phys. 56 (1984) 1785.
- [51] P.W.Yu, Phys.Rev.B 27 (1983) 7779.
- [52] Z-G.Wang, L-].Ledebor and H.G.Grimmeiss, J.Phys.C  
17 (1984) 259.
- [53] W.Poetz and D.K.Ferry, Phys.Rev. B 29 (1984) 5687.
- [54] Y.P.Varshni, Physica 39 (1967) 149.
- [55] C.D.Thurmond, J.Electrochem.Soc. 122 (1975)  
1133.

[56] B.V.Shanabrook, W.J.Moore and S.G.Bishop,  
J.Appl.Phys. 59 (1986) 2535.

## CHAPTER 6

### SILICON MIGRATION IN MODULATION DOPED $\text{Al}_x\text{Ga}_{1-x}\text{As}/\text{GaAs}$ HETEROJUNCTIONS

#### 6.1 Introduction

At low temperatures the scattering caused by ionised impurities is the dominant mechanism limiting the mobility of carriers in a doped semiconductor. It was first proposed by Esaki and Tsu [1] that ionised impurity scattering could be minimised by using a selectively doped heterojunction structure. In a selectively - or modulation - doped heterojunction the ionised donors are located in the wide band gap material ( $\text{Al}_x\text{Ga}_{1-x}\text{As}$ ). The free electrons diffuse across the heterojunction into the narrower band gap material (GaAs) where they are confined in the potential well formed by the conduction band discontinuity at the heterojunction and the band bending of GaAs. The lateral dimension of the potential well is so small that the electrons are only free to move in the two dimensions parallel to the heterojunction, forming a two dimensional electron gas (2DEG). In a similar way, if the AlGaAs layer is doped with acceptor impurities, a two dimensional holegas is formed at the top of the valence band. Mobility enhancement in a modulation doped AlGaAs/GaAs heterostructure was first obtained by Dingle et al. [2]. By separating the doped AlGaAs region from the interface with an undoped AlGaAs spacer layer the impurity scattering can be further reduced [3],[4]. The mobility of electrons in the 2DEG increases with the spacer layer thickness  $d$  [4],[5],[6] reaching a peak at some value of  $d$ , which can be up to  $800\text{\AA}$  in high purity material [6].

The modulation doped heterojunction is called "normal" when the AlGaAs layer is grown on top of the undoped GaAs layer. If the AlGaAs layer is grown first and the 2DEG is formed in GaAs on top of AlGaAs, the structure is referred to as "inverted". Ideally, of course, the transport properties of normal and inverted structures should be identical. In practice, however, normal structures have superior properties, the highest mobility reported so far being  $3.1 \times 10^6 \text{ cm}^2/\text{Vs}$  [6], over an order of magnitude higher than the best mobility achieved in an inverted structure [7].

There are believed to be three principal reasons for the inferior performance of the inverted structure: interface roughness, impurity buildup near the interface and Si migration from the doped AlGaAs layer. In this work, however, evidence is presented that the mobility may be limited by the strong localisation of the 2D electrons.

### 6.1.2 Interface roughness

It has been found that GaAs/AlGaAs multiple quantum well (MQW) structures and AlGaAs layers with  $x > 0.3$  have wavy surfaces when grown at intermediate temperatures  $T_S = 630-690^\circ\text{C}$  [8],[9] with a maximum roughness at about  $T_S = 650^\circ\text{C}$  and Al mole fraction  $x = 0.5$  [11],[12]. The surface roughening can be reduced by using a lower growth rate [12], a low ( $R=2.1$ ) or high ( $R=11$ )  $\text{As}_4$ :Ga flux ratio [9],[12], thermally cracked  $\text{As}_2$  instead of  $\text{As}_4$  [13], a lower aluminium concentration, a growth temperature outside the 'forbidden' range [8],[9],[10] or a GaAs substrate misoriented from the (100) plane [14]. No surface roughness in this temperature range has been observed for either GaAs or AlAs.

Among the causes proposed to explain the surface roughening are inhomogeneous nucleation [11] due to the low surface mobility of Al compared to Ga [15], an As deficiency of the AlGaAs layer resulting from the short lifetime of  $As_4$  on the GaAs surface at high temperatures [13], Ga segregation [16], and the accumulation of a nucleation inhibiting impurity such as carbon on the growing surface [17].

### 6.1.3 Impurity accumulation

GaAs/AlGaAs single and multiquantum well structures have shown weak extrinsic photoluminescence due to neutral acceptors, probably carbon [18]. It is believed that carbon segregates on the surface during the growth of the ternary layer, degrades the smoothness of the interface because of its growth inhibiting nature and is finally incorporated in the GaAs layer where its solubility is higher [12],[17],[19],[20],[21]. DLTS analysis has shown qualitatively that impurities or traps are confined in a thin layer of GaAs near the interface [10]. The use of a superlattice buffer layer or GaAs quantum wells improves the purity of AlGaAs because C and Si are trapped near the first inverted interface [17],[22].

### 6.1.4 Silicon migration

There is good experimental evidence to suggest that a major reason for the inferiority of the inverted structure - at least at elevated temperatures - is caused by the migration of Si atoms from the doped AlGaAs layer towards the quantum well. Sasa et al. [23] measured the mobility of the 2DEG as a function of the quantum well width in structures which had a doped

AlGaAs layer grown on both sides of the well at  $680^{\circ}\text{C}$ . Two different kinds of 2DEG were found to exist in the well, a high mobility 2DEG near the normal interface and a low mobility 2DEG near the inverted interface. The decreased mobility was explained by assuming Si-migration through the 60Å undoped spacer layer.

The best evidence for Si migration has been obtained by Inoue et al [25],[24] who grew GaAs single quantum wells which were doped symmetrically on both sides. The 2DEG mobility depended on the growth temperature  $T_s$  reaching a maximum at  $530^{\circ}\text{C}$  and decreasing considerably when  $T_s = 600^{\circ}\text{C}$ . This reduction was supposed to be due to the diffusion or segregation of Si from the bottom n-AlGaAs layer. Inoue et al. [25] also used a 150Å superlattice in the spacer layer to improve the inverted interfaces. Samples grown at  $530^{\circ}\text{C}$  had high mobilities ( $\mu_{77\text{K}} = 120000\text{cm}^2/\text{Vs}$ ) but a sample grown at  $630^{\circ}\text{C}$  showed a much degraded mobility and a high electron concentration ( $2.3 \times 10^{12}\text{cm}^{-2}$ ). The Si distribution was measured by secondary ion mass spectrometry (SIMS). No evidence of Si migration was seen in the low temperature sample but in the sample grown at  $630^{\circ}\text{C}$  Si was seen to accumulate near the surface. Also Si had clearly migrated into the well from the bottom doped layer. Therefore the superlattice did not prevent Si migration.

Whether the Si migration is caused by surface segregation during the growth of the layer or subsequent diffusion is not known. Heiblum et al. found from SIMS measurements that Si tends to accumulate near the surface [26],[27]. This accumulation is not necessarily proof of surface segregation. It can be an artefact of the SIMS measurement or caused by the diffusion of dopant atoms to the depletion zone created by the pinning of the Fermi level at the surface.

When AlGaAs is doped with silicon below  $2 \times 10^{18} \text{ cm}^{-3}$  Si is incorporated only as a donor but at higher doping levels the free electron concentration saturates [28]. This saturation effect may be due to Si being incorporated with equal probability on both donor and acceptor sites, possibly forming Si-Si pairs. However, Maguire et al. have found evidence that  $\text{Si}_{\text{Ga}}$  donors in highly doped GaAs are primarily compensated by complexes of silicon and a native defect, probably gallium vacancy [29]. A similar compensation mechanism could also be operative in AlGaAs.

At the high doping levels of  $> 2 \times 10^{18} \text{ cm}^{-3}$  the diffusion coefficient of silicon is also high and the diffusion of silicon can disorder AlAs-GaAs superlattices [28],[30]. SIMS studies of silicon in the low doping regime have shown that Si-migration is slightly asymmetric being faster towards the growth direction [28]. In highly doped AlGaAs no asymmetry has been observed.

#### 6.1.5 The improvement of inverted heterostructures

Several techniques have been used to improve the quality of the inverted AlGaAs/GaAs interface [31]. To reduce surface roughening and impurity accumulation growth at a high temperature ( $T_s = 700^\circ\text{C}$ ), a slow growth rate, the use of  $\text{As}_2$  instead of  $\text{As}_4$ , superlattice or MQW buffer layers or a thin GaAs prewell have been utilised. Drummond et al. [7] used a 150Å thick AlGaAs/GaAs three period superlattice in place of the undoped AlGaAs spacer layer and obtained 10K mobilities of up to  $256000 \text{ cm}^2/\text{Vs}$ . They attributed this improvement to the relief of strain caused by the superlattice. It has been observed, however, that a superlattice is not effective in preventing Si migration at high doping levels due to the high diffusion constant [24],[28].

Drummond et al. have investigated the Hall mobility of inverted AlGaAs/GaAs heterostructures as a function of the growth temperature [32]. They found that maximum mobilities ( $8000 \text{ cm}^2/\text{Vs}$ ) were obtained at  $T_s=700^\circ\text{C}$ . Mobilities dropped sharply for  $T_s < 680^\circ\text{C}$ . This should be contrasted with the behaviour of the normal structures which exhibit maximum mobilities when grown at temperatures between  $620\text{-}650^\circ\text{C}$  and much lower mobilities at higher temperatures [5],[6],[10]. Harris and Foxon, however, have shown that by reducing the silicon concentration in the doped layer to  $4 \times 10^{17} \text{ cm}^{-3}$  the critical temperature for 2DEG mobility degradation was increased to above  $680^\circ\text{C}$  [33]. This is believed to be due to the much lower diffusion coefficient of silicon in the low doping regime [28].

## 6.2 On the purpose of the experiment

The goal of the experiments described here was to develop a test structure which would allow silicon migration to be distinguished from the other effects influencing the mobility of the 2DEG in both normal and inverted structures, and to determine whether the surface segregation or the diffusion of silicon is the dominant migration mechanism.

It is difficult to grow normal and inverted interfaces which are of comparable quality, therefore it is desirable for the 2DEG to see both interfaces simultaneously. This can be accomplished by using a thin quantum well in which the electron wave function is symmetrically confined by both interfaces.

As shown in Figure (6-1) the complete structure consists of a thick undoped GaAs layer, a  $0.2 \mu\text{m}$   $\text{Al}_x\text{Ga}_{1-x}\text{As}$  buffer layer, a  $400\text{\AA}$  thick doped AlGaAs layer and an undoped AlGaAs spacer, a  $100\text{\AA}$  thick GaAs quantum well, an undoped AlGaAs spacer, another doped  $400\text{\AA}$  AlGaAs

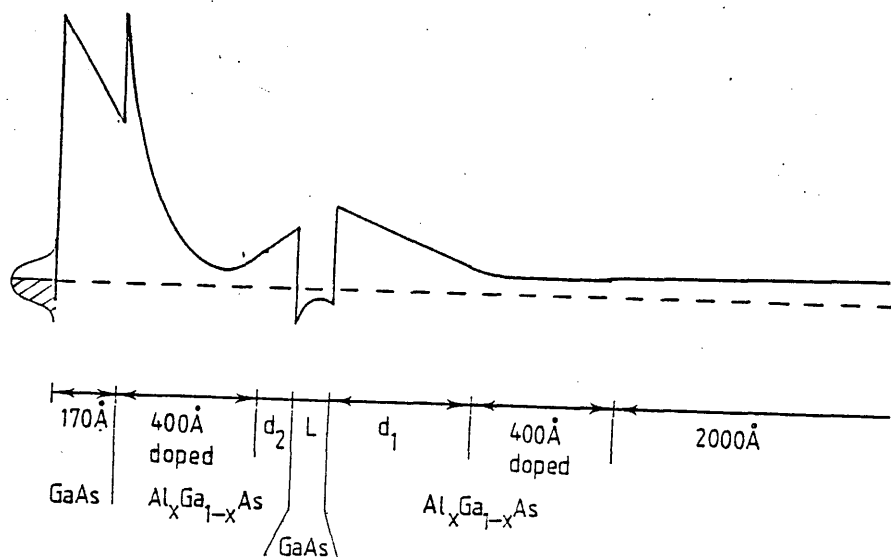


Figure (6-1). A schematic energy band diagram of the test structure.

Normal structure:  $d_1 = 400\text{\AA}$ ,  $d_2 = 100\text{\AA}$ .

Inverted structure:  $d_1 = 100\text{\AA}$ ,  $d_2 = 400\text{\AA}$ .

layer and a  $170\text{\AA}$  thick undoped GaAs contact layer.

To prevent the quantum well from being excessively distorted by the electric fields, doped AlGaAs layers were grown on both sides of the well. A fully symmetric structure could not be used because the purpose was to investigate the difference in the silicon migration in normal and inverted structures. Therefore the "normal" structure was grown with a thick undoped spacer layer on the substrate side of the well and a thin spacer on the other side (Figure 6-1). In the "inverted" structure the thicknesses of the spacers were inverted compared to the normal structure. It was assumed that the well was thin enough to prevent the asymmetric doping from distorting the well significantly. As will be seen later this assumption is not quite correct.

It was originally envisaged to grow pairs of normal and inverted samples at several different growth temperatures ( $T_g$ ) to find out the effect of varying  $T_g$  on the mobility of the 2DEG. Due to the usual practical difficulties associated with MBE only one pair of samples was grown successfully at a low temperature of  $600^\circ\text{C}$ . These samples were subsequently annealed at higher temperatures of up to  $700^\circ\text{C}$  to see whether post-growth silicon diffusion occurred. The samples were characterised by measuring the electron mobilities at 4.2K.

In the following, after the experimental methods have been described, the 2DEG density in the well and the distortion of the quantum well due to the asymmetric doping profile are calculated in Sections 6.4 and 6.5. In Section 6.6 the theoretical dependence of mobility on the 2DEG density for each scattering mechanism is calculated. These results are used in Section 6.7 for explaining the experimental results, and to determine the probable scattering mechanism limiting the mobility in the single quantum well samples.

### 6.3 Experimental

The samples were grown at Philips Research Laboratories in a modified commercial MBE machine (Varian 360) which has been described elsewhere [34]. The 360 was equipped with computerised shutter and temperature control allowing automatic growth of complicated structures. A graphite  $As_4$  source and pBN Al and Ga cells were used. The undoped semi-insulating GaAs substrates were cleaned with solvents and etched for 3 minutes in a 3:1:1 ( $H_2SO_4:H_2O_2:H_2O$ ) solution prior to mounting on Mo-blocks with an In-Ga eutectic alloy. The substrates were heat cleaned under an  $As_4$  flux. The substrate temperature was measured with an Ircon pyrometer. The oxide removal temperature was assumed to be  $600^\circ C$  and used as a reference point to calibrate the emissivity setting of the pyrometer prior to each growth run. Oxide removal was monitored with Reflection High Energy Electron Diffraction (RHEED). RHEED oscillations caused by the interrupted growth of GaAs and AlAs on a reference wafer were used to calibrate both Ga and Al fluxes prior to growth. The growth rates were about  $2.06\mu m/h$  for GaAs and  $1.10\mu m/h$  for AlAs giving a growth rate of  $3.2\mu m/h$  for AlGaAs. The closing and opening of the Al-shutter caused transients in the cell temperature which changed the Al-flux by up to 7%.

The Al-concentrations ( $x$ ) of the grown structures were estimated from the composition dependent position of the absorption edge obtained by measuring the surface photovoltage signal with a modified Polaron electrochemical plotter. The values for the normal and for the inverted structure were  $x = 37\%$  and  $x = 35.5\%$ , respectively.

The morphology of the grown wafers was excellent with less than  $10^3 cm^{-2}$  oval or other visible defects. Samples of  $10 \times 20 mm^2$  were cleaved from the wafers and typically 6 Hall bars and 2 Van der Pauw patterns were etched on each sample using a photolithographic process

and Ni-AuGe ohmic contacts were deposited by vacuum evaporation. A pair of normal and inverted samples was always processed simultaneously to minimise the effects of processing induced deviations in the samples.

The Hall mobilities of the Van der Pauw samples were measured in a conventional Hall apparatus at 4.2K. A superconducting coil producing 34 mT was used. The samples could be illuminated with white light to increase the 2DEG density. Also a GaAs filter was used in some measurements to check the effect of infrared radiation on the emptying of the traps in the AlGaAs layer.

Shubnikov-de Haas measurements were done at 4.2K using a superconducting coil which produced magnetic fields of up to 6T. Illumination with both infra-red and white light could be used for emptying the traps in the AlGaAs.

#### 6.4 The electron density in the undistorted quantum well

The calculation of the 2D electron density  $n_s$  for a modulation doped structure is complicated by two effects. The surface states on the thin GaAs contact layer pin the Fermi level near the middle of the band gap and some of the free electrons are used to fill surface states causing a decrease of  $n_s$  if the doped layer is fully depleted. Additionally, the doped AlGaAs layer is compensated by deep electron traps, the so called DX centres. The origin of these centres is still a matter of some controversy but they are known to be related to dopant impurities and their concentration is very strongly dependent of the Al concentration [36]. Below 80K empty DX-centres cannot recapture free electrons which have been generated from the traps by for instance illumination. This is the cause of the persistent photoconductivity (PPC) effect in the modulation doped structure.

The calculation of the electron density in the asymmetrically doped quantum well is quite laborious, requiring the self-consistent solution of the electron distribution in the well. Because the model will contain several adjustable variables which are not known very accurately, it is sufficient to solve the simpler problem of calculating the electron density in the symmetrically doped ( $d_1 = d_2$  in Figure (6-2)) quantum well. Due to the symmetry the skewing  $E_s=0$  and the depletion widths are equal:  $D_1 = D_2 = D/2$ . The conduction band discontinuity is

$$\Delta E = E_c(L/2) - E_F + (E_F - E_0) + \Delta E_0 \quad (6-1).$$

The position of the conduction band edge at the interface  $E_c(L/2)$  can be obtained from Poisson's equation

$$E_c\left(\frac{L}{2}\right) = \frac{e^2 n_s}{2 \epsilon_2} \left( \frac{n_s}{4N_b} + d \right) \quad (6-2)$$

where the relation between  $n_s$  and the depletion width  $D$  has been utilised:

$$n_s = N_D D \quad (6-3)$$

The ground state energy level,  $E_0$ , for the ideal, flat well can be solved numerically [35] from simple transcendental equations. For a 250 meV deep GaAs well  $E_0$  can be approximated quite well by the expression

$$E_0 = \frac{35 \text{meV}}{(L/100\text{\AA})^{1.1}} \quad \text{when } 30\text{\AA} < L < 120\text{\AA}$$

The 2DEG has a constant density of states, therefore in the degenerate case  $n_s$  is given by

$$n_s = \frac{gm^*(E_F - E_0)}{2\pi h^2} \quad (6-4)$$

with the degeneracy  $g=2$ .  $m^*$  is the effective mass and  $h$  the reduced Planck's constant.

The position of the Fermi level in the doped region can be assumed to be pinned by the Si donor level which is strongly dependent on the composition of the AlGaAs layer, and is taken as a constant  $E_F = 60 \text{meV}$ . The correct value of the conduction band discontinuity  $E_c$  is not quite certain, a value  $E_c = 250 \text{meV}$  is adopted here. Then  $n_s$  can be solved from equations (6-1, ..., 6-4)

$$n_s = \left\{ \sqrt{(2d+79.2)^2 N_D^2 + 84290 N_D} - \frac{13921 N_D}{(L/100\text{\AA})^{1.1}} - (2d+79.2) N_D \right\} \quad (6-5)$$

Equation (6-5) gives  $n_s$  in units of  $10^{10} \text{cm}^{-2}$ ,  $d$  is in units of  $\text{\AA}$  and  $N_D$  in  $10^{18} \text{cm}^{-3}$ . The calculated values from (6-5) are shown in Figure (6-3).

## 6.5 The distortion of the asymmetrically doped well

The amount of distortion,  $E_s$ , in the asymmetrically doped quantum well (Figure 6-2) can be calculated by integrating the band bending caused by the charge on the substrate side [37]:

$$E_s = E_F + E_I + \frac{e^2}{2\epsilon_2} N_D \cdot D_1^2 + \frac{e^2}{\epsilon_2} N_D \cdot D_1 (L + d_1) - e\delta_1 - \Delta E_c \quad (6-6)$$

where  $e\delta_1$  is the band bending caused by the 2DEG in the well. If unintentional impurities are ignored Poisson's law gives for  $e\delta_1$

$$e\delta_1 = \frac{e^2}{\epsilon_1} \int dz \int_i N_i \varphi_i^2(z') dz' \quad (6-7)$$

where  $\varphi_i$ ,  $N_i$  are the wavefunction and electron density in each sub-band  $i$  ( $i=0,1,\dots$ ). A similar equation determines  $e\delta_2$ .

The second depletion width  $D_2$  is determined by

$$E_F + E_I + \frac{e^2}{2\epsilon_2} N_D \cdot D_2^2 + \frac{e^2}{\epsilon_2} N_D \cdot D_2 \cdot d - \Delta E_c = E_s \quad (6-8)$$

By defining the total depletion width  $D$  caused by the 2DEG:

$$D = n_s / N_D$$

and by using (6-6),  $D_2$  from equation (6-8) can be solved

$$D_2 = \frac{\frac{1}{2}D^2 + (d_1 + L)D - \frac{\epsilon_2}{eN_D} \delta_1}{d_1 + d_2 + L + D} \quad (6-9)$$

The position of the Fermi level is determined by

$$E_F + E_I + \frac{e^2}{2\epsilon_2} N_D \cdot D_1^2 + \frac{e^2}{\epsilon_2} N_D \cdot D_1 \cdot d = \Delta E_c \quad (6-10)$$

From (6-6) and (6-10) the skewing  $E_s$  is found to be

$$E_s = \frac{e^2 N_D}{\epsilon_2} \cdot D_1 \cdot L - e\delta_1 \quad (6-11)$$

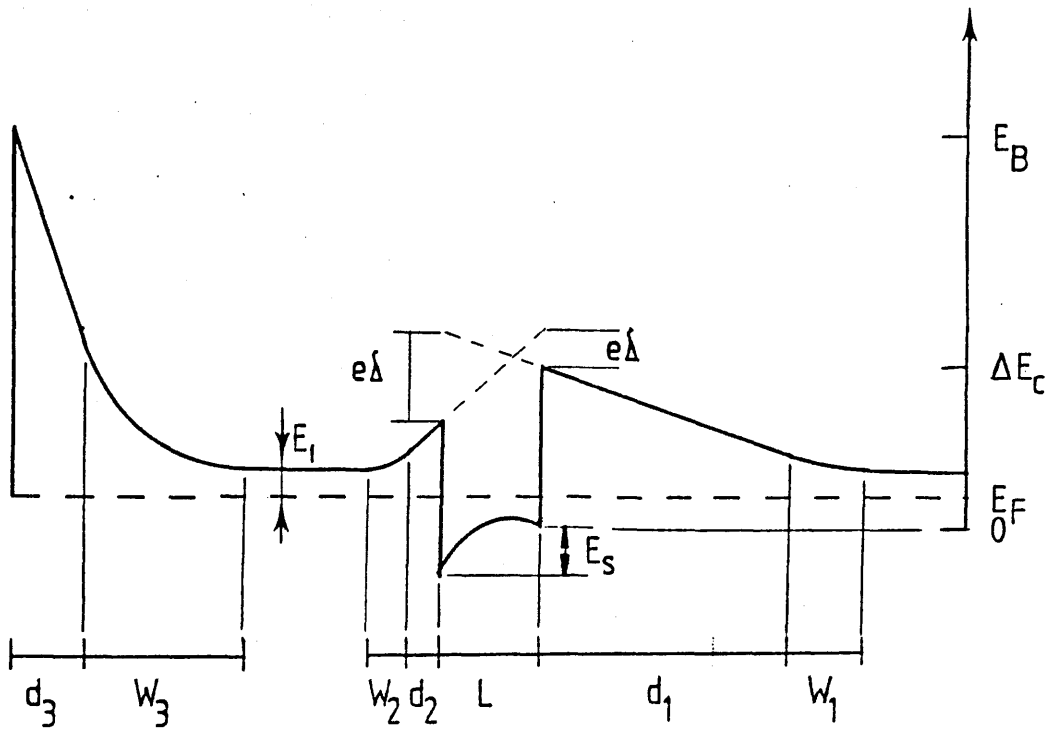


Figure (6-2). A schematic conduction band diagram of the asymmetrically doped single quantum well.

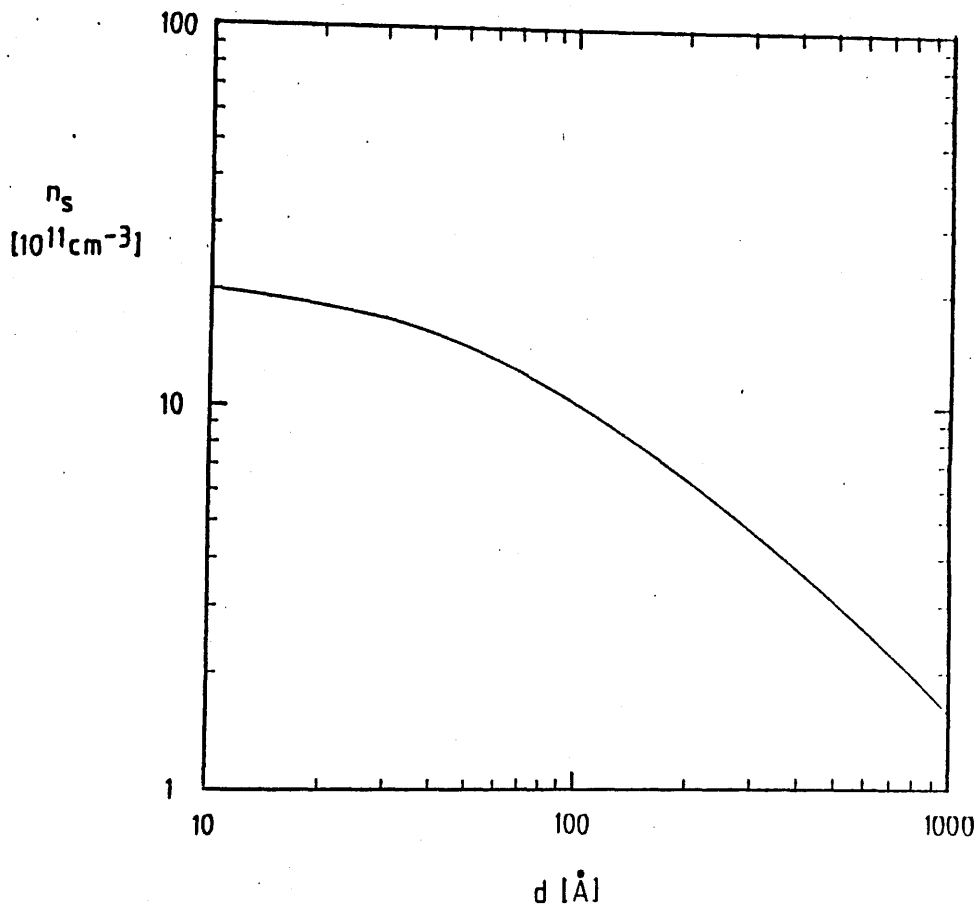


Figure (6-3). The calculated maximum 2D electron density  $n_s$  as a function of the spacer layer thickness in a symmetrically doped single quantum well ( $N_D = 1.5 \times 10^{18} \text{ cm}^{-3}$ ).

By using equation (6-11) and the analogous equation for  $e\delta_2$  the sum of the two band bending terms can be solved:

$$e(\delta_1 + \delta_2) = \frac{e^2 L n_s}{\epsilon_2} \quad (6-12)$$

To obtain  $e\delta_1$  and  $e\delta_2$  accurately it is necessary to solve  $\psi_i$  and  $N_i$  self-consistently, i.e. the potential in the square well must include both the electrostatic potential of the 2DEG and the exchange-correlation interaction. Such a calculation involves the numerical solution of the Schrodinger equation and Poisson's equation [37].

However, the exact solution of equation (6-9) is not necessary for the purposes of this work, the aim being just obtaining an estimate whether the skewing  $E_s$  is significant compared to the separation of the ground state energy level from the bottom of the well. A good approximation is to assume a symmetric charge distribution in the well, and to take  $\delta_1$  and  $\delta_2$  as equal. Then from (6-9) and (6-11)  $E_s$  is easily solved

$$E_s = \frac{e^2 L}{2\epsilon_2} \cdot n_s \cdot \frac{(d_2 - d_1)}{d_1 + d_2 + L + D} \quad (6-13)$$

At high 2DEG densities the total depletion width  $D$  is of the order of  $100\text{\AA}$ . An estimate of the maximum skew from equation (6-13) is shown in Figure (6-4) as a function of the well width  $L$ . For the test structure with  $L=100\text{\AA}$  the maximum skew can exceed the separation of the ground state energy level from the well bottom. It is therefore likely that the 2DEG does not 'see' both interfaces equally well. From Fig. (6-4) it is clear that a well thickness of about  $50\text{\AA}$  should be used to ensure a reasonably symmetric well. The first sub-band of  $50\text{\AA}$  thick well is also at a sufficiently high energy to ensure that only the ground state will be occupied.

The sign of the skewing energy is such that the well is tilted towards the nearest doped region. If the inverted interface is of poorer quality than the normal interface, the mobility of the 2DEG can be expected to be higher in the normal than in the inverted structure. However, if the quality of the interfaces is the main factor limiting the mobility, the  $\mu$  vs.  $n_s$  plot of the normal structure should be steeper than that of the inverted structure because at higher 2DEG densities the well becomes more distorted therefore moving the electron distribution away from the inverted interface in the normal structure and towards the inverted interface in the inverted structure.

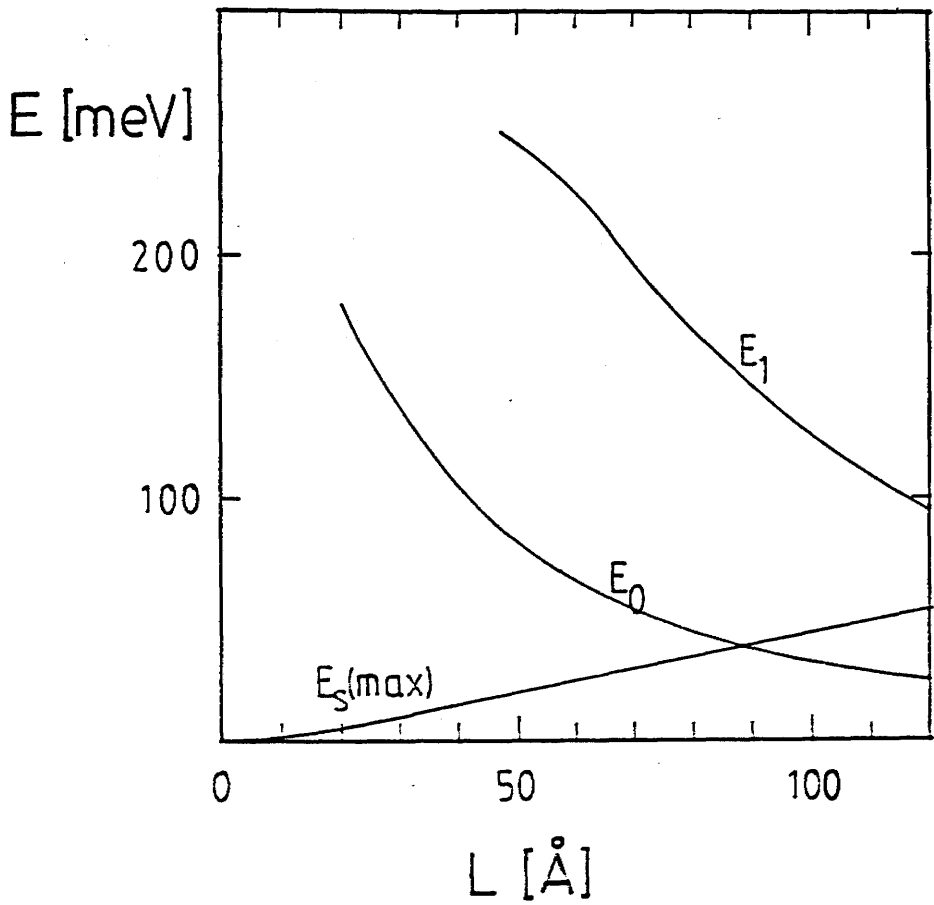


Figure (6-4). The calculated two lowest energy levels ( $E_0$ ,  $E_1$ ) in a square 250meV deep GaAs/AlGaAs quantum well [35]. As a comparison, the estimated maximum skew ( $E_S(\text{max})$ ) of the test structure from equation (6-13) is shown.

## 6.6 Mechanisms limiting the mobility in GaAs/AlGaAs quantum wells

At temperatures below 80K the mobility of the 2D electrons is limited mainly by [10],[38],[39]

- ionised impurity scattering
- interface roughness scattering
- scattering by acoustic phonons
- alloy scattering
- intersub-band scattering
- strong localisation by interface potential fluctuation.

Of these neither the intersub-band scattering nor strong localisation is a distinct scattering mechanism. Intersub-band scattering occurs when the second sub-band becomes populated at high 2D electron densities and the scattering rate of the electrons increases due to the increase in phase space leading to a sudden drop in the mobility [38].

Strong localisation is the result of potential fluctuations at the interface, which inhibit the movement of the 2DEG electrons. Foxon et al. [40] have found evidence of strong localisation at the normal interface of some SH samples. The mobility of the 2DEG in such samples increases very steeply with  $n_s$  due to the increase in the Fermi level resulting in power law exponents  $\alpha > 3$ .

In the following sections 6.6.x the theoretical dependence of the mobility on the 2DEG density  $n_s$  for each scattering mechanism is derived. The power law dependencies thus obtained are used in section 6.7 to explain the experimental results for the asymmetrically doped samples.

### 6.6.1 Scattering by remote ionised impurities

The electrons in the 2DEG are scattered through the Coulombic interaction by the ionised impurities located either in the GaAs well, at the heterojunction or in the AlGaAs layer. The purity of high quality GaAs grown by MBE is such that unintentional ionised impurities are not a significant source of scattering in high mobility single interface samples [10],[41], the scattering being dominated by the remote ionised impurities [39].

Lee et al. have considered remote impurity scattering within the 0th sub-band [42]. Their analysis gives the mobility limit in the SH 2DEG as

$$\mu = \frac{32e(2\pi n_s)^{3/2}}{\pi N_D \hbar} \cdot \left[ \frac{1}{(d+z)^2} + \frac{1}{(d+z+D)^2} \right]^{-1} \quad (6-14)$$

where  $d$  is the thickness of the undoped spacer layer and  $D$  is the width of the layer containing ionised scatterers.  $z$  is the average distance of the electron wavefunction from the heterojunction into GaAs and depends on  $n_s$ :

$$z = (n_s/10^{12} \text{cm}^{-2})^{-1/3} \cdot 55 \text{\AA} \quad (6-15)$$

The 2DEG density is changed by emptying electron traps in the doped AlGaAs layer by illumination. It can therefore be assumed that the density of scattering centres is roughly equal to the density of ionised donors which is constant ( $N_D$ ). Also the width of the doped layer, which contains the scattering centres is constant ( $D$ ). Figure (6-10) shows the calculated values of the mobility for  $D=400 \text{\AA}$  and  $N_D = 1 \times 10^{18} \text{cm}^{-3}$ . The experimental values are well below the theoretical mobilities.

When the doped AlGaAs layer is not fully depleted, the scattering by ionised donors is reduced by the image charges [43], which effectively move the fixed charge

further away from the 2DEG. Hence the inclusion of image charges would increase the discrepancy between the theoretical mobilities limited by the remote ionised impurities and the experimental mobilities measured for the asymmetrically doped quantum wells.

### 6.6.2 Ionised impurity scattering due to interface charge

The momentum relaxation time due to scattering by an ionised background impurity density  $N$  in the well or at the interface is given by [42]

$$\tau = \left[ \frac{4\pi\epsilon}{e^2} \right]^2 \cdot \hbar^3 \cdot \frac{n_s}{m^*N} \cdot I^{-1}(\beta) \quad (6-16)$$

$$\text{where } I = \int_0^\pi \frac{m^* \theta d\theta}{(m^* \theta + \beta)^2}$$

$$\text{and } \beta = \frac{S_0}{2\sqrt{2\pi n_s}}$$

For GaAs  $S_0 = 2 \times 10^8 \text{ m}^{-1}$ . The integral  $I$  can be solved numerically. For electron densities  $n_s$  between  $2 - 18 \times 10^{11} \text{ cm}^{-3}$   $I$  can be approximated accurately by

$$I(n_s) = 0.395 \{n_s / 10^{11} \text{ cm}^{-3}\}^{0.445}.$$

Therefore, the mobility limit due to the interface charge is

$$\mu = 17500 \frac{\text{cm}^2}{\text{Vs}} \frac{(n_s / 10^{11} \text{ cm}^{-3})^{0.55}}{(N / 10^{10} \text{ cm}^{-2})} \quad (6-17)$$

### 6.6.3 Interface roughness scattering

By assuming a Gaussian form for the correlation of the surface roughness Ando [44] obtained for the inverse of the relaxation time due to the interface roughness scattering

$$\frac{1}{\tau} = \frac{2q}{\hbar} \sum_{\bar{q}} \pi \left[ \frac{\Delta \Lambda E_{\text{eff}}}{\epsilon(q)} \right]^2 \cdot \exp\left\{-\frac{q^2 \Lambda}{4}\right\} \quad (6-18)$$

where  $\bar{q}$  is the wave vector,  $\Delta$  the average displacement of the interface and  $\Lambda$  is the order of the range of the spatial variation parallel to the interface. The effective field is given by

$$E_{\text{eff}} = \int dz |\psi(z)|^2 \frac{\partial v(z)}{\partial z} = \frac{e^2}{2\epsilon_s} n_s$$

and the dielectric function by

$$\epsilon(q) = 1 + \frac{2\pi e^2}{\epsilon q} \cdot F(q) \cdot P(q)$$

where  $F$  is the form function and  $P$  the polarisation.

If the depletion charge is ignored, (6-18) can be written as an integral over the circumference of the Fermi circle and the inverse of the relaxation time is proportional to

$$\frac{1}{\tau} = n_s^2 \int_0^{2\pi} \frac{\sin^2(\frac{\theta}{2}) \cdot \exp\left\{-q_F^2 \Lambda^2 \sin^2(\frac{\theta}{2})\right\} d\theta}{\left\{\epsilon(2q_F \sin \frac{\theta}{2})\right\}} \quad (6-19)$$

To obtain the functional dependence of  $1/\tau$  on the 2DEG density  $n_s$  the integral in (6-19) needs to be evaluated. If the lateral spatial decay rate of roughness,  $\Lambda$ , is large  $\tau \rightarrow \infty$ , therefore the interface roughness scattering can only be significant if  $\Lambda$  is small, i.e.

$$\Lambda < 1/(q_F \sin \frac{\theta}{2})$$

Then the exponential in the integrand of (6-19) is almost constant and the only term dependent on  $n_s$  in the integral is the dielectric function  $\epsilon$ . To solve  $\epsilon$ , the polarisation can be written [45]

$$P(q) = \frac{2m_t}{\pi \hbar^2} \left\{ 1 - u(q - 2q_F) \left[ 1 - \left( \frac{2q_F}{q} \right)^2 \right] \right\}^{\frac{1}{2}}$$

where  $u$  is the step function. Because the integration only needs to be done over the circumference of the Fermi circle,  $P(q)$  can be taken as a constant:

$$P(q) = 2m_t / \pi \hbar^2 .$$

The form factor  $F(q)$  is

$$F(q) = \frac{1}{2} \left\{ \left( 1 + \frac{\epsilon_1}{\epsilon_2} \right) \left[ 1 + \frac{q}{8} \frac{q}{b} + \frac{3}{8} \left( \frac{q}{b} \right)^2 \right] \left( 1 + \frac{q}{b} \right)^{-3} + \left( 1 - \frac{\epsilon_1}{\epsilon_2} \right) \left( 1 + \frac{q}{b} \right)^{-6} \right\}$$

where  $b$  is the variational parameter in the Stern-Howard variational wave function [45]. It is straightforward to show that for the GaAs/AlGaAs heterojunction,  $q/b \gg 1$  except for very small values of  $\theta$ . Therefore  $F(q)$  vanishes everywhere except near  $\theta = 0$ . When  $q/b < 1$ ,  $F(q)$  can be taken, as a first approximation to be a constant. Therefore the dielectric function is only weakly dependent on  $n_s$  and

$$\mu \sim n_s^{-2}$$

The interface roughness scattering in a single heterojunction quantum well is inversely proportional to the square of the 2DEG density.

#### 6.6.4 Scattering by acoustic phonons

At low (<70K) temperatures the lattice scatters electrons by acoustic phonons through the deformation potential and the piezoelectric field. The momentum relaxation time due to the deformation potential scattering is [42] proportional to

$$\tau_A \sim b \cdot I_A^{-1}$$

where  $b$  is the effective width of the 2DEG and the integral  $I$  can be interpolated by

$$I_A = \sqrt{1 + \frac{n_s}{2.45 \cdot 10^{11} \text{ cm}^{-2}}}$$

Because  $b$  is proportional to  $n_s^{-1/3}$ , the mobility limit due to the deformation potential decreases when the 2DEG density increases:

$$\mu_A \sim n_s^{-1/3} \left[ 1 + \frac{n_s}{2.45 \cdot 10^{11} \text{ cm}^{-2}} \right]^{-1/2}$$

The mobility limit due to piezoelectric scattering is independent of  $n_s$  [44]:

$$\mu = 13.7 \times 10^6 \text{ cm}^2/\text{Vs} \quad (6-20)$$

## 6.7 Results and discussion

### 6.7.1 Shubnikov-de Haas measurements

In Shubnikov-de Haas (S-dH) measurements the resistivity of the Hall bar is measured as a function of the magnetic field strength. The measurements were repeated at 4.2K both in the dark and after illumination with an infrared light emitting diode (LED), and a red LED and finally white light to increase the 2DEG density. Figure (6-5) shows S-dH results for the normal sample. There is only one period of oscillation indicating that only one sub-band is occupied. In contrast, the resistivity of the inverted sample saturated with white light (Figure (6-6)) displays two different periods of oscillation, indicating the existence of a parallel conducting channel.

There are two possibilities for such a parallel conducting layer, either it is due to the free electrons in one of the doped AlGaAs layers or to the occupation of the first sub-band in the 2DEG, which in an ideal, flat, 250meV deep and 100Å thick GaAs quantum well is 93meV above the ground energy level (Figure 6-4). This theoretical value can be compared to the separation of the Fermi-level and the ground state energy level at the onset of the second period of oscillation, which can be estimated by using the equation for the electron density in the 2DEG:

$$n_s = \frac{m^*}{\pi \hbar^2} (E_F - E_0) \quad (6-21)$$

Equation (6-21) is valid when  $E_F - E_0 \gg kT$ . The onset of the second period of oscillation in the inverted sample occurs at  $n_s = 1.3 \times 10^{12} \text{cm}^{-2}$ , hence the separation of the Fermi- and the ground state energy levels is  $E_F - E_0 = 46.5 \text{meV}$ , only one half of the calculated value for the ideal well.

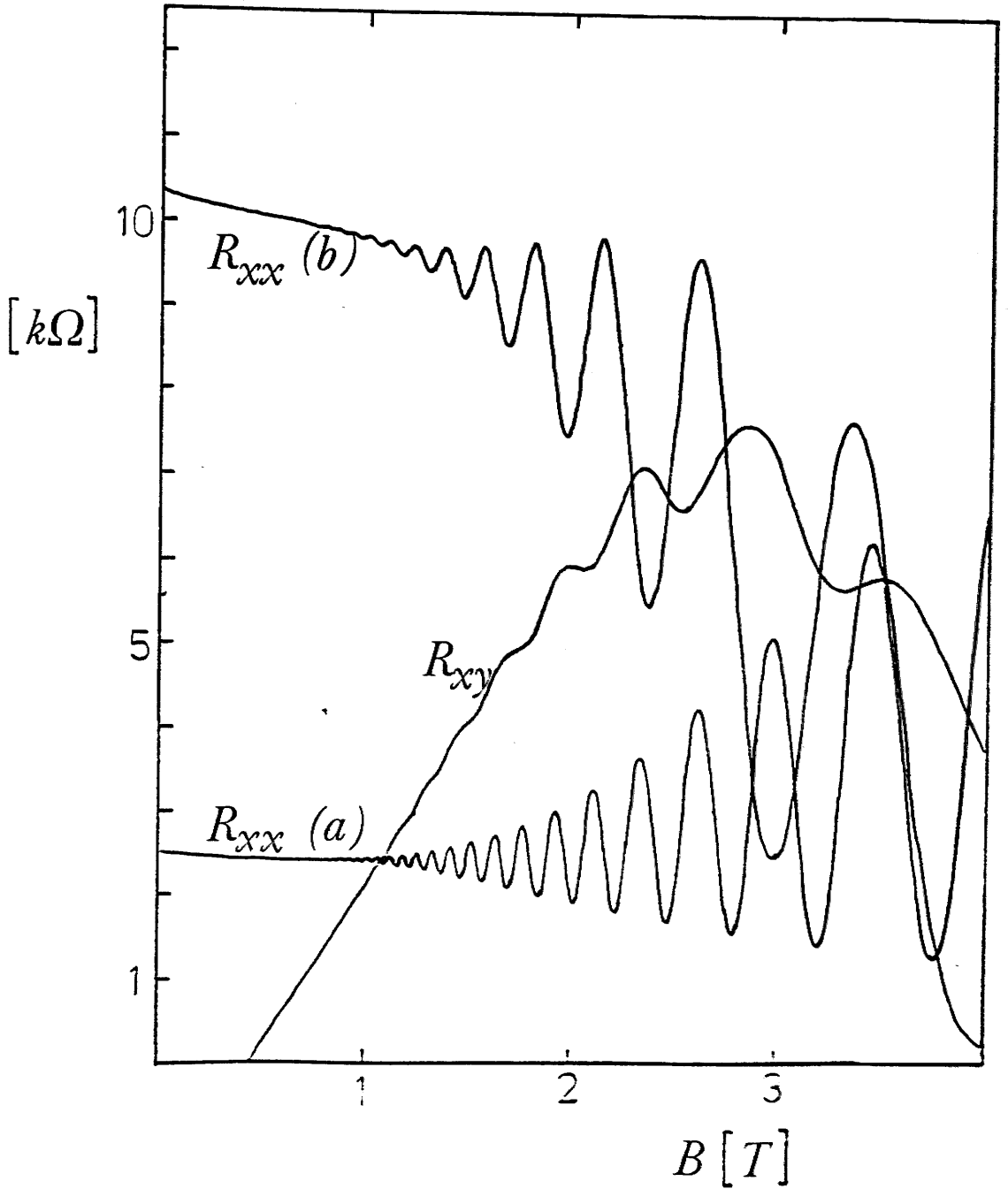


Figure (6-5). The magnetoresistance ( $R_{xy}$ ) after saturation by white light and the resistivity ( $R_{xx}$ ) both before (b) and after (a) saturation by white light of the normal structure at 4.2K as a function of the magnetic field strength.

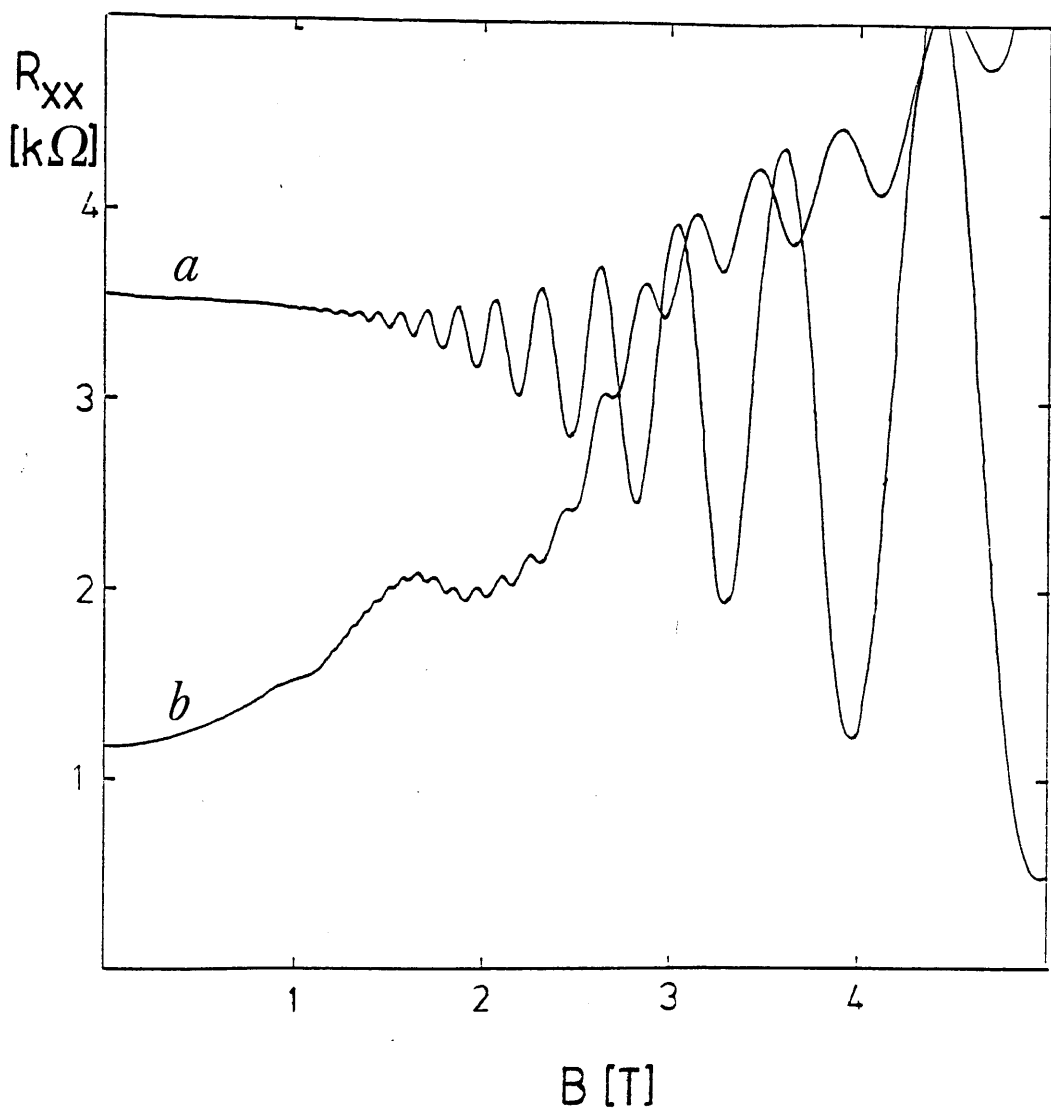


Figure (6-6). The resistivity of the inverted structure as a function of the magnetic field strength in the dark (a) and after saturation by white light (b). The second period of oscillation in (b) indicates parallel conduction in another subband.

The large discrepancy between the calculated ideal energy level separation and that measured from the S-dH data indicates that the parallel conduction is more likely due to the doped AlGaAs rather than the first sub-band in the quantum well. This interpretation is supported by the Hall scattering coefficient data of Section 6.7.2. However it should be noted that the distortion of the quantum well reduces the separation of the energy levels. In fact a severely distorted well is similar to a single heterojunction, in which the separation of the first and ground energy levels is about 33meV at  $n_s = 1.2 \times 10^{12} \text{cm}^{-2}$  [47].

The number of filled Landau levels in the 2DEG,  $\nu$ , is given by

$$\nu \hbar \omega_c = E_F - E_0 \quad (6-22)$$

where  $\omega_c$  is the cyclotron frequency. Therefore from (6-21) and (6-22) the 2DEG density can be solved as a function of the filling factor  $g$  and the magnetic field strength  $B$ :

$$n_s = 2.42 \cdot 10^{10} \text{cm}^{-2} (g\nu)B/[T] \quad (6-23)$$

$n_s$  is obtained from the resistivity  $R_{xx}(B)$  by plotting the filling factor  $g\nu$  as a function of the inverse of the magnetic field strength  $1/B$ . The filling factor in turn is calculated from the plateaus in the Hall resistance which are given by [48]

$$R_{xy} = B/en_s = \frac{25.812 \text{ k}\Omega}{g\nu} \quad (6-24)$$

In Figure (6-10) the relation between the mobility and the 2DEG density obtained from S-dH measurements at 4.2K is plotted for both the normal and the inverted samples. For comparison also the results of Hall measurements of Van der Pauw (VdP) patterns are shown. The normal sample has higher mobilities but a lower  $n_s$  than the inverted sample indicating that silicon has migrated further towards the quantum well from the first doped layer than from the second. For the inverted sample the data from the Hall measurement does not agree with the results from the S-dH measurement giving further support to the presence of parallel conduction in of the AlGaAs-layers.

### 6.7.2 The Hall scattering coefficient

The Hall coefficient  $R_H$  is defined as the transverse field  $E_y$  divided by the product of the magnetic field strength  $B$  and the current  $J_x$ :

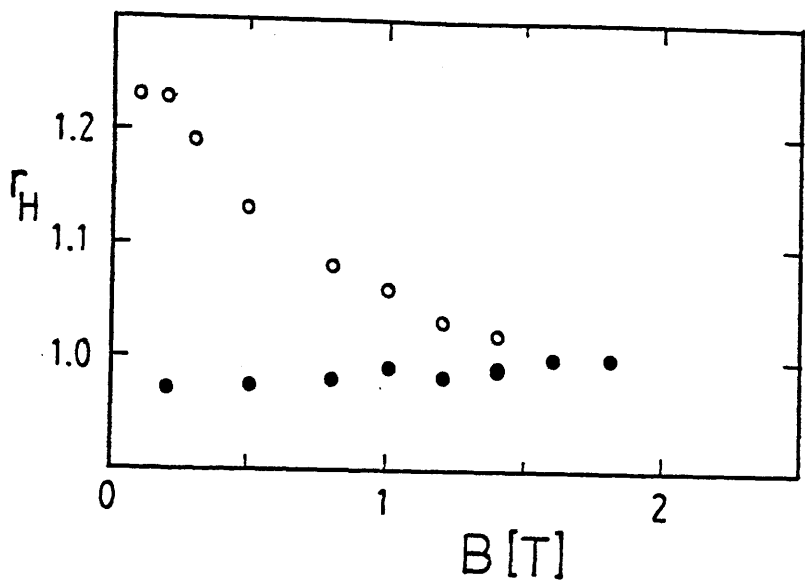
$$R_H = E_y / (BJ_x) \quad (6-25)$$

The free electron concentration  $n$  can be calculated from  $R_H$  by using the equation

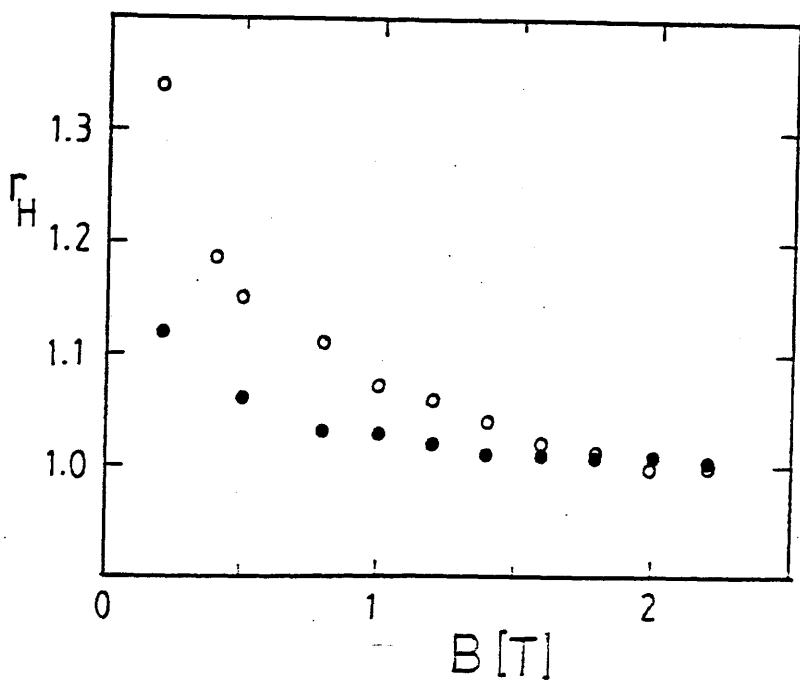
$$R_H = r_H / (e \cdot n) \quad (6-26)$$

The value of the Hall scattering coefficient,  $r_H$ , can be obtained by measuring the Hall coefficient at high magnetic fields [50]:

$$r_H(B) = \frac{R_H(B)}{R_H(B \gg 1/\mu)} \quad (6-27)$$



(a)



(b)

• dark

○ light

Figure (6-7). a) The Hall scattering coefficient  $r_H(B)$  at 4.2K calculated from the S-dH data for the normal sample: I) in the dark (low  $n_s$ )

II) saturated by white light (high  $n_s$ ).

b) Same as (a) but for the inverted sample.

### 6.7.3 Mobility vs. temperature

The Hall mobility and 2DEG concentration of both structures was measured as a function of the temperature from 300K to 4.2K (dark) and from 4.2K to 300K (after illumination). The results are plotted in Figures (6-8a and b). Before illumination the mobility of both samples shows a broad maximum at about 80K (normal sample) to 60K (inverted) before decreasing at lower temperatures. After illumination the mobility of the normal structure increases monotonically towards 4.2K having only a small peak around 80K, whereas the inverted structure has a large peak at 30K.

Before illumination the 2DEG density of both samples declines monotonically with temperature, illuminated structures, however, show a peak at 30K to 50K. The inverted sample has interesting variations in  $n_s$  between 15-50K depending on the pair of contacts used for measuring the Hall voltage (see inset of Figure 8(a)).

The decrease of the Hall mobility at low temperatures is probably caused by the strong localisation of the 2D electrons by potential fluctuations at the interface [40]. It seems that the localisation is stronger in the inverted structure, i.e. at the inverted interface. Since the localisation is evident in samples with  $n_s = 1-2 \times 10^{12} \text{cm}^{-2}$  the average potential fluctuation can be estimated to be at least 50-70meV. The cause of the fluctuations is not certain, but interface roughness and interface charges or alloy composition fluctuations are most likely candidates [40]. As shown in Section 6.5 the 2DEG in the normal structure is probably quite far away from the inverted interface due to the distortion of the quantum well; therefore if - as appears likely - the potential fluctuations are mainly due to the inverted interface, the fluctuations must be quite long range.

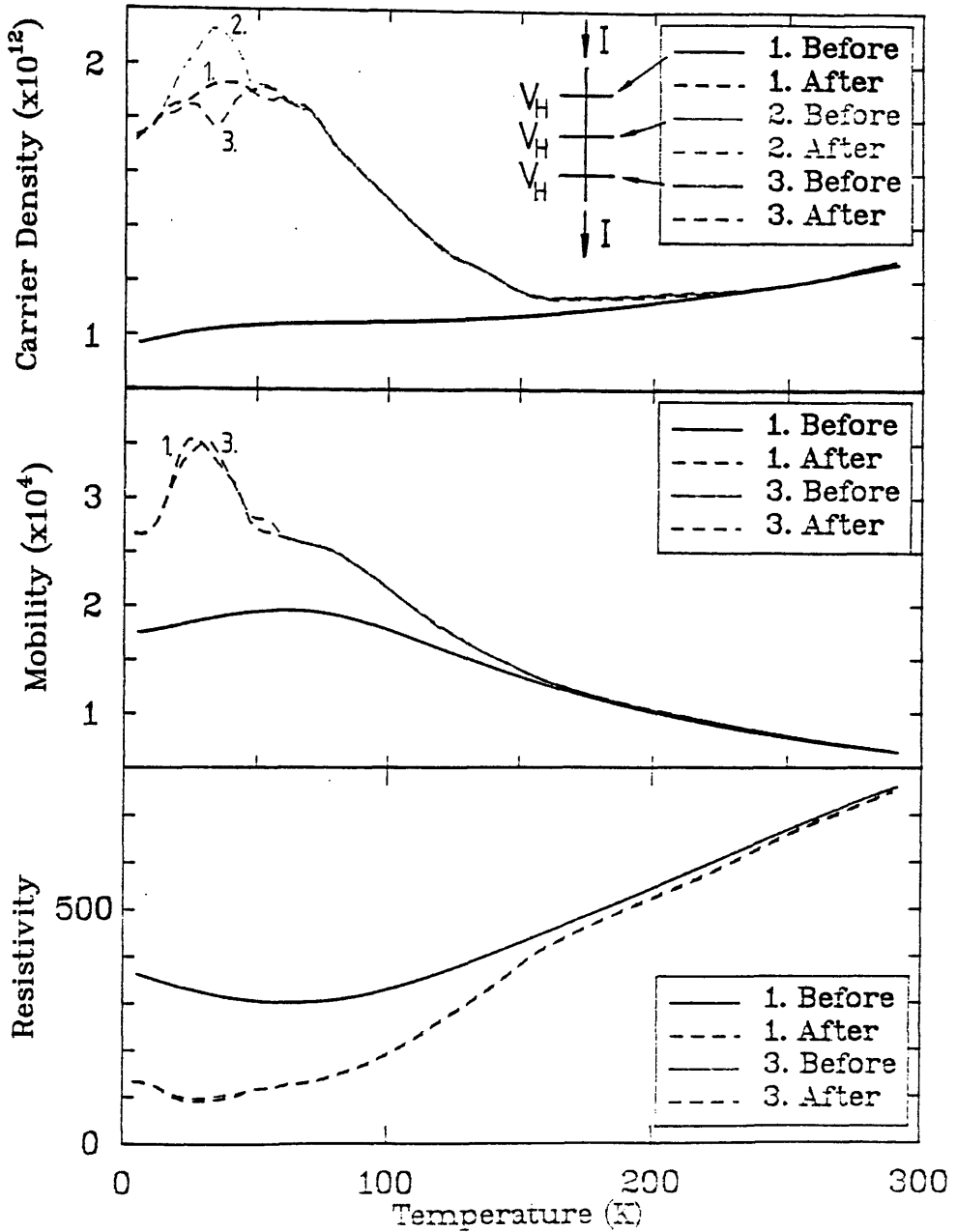


Figure (6-8). The Hall mobility, free electron concentration and resistivity as a function of temperature (Before = before illumination, After = after illumination).

a) Inverted structure. 1,2,3 refer to different pairs of probes used for measuring the Hall voltage of the Hall bar (inset).

#### 6.7.4 Annealing experiments

Pairs of samples cleaved from both the normal and inverted wafers grown at 600°C were cleaned in the usual manner but with the final etch being omitted. The samples were mounted on Mo-blocks and loaded into the growth chamber where they were annealed in a stabilising As<sub>4</sub> flux of  $3 \times 10^{15}$  molecules cm<sup>-2</sup>s<sup>-1</sup> for 15 minutes. Annealing temperatures were 650°C, 680°C and 700°C.

The Hall mobilities at 4.2K as a function of the 2DEG density for both annealed and unannealed samples are shown in Figure (6-9). The samples were cooled down to 4.2K in the dark. Pulses of white light were used to empty some of the electron traps and to change  $n_s$ .

An anneal at 650°C does not affect the mobility of the 2DEG. Annealing at 680°C and 700°C however causes a marked decrease in the mobility indicating that silicon diffuses towards the quantum well in both structures during the high temperature anneal. In the inverted sample annealed at 700°C a Hall voltage could only be measured when the sample was saturated by white light. This was probably caused either by an increase in the electron trap density or by a deterioration of the ohmic contacts.

In the normal sample the  $\mu$  vs.  $n_s$  curves are extended to lower values of  $n_s$  as the annealing temperature increases. If silicon dopant atoms diffuse towards the quantum well,  $n_s$  can be expected to increase. The decrease in the minimum value of  $n_s$  is probably due to the evaporation of the surface GaAs contact layer at high temperatures. According to Imura et al. [52] the desorption rate of GaAs should be about 70Å/min at 700°C, sufficient to remove the entire contact layer of 170Å during the 15min anneal. At low  $n_s$  the entire doped surface layer may be depleted, therefore as the GaAs layer desorbs the shifting surface depletion

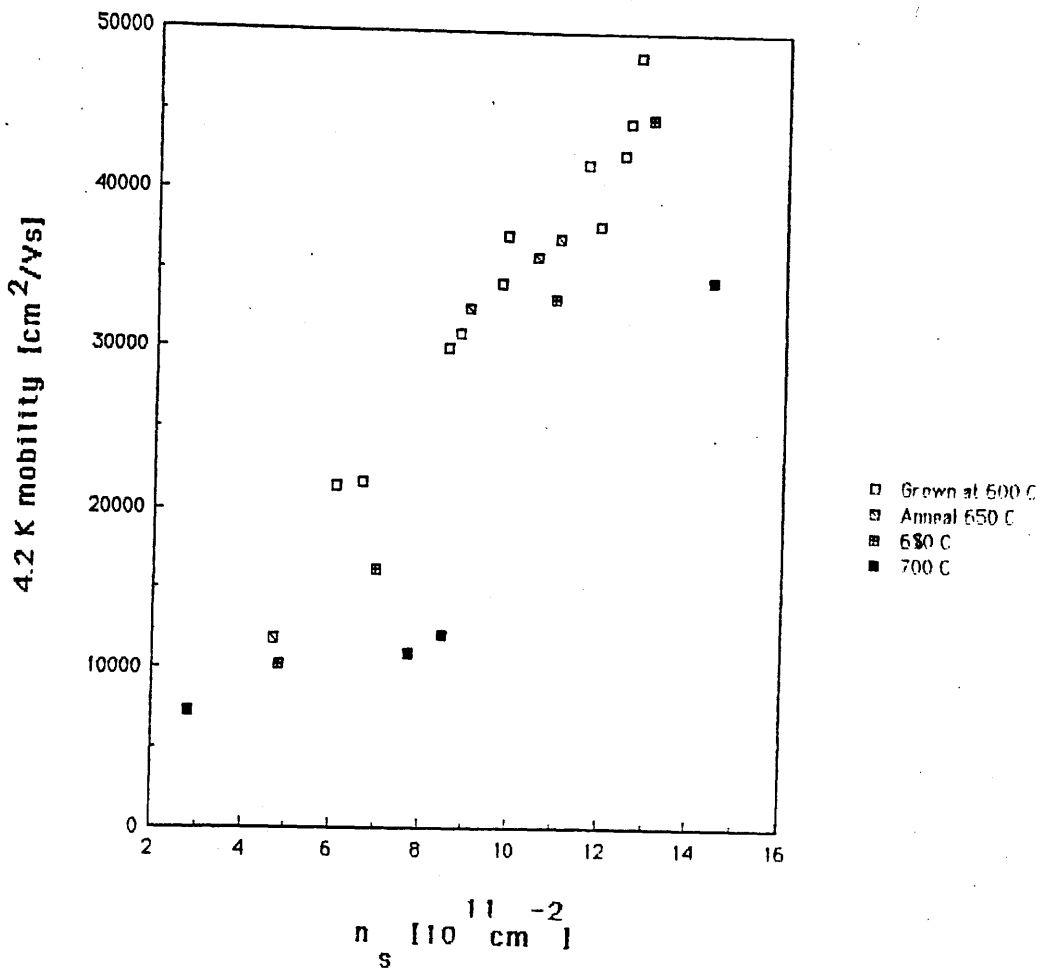


Figure (6-9). Hall mobilities vs.  $n_s$  at 4.2K for the sample grown at  $600^\circ\text{C}$  and after annealing at  $650^\circ\text{C}$ ,  $680^\circ\text{C}$ , and  $700^\circ\text{C}$ .

a) Normal structure.

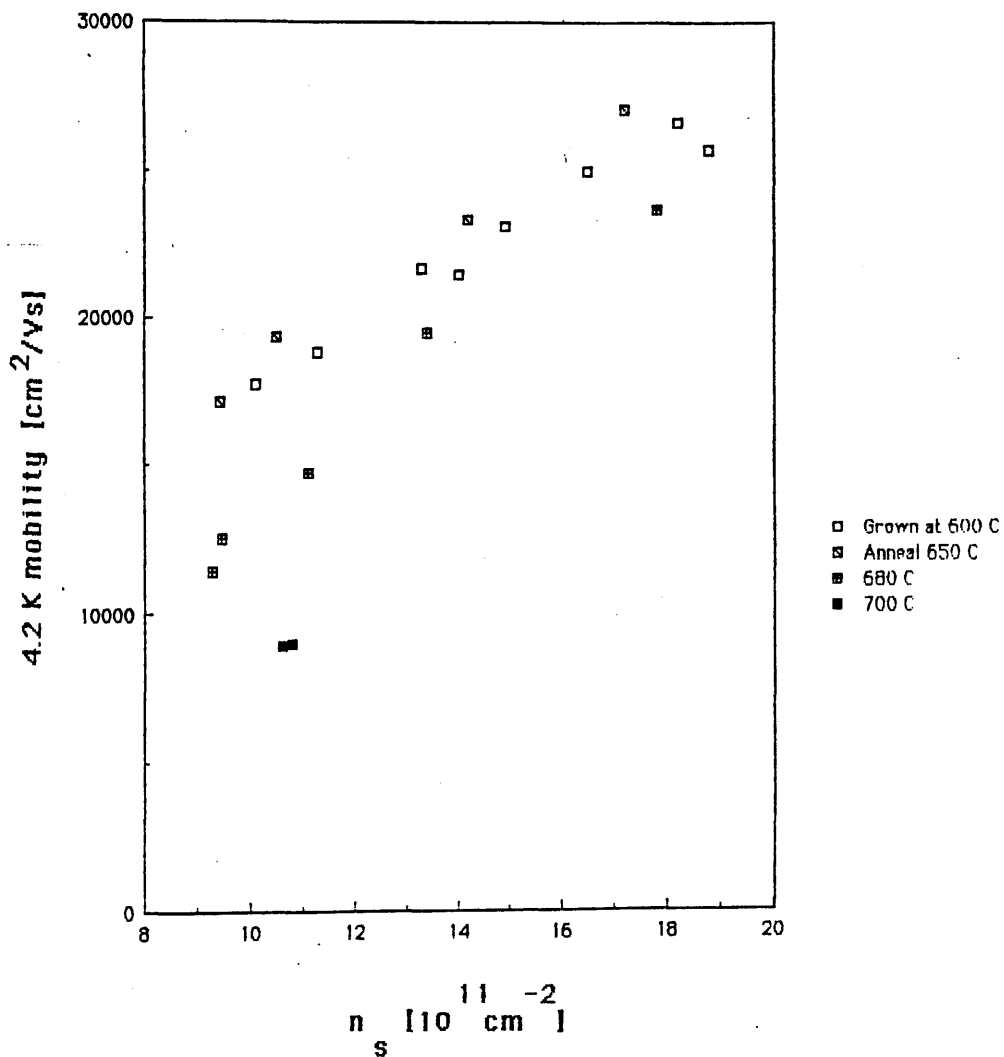
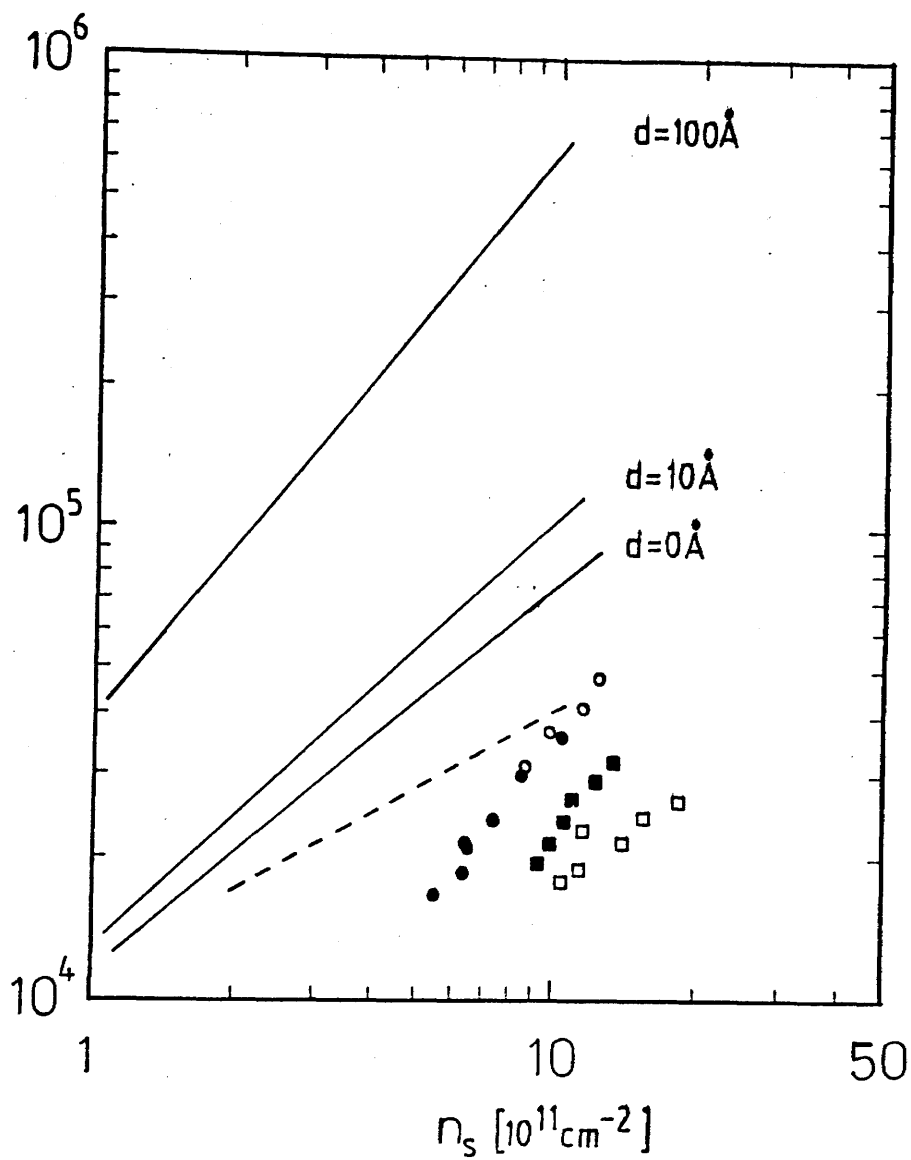


Figure (6-9)<sup>A</sup>. Hall mobilities vs.  $n_s$  at 4.2K for the sample grown at 600°C and after annealing at 650°C, 680°C, and 700°C.

b) Inverted structure.



Normal:	Inverted:
● S-dH	■
○ Hall	□

Figure (6-10). The Hall mobilities vs. the 2DE density calculated from Lee et al.'s model [44] of remote impurity scattering (solid lines,  $N = 1 \times 10^{18} \text{ cm}^{-3}$ ,  $D = 400\text{\AA}$ ) and the model for interface charge scattering ( $N = 1.5 \times 10^{10} \text{ cm}^{-2}$ , broken line). For comparison the experimental results of the normal and inverted quantum well structures are shown.

region moves towards the quantum well thus reducing the total charge available for the 2DEG.

It has been suggested that a possible reason for the migration of silicon towards the inverted interface is the buildup of native defects in the thick AlGaAs buffer layer which might increase the diffusion coefficient of Si [53]. Such effects, if they exist, can be eliminated by the use of thin GaAs prewells before the doped AlGaAs region. However, it should be noted that the annealing experiments of this work do not indicate any major difference in the rate of diffusion between the normal and the inverted structures.

#### 6.7.5 The mobility vs. the 2D electron density

Experimentally the 2DEG mobility is found to be proportional to some power  $\alpha$  of the 2DEG density  $n_s$ :

$$\mu \sim n_s^\alpha \quad (6-28)$$

For high mobility samples with thick spacers  $\alpha$  is usually about 1.5 [40].  $\alpha$  has been calculated from Lee's model for remote ionised impurity scattering (equation (6-21)) and the result is shown in Figure (6-11).  $\alpha$  is indeed 1.5 for thick spacers, and decreases to about 0.82 when the thickness of the spacer ( $d$ ) is reduced to zero. Such a reduction of  $\alpha$  as a function of  $d$  has been observed by Hirakawa et al. [54]. The calculated values of  $\alpha$  for other scattering mechanisms are also shown in Figure (6-11).

It is reasonable to conclude that since  $\alpha$  is about 1 for both normal and inverted structures, the scattering due to surface roughness ( $\alpha = -2$ ) and acoustic phonons ( $\alpha = -1/3 \dots -5/6$ ) can be excluded as probable mechanisms limiting the mobility. Only the ionised impurity scattering due to remote impurities with a spacer thickness of  $d = 100\text{\AA}$  has the correct value of  $\alpha \sim 1.2$ .

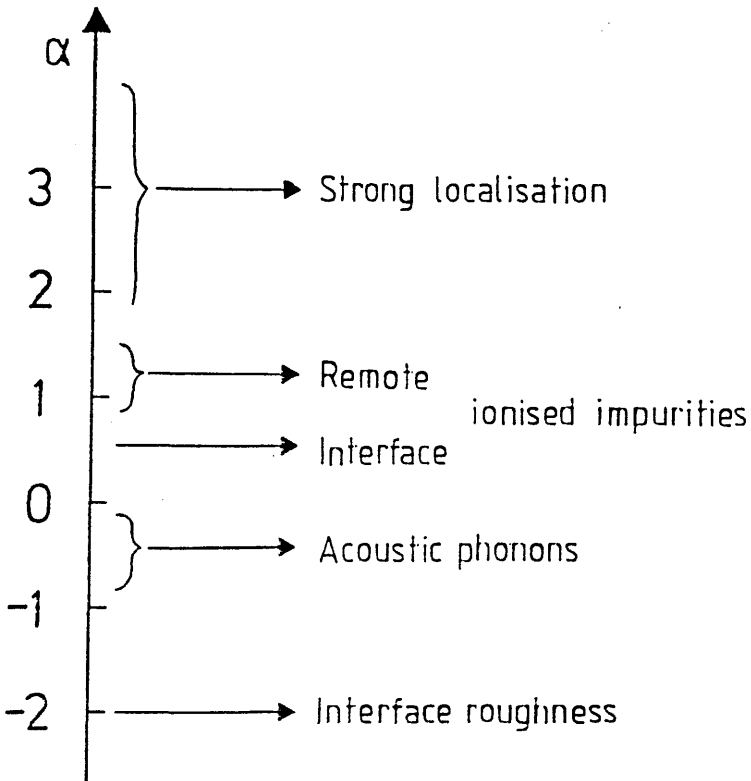
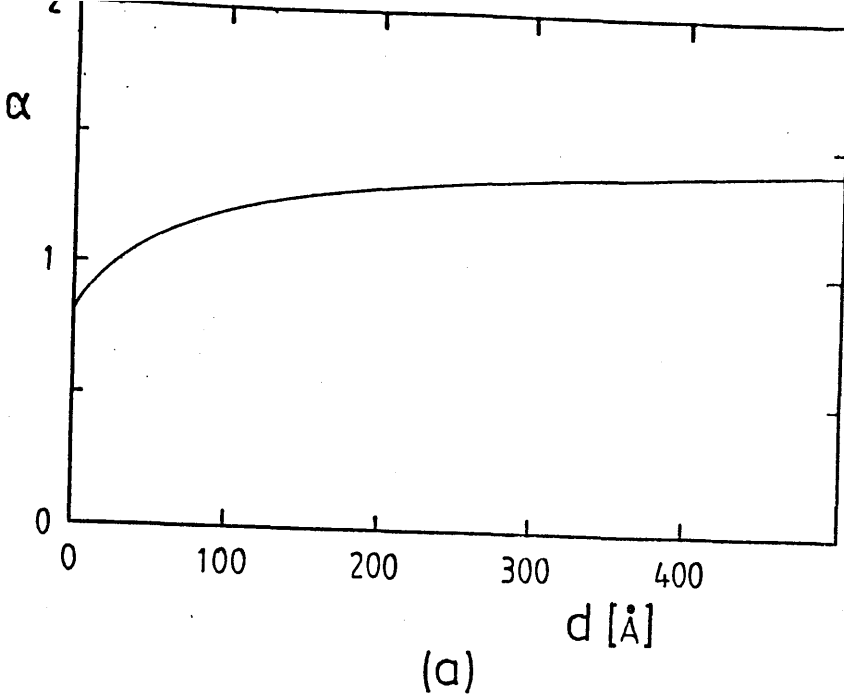


Figure (6-11).

a) The power law ( $\mu^{-\alpha} n_s^\alpha$ ) exponent for ionised impurity scattering as a function of the spacer layer thickness ( $N_D = 1.5 \times 10^{18} \text{ cm}^{-3}$ ) calculated from the model by Lee et al. [44].

b) The power law exponents for the different scattering mechanisms.

However, the theoretical mobilities are much higher than the measured values even if the effective spacer layer thickness is assumed to be 0.

Scattering by ionised interface or background impurities can explain the observed mobilities if a very high interface charge density ( $>10^{10} \text{ cm}^{-2}$ ) is assumed. The theoretical exponent for ionised interface scattering is only 0.55. However, the interface charge density is probably not independent of the Fermi level [42], i.e. an increase in the Fermi-level may compensate some of the interface charge leading to a higher value of  $\alpha$  than that predicted by assuming a constant density of scattering centres.

Foxon et al. [40] have measured values of  $\alpha > 3$  for the high mobility samples showing strong localisation, yet it is not known whether localisation always causes such high values of  $\alpha$ . Therefore strong localisation cannot be excluded as the possible cause of the poor mobility at 4.2K even though the exponent  $\alpha = 1.2$  is smaller than observed by Foxon et al.

## 6.8 Proposals for future work

In this work only one pair of quantum well samples was successfully grown at  $600^\circ\text{C}$ . It would be interesting to grow pairs of samples at several different temperatures and compare their 2DEG mobilities with those of annealed samples.

The 2DEG mobilities of the asymmetrically doped quantum wells were quite low, probably due to the strong localisation caused by potential fluctuations at the inverted interface. It is important that the mobilities are as high as possible. Some of the techniques mentioned in Section 6.1.5 could be utilised to improve the inverted interface. Specifically, a slightly higher growth temperature for the low

temperature sample ( $630^{\circ}\text{C}$ ) and a lower growth rate could be used. To getter impurities in the thick AlGaAs buffer layer very thin GaAs prewells should be used immediately prior to the first doped AlGaAs layer.

The skewing of the asymmetrically doped quantum well can be minimised by reducing the thickness of the well. To achieve an electron distribution which is reasonably symmetric in relation to both interfaces the ground state energy  $E_0$  must be several times the maximum skew  $E_s(\text{max})$ . As shown in Figure (6-4) a well thickness of  $50\text{\AA}$  fulfils this requirement and still allows a reasonable maximum 2DEG density. An additional benefit from the use of a narrow well is that the separation of the energy levels is increased and only one level will be occupied even at high  $n_s$ .

The nominal doping level of  $1.5 \times 10^{18} \text{cm}^{-3}$  used in this work is quite high and very near the level at which Gonzalez et al. [28] observed a higher diffusion coefficient of silicon in AlGaAs. A comparison with annealed samples of a lower ( $\sim 5 \times 10^{17} \text{cm}^{-3}$ ) doping level would reveal whether the concentration dependent diffusion coefficient affects the post growth migration.

The quality of the quantum well could be analysed by photoluminescence measurements to check whether unwanted impurities are present in the well.

It seems that strong localisation may be one of the reasons for the inferior electron mobilities in inverted structures. It would therefore be useful to measure the mobility as a function of the temperature in such structures to reveal whether the characteristic "bump" in the  $\mu$  vs.  $T$  curve exists.

## 6.9 Conclusions

Hall and Shubnikov-de Haas measurements of the asymmetrically doped single quantum well test structures show that similar 2DEG densities can be achieved in both the normal and the inverted structures. The maximum electron density  $n_s$  of the inverted structure is slightly higher indicating that the silicon dopant has migrated towards the quantum well during the growth. The mobility of the 2DEG in the normal structure at 4.2K is higher than in the inverted structure which may be another indication of the migration of the ionised impurities from the first doped layer. However it is not known how much the possible differences in the quality of the two interfaces affect the results. Calculations show that the  $100\text{\AA}$  wide quantum well is tilted towards the nearest doped region to such an extent that the 2DEG distribution is strongly asymmetric.

The measured power law exponents of the  $\mu$  vs.  $n_s$  curves indicate that neither the surface roughness scattering nor the acoustic phonons are responsible for the rather low mobilities in the single quantum wells. Remote ionised impurity scattering has the correct power law dependence but the theoretical mobilities are much higher than those measured for the asymmetric test structures.

The ionised impurity scattering by interface (or background) impurities can explain the observed mobilities if a high interface charge density of  $N > 10^{10}\text{cm}^{-2}$  is assumed.

However, on the basis of the mobility vs. temperature measurements the strong localisation of the 2DEG by potential fluctuations at the inverted interface can be considered the most likely mechanism responsible for the low 4.2K mobility. The power law exponent  $\alpha = 1.2$  is lower than that observed by Foxon et al. [40] possibly indicating that the potential fluctuations causing the

strong localisation are larger at the inverted interface than at the normal single heterojunction. This is the first time strong localisation has been suggested as a cause of the poor mobility of inverted heterointerfaces.

Both normal and inverted samples annealed at 680°C and 700°C show a reduction in the 2DEG mobility at 4.2K indicating that silicon atoms diffuse away from the doped regions at high temperatures. However an anneal at 650°C did not affect the 2DEG mobilities of either sample. It is not known whether the mechanism limiting the mobility of the unannealed samples is due to silicon migration during the growth. Therefore it cannot be concluded whether or not the surface segregation or the diffusion is the dominant migration mechanism of silicon at the growth temperature of 600°C.

## 6.10 References

- [1] L.Esaki and R.Tsu, Internal Report RC 2418, IBM Research, March 1969.
- [2] R.Dingle, H.L.Stoermer, A.C.Gossard and W.Wiegmann Appl.Phys.Lett. 37 (1978) 805.
- [3] T.J.Drummond, H.Morkoc and A.Y.Cho J.Appl.Phys. 52 (1981) 1380.
- [4] H.L.Stoermer, A.Pinczuk, A.C.Gossard and W.Wiegmann Appl.Phys.Lett 38 (1981) 1380.
- [5] G.Weimann and W.Schlapp, Appl.Phys.Lett. 46 (1985) 411.
- [6] J.J.Harris, C.T.Foxon, K.W.J. Barnham, D.E. Lacklison, J.Hewett and C.White "Two-dimensional electron gas structures with mobilities in excess of  $3 \times 10^6$  cm<sup>2</sup>/Vs" To be published in J.Appl.Phys., February 1987.

- [7] T.J.Drummond, J.Klein, D.Arnold, R.Fischer, R.E.Thorne, W.G.Lyons and H.Morkoc, Appl.Phys.Lett. 42 (1983) 615.
- [8] C.Weisbuch, R.Dingle, P.M.Petroff, A.C.Gossard and W.Wiegmann, Appl.Phys.Lett. 38 (1981) 840.
- [9] H.Morkoc, T.C.Drummond, W.Kopp and R.Fischer, J.Electrochem.Soc. 129 (1982) 824.
- [10] K.Mitsunaga, K.Kanamoto, M.Nunoshita and T.Nakayama, J.Vac.Sci.Technol. B3 (1985) 627.
- [11] F.Alexandre, L.Goldstein, G.Leroux, M.C.Joncour, H.Thibierge and E.V.K.Rao, J.Vac.Sci.Technol. B3 (1985) 950.
- [12] F.Alexandre, J.L.Lievin, M.H.Meynadier and C.Delalande, Surf.Sci. 168 (1986) 454.
- [13] L.P.Erickson, T.J.Mattord, P.W.Palmberg, R.Fischer, H.Morkoc, Electron.Lett. 19 (1983) 632.
- [14] R.K.Tsui, G.D.Kramer, J.A.Curless and M.S.Peffley, Appl.Phys.Lett. 48 (1985) 940.
- [15] B.A.Joyce, P.J.Dobson, J.H.Neave and K.Woodbridge, Surf.Sci. 168 (1986) 423.
- [16] R.A.Stall, J.Zilko, V.Swaminathan and N.Shumaker, J.Vac.Sci.Technol. B3 (1985) 524.
- [17] R.C.Miller, W.T.Tsang and O.Munteanu, Appl.Phys. Lett. 41 (1982) 374.
- [18] R.C.Miller, A.C.Gossard, W.T.Tsang and O.Munteanu, Phys.Rev. B25 (1982) 3871.
- [19] P.M.Petroff, R.C.Miller, A.C.Gossard and W.Wiegmann Appl.Phys.Lett. 44 (1984) 217.
- [20] J.C.Phillips, J.Vac.Sci.Technol. 19 (1981) 545.
- [21] A.M.White in Proceedings of the XIV International Conference on the Physics of Semiconductors, Edinburgh 1978, ed B.C.H.Wilson (Institute of Physics, London 1979) pl23.
- [22] T.Hayakawa, T.Suyama, M.Kondo, K.Takahashi, S.Yamamoto, S.Yarro and T.Hijikata, J.Appl.Phys. 58(1985) 4452.

- [23] S.Sasa, J.Saito, K.Nanbu, T.Ishikawa and S.Hiyamizu  
Japan.J.Appl.Phys. 23 (1984) L573.
- [24] K.Inoue, H.Sakaki and J.Yoshino, Japan.J.Appl.Phys.  
23 (1984) L767.
- [25] K.Inoue, H.Sakaki, J.Yoshino, Y.Yoshioka, Appl.  
Phys.Lett. 46 (1985) 973.
- [26] M.Heiblum, J.Vac.Sci.Technol. B3 (1985) 820.
- [27] M.Heiblum, W.I.Wang, L.E.Osterling and V.Deline,  
J.Appl.Phys. 54 (1983) 6751.
- [28] L.Gonzalez, J.B.Clegg, D.Hilton, J.P.Gowers,  
C.T.Foxon and B.A.Joyce, To be published.
- [29] J.Maguire, R.Murray, R.C.Newman, R.B.Beall and  
J.J.Harris, to be published in Appl.Phys.Lett.
- [30] M.Kawabe, N.Matsuura, N.Shimizu, F.Hasegawa and  
Y.Nannichi, Japan.J.Appl.Phys. 23 (1984) L623.
- [31] R.Fischer, Y.L.Sun, W.T.Masselink, J.Klem, M.V.  
Klein and H.Morkoc, Japan.J.Appl.Phys. 23 (1984)  
L126.
- [32] T.J.Drummond, R.Fischer, P.Miller, H.Morkoc and  
A.Y.Cho, J.Vac.Sci.Technol. 21 (1982) 684.
- [33] J.J.Harris and C.T.Foxon, Private Communication.
- [34] J.M.Woodcock, J.J.Harris and J.M.Shannon, J.Vac.  
Sci.Tech. B4 (1986) 609.
- [35] E.Merzbacher, "Quantum Mechanics", 2nd ed. (Wiley,  
New York, 1970), p. 106.
- [36] N.Chand, R.Fischer, J.Klem, T.Henderson, P.Pearah,  
W.T.Masselink, Y.C.Chang and H.Morkoc, J.Vac.Sci.  
Technol. B 3 (1985) 644.
- [37] K.Inoue, H.Sakaki, J.Yoshino and T.Hotta, J.Appl.  
Phys 58 (1985) 4277.
- [38] H.L.Stormer, Surf.Sci. 132 (1983) 519.
- [39] J.J.Harris, C.T.Foxon, D.E.Lacklison and K.W.J.  
Barnham, To be published in Superlattices and  
Microstructures.
- [40] C.T.Foxon, J.J.Harris, R.G.Wheeler and D.E.  
Lacklison, J.Vac.Sci.Technol. B4 (1986) 511.

- [41] H.Morkoc, Chapter 7 in "The Technology and Physics of Molecular Beam Epitaxy", Ed. E.H.C.Parker (Plenum, New York, 1985) p.185.
- [42] K.Lee, M.S.Shur, T.J.Drummond and H.Morkoc, J.Appl. Phys. 54 (1983) 6432.
- [43] A.A.Grinberg and M.S.Shur, J.Appl.Phys. 58 (1985) 382.
- [44] T.Ando, J.Phys.Soc.Japan 51 (1982) 3900.
- [45] T.Ando, J.Phys.Soc.Japan 43 (1977) 1616.
- [46] P.J.Price, Ann.Phys. (NY) 133 (1981) 217.
- [47] T.Ando, J.Phys.Soc.Japan 51 (1982) 3893.
- [48] Zhong-Hua, Acta Metall. Sinica 4 (1983) 241.
- [49] A.C.Beer "Galvanomagnetic effects in semi-conductors", p.120 in vol. 4 of Solid State Physics, ed. F.Seitz and D.Turnbull (Academic Press, 1963).
- [50] D.A.Anderson and N.Apsley, Semic.Sci.Technol. 1 (1986) 187.
- [51] M.J.Kane, N.Apsley, D.A.Anderson, L.L.Taylor and T.Kerr, J.Phys.C 18 (1985) 5629.
- [52] Y.Imura, H.Takasugi and M.Kawabe, Japan.J. Appl.Phys. 25 (1986) 95.
- [53] Reference [7.42] in: R.L.S.Devine, PhD Thesis (University of Glasgow, 1985) p.93.
- [54] K.Hirakawa, H.Sakaki and J.Yoshino, Surf.Sci. 170 (1986) 440.

## CHAPTER 7

### CONCLUSIONS AND PROPOSALS FOR FUTURE WORK

The flux calibration measurements of Chapter 2 reveal that the beam equivalent pressure (BEP) measured by the ion gauge is an underestimate of the true pressure, defined as the pressure of an ideal gas which causes a flux equal to that caused by the molecular beam. The pressure of the In beam is found to be 26 times of the beam equivalent pressure (BEP) given by the ion gauge. The  $P_2$ -flux can be calibrated indirectly from the weight of the phosphorus charge and the geometry of the cracker-substrate system giving a correction factor  $C_f=8$  which is in good agreement with the calculated value. However, a less inaccurate method for calibrating the phosphorus flux is needed.

If InP is grown in an insufficient  $P_2$ -flux, In droplets are eventually formed on the surface. The experimental phase diagram for this In-rich transition under typical MBE conditions can be explained by assuming that the minimum  $P_2$ -flux necessary for preventing the surface from becoming In-rich is the sum of the flux needed for growth and of the flux needed to stabilise the surface against the desorption of  $P_2$ . The experimental data fits the model well if an accommodation coefficient of 0.2 is assumed for  $P_2$ .

When III-V alloys are grown at high temperatures, the desorption rate of the group III element with the highest vapour pressure may become sufficient to affect the nett growth rate or the composition of the alloy. The thermodynamic equilibrium model [1] developed by Heckingbottom for explaining the desorption of Ga from GaAs predicts that the desorption rate of In is negligible even at the highest growth temperatures ( $560^\circ$ ). Experimental results confirm that the upper limit of the desorption rate is less than 0.1um/h at

560<sup>o</sup>. More accurate measurements of the desorption rate, preferably at even higher temperatures than 560<sup>o</sup>C are necessary to check the applicability of the equilibrium model [1] to the desorption of In from InP.

As shown in Chapter 3, the desorption of sulphur from InP becomes significant when the growth temperature exceeds 500<sup>o</sup>. The activation energy of desorption is about 4.5eV in the high doping regime. It still remains to be resolved whether the result of Iliadis et al. [2] of a lower activation energy of desorption (1 eV) at low sulphur concentrations ( $\approx 10^{16} \text{ cm}^{-3}$ ) is correct. Since electrochemical C-V profiling cannot be used for estimating the sulphur concentration at such low doping levels, SIMS analyses should be used instead.

Thermodynamic calculations based on VPE growth data show that In<sub>2</sub>S rather than InS is the most likely desorbing species. From the calculated equilibrium desorption rates it is concluded that the sulphur taking part in the desorption reaction should be considered in equilibrium with the crystal rather than the vapour phase. The calculated enthalpies of equilibrium desorption reactions between the bulk crystal and the vapour phase are in good agreement with the activation energies of desorption of S in InP and S, Se and Te in GaAs.

In Chapter 4 the effect of growth conditions on the incorporation of sulphur in MBE grown InP is found to provide information on the kinetics of the dopant incorporation and desorption reactions. On the basis of the kinetic model by Wood and Joyce [3] the linear dependence of the concentration of incorporated sulphur atoms on the incident sulphur flux in the high desorption regime implies equal kinetic orders of the incorporation and desorption reactions.

From the growth rate dependence of the sulphur concentration in InP grown at a high substrate

temperature the ratio of the rate constants of incorporation and desorption is shown to be proportional to the growth rate. It is assumed that the incorporation rate is directly proportional to and the desorption rate is independent of the growth rate.

The desorption rate of sulphur can be reduced only slightly by increasing the  $P_2$  overpressure, hence the strong desorption limits the use of S as a dopant for MBE grown InP to temperatures below  $500^{\circ}\text{C}$ . The observed difference in the effect of the group V element overpressure on the incorporation behaviour of S in GaAs and InP can be explained by an incorporation rate constant which is not a function of the applied  $\text{As}_4$  pressure in the case of GaAs and an incorporation rate which is inversely proportional to the applied  $P_2$  pressure in InP. It seems that equilibrium calculations alone cannot explain the relative insensitivity of the desorption of sulphur to the  $P_2$  pressure.

As discussed in Chapter 5, the concentrations of native defects formed in the crystal during the growth under equilibrium conditions can be calculated by utilising the Law of Mass Action. However, due to the lack of reliable thermodynamic data the self-consistent calculation of defect concentrations in III-V compounds is an overambitious goal. The thermodynamic model can be simplified by taking the Fermi-level of the crystal as an adjustable parameter. Therefore, the calculation of the defect concentrations can be formulated without any need for self-consistency in regard of the charge neutrality condition. Moreover, by choosing the defect formation reactions so that only the group V element in the vapour phase, and the group III and V elements on their proper sites in the crystal are involved in the reaction, the concentrations of all isolated point defects can be calculated independently of each other. Hence only those defects which are of interest or for

which the thermodynamic data exists need to be included in the model.

It is found that the virtual formation reactions of isolated point defects in a binary III-V compound can be written as physically realisable reactions if the surface atoms are taken explicitly into account. Such a formulation allows the "virtual" enthalpies and entropies of formation to be determined unequivocally to form a self-consistent system. The virtual free energy of incorporation of the group V element from the vapour phase is calculated correctly from the vapour pressure of the element over the compound during the growth.

A review of the available literature reveals that experimental data of the virtual enthalpies and entropies of formation is lacking. However, good theoretical calculations for the enthalpies of formation of vacancies and antisites exist. Especially the enthalpies of formation of antisites and neutral antistructures from the two completely different model by Van Vechten [4], and Kraut and Harrison [5] can be shown to agree well.

For the entropies of formation neither experimental nor theoretical data is available and their assumed values are almost pure speculation. The entropies of ionisation can be estimated as shown by Van Vechten [4].

Plenty of both experimental and theoretical results of the ionisation levels of native defects exist. The theoretical models are not accurate enough to provide exact values of the ionisation enthalpies, whereas the utility of the experimental data is limited by the difficulty of identifying the defects correctly.

The best available data suggests that anion antisites are the most common native defects in InP and GaAs grown at typical MBE temperatures whilst also ionised cation vacancies should occur at relatively high concentrations.

An asymmetrically doped single quantum well structure was developed in Chapter 6 for studying the effect of silicon migration on electron mobility in modulation doped GaAs/AlGaAs structures. The 100Å wide quantum well is shown to be significantly distorted especially at high two dimensional electron densities ( $n_s$ ) making the interpretation of the measurements more difficult.

Hall and Shubnikov-de Haas measurements show that similar values of  $n_s$  can be achieved in both the normal and the inverted structures. The maximum electron density of the inverted structure is slightly higher indicating that the silicon dopant has migrated towards the quantum well during the growth. The mobility of the 2DEG in the normal structure at 4.2K is higher than in the inverted structure which may be another indication of the migration of the ionised impurities from the first doped layer. However it is not known how much the possible differences in the quality of the two interfaces affect the results.

The measured power law exponents of the  $\mu$  vs.  $n_s$  curves indicate that neither the surface roughness scattering nor the acoustic phonons are responsible for the rather low mobilities in the single quantum wells. Remote ionised impurity scattering has the correct power law dependence but the theoretical mobilities are much higher than those measured for the asymmetric test structures. The ionised impurity scattering by interface (or background) impurities can explain the observed mobilities if a high interface charge density of  $N > 10^{10} \text{cm}^{-2}$  is assumed. However, on the basis of the mobility vs. temperature measurements the strong localisation of the 2DEG by potential fluctuations at the inverted interface can be considered the most likely mechanism responsible for the low 4.2K mobility. The power law exponent  $\alpha = 1.2$  is lower than that observed by Foxon et al. [40] possibly indicating that the potential fluctuations causing the strong localisation

are larger at the inverted interface than at the normal single heterojunction. This is the first time strong localisation has been suggested as a cause of the poor mobility of inverted heterointerfaces. However, the evidence for the strong localisation is still somewhat circumstantial. It would be useful to have a more direct measurement of localisation, one possibility being conductivity measurements at 4.2K, which should reveal negative differential resistance due to the localising potential fluctuations.

Both normal and inverted samples annealed at 680°C and 700°C show a reduction in the 2DE mobility at 4.2K indicating that silicon atoms diffuse away from the doped regions at high temperatures. However an anneal at 650°C did not affect the 2DE mobilities of either sample. It is not known whether the surface segregation or the diffusion is the dominant migration mechanism of silicon at the growth temperature of 600°C.

It is suggested, that in further studies the quality of the inverted interface should be improved to prevent strong localisation. The quantum wells should be thinner (50Å) to prevent the distortion of the well from having an effect on the mobilities and test structures should be grown at several different temperatures to allow comparison with annealed samples.

## 7.2 References

- [1] R.Heckingbottom, J.Vac.Sci.Technol. B3 (1985) 572.
- [2] A.Iliadis, T.Martin and C.R.Stanley, unpublished data.
- [3] C.E.C.Wood and B.A.Joyce, J.Appl.Phys. 49 (1978) 4854.
- [4] J.A.Van Vechten, Chapter 1 in "Handbook on Semiconductors, Vol. 3", ed. S.P.Keller (North Holland, Amsterdam 1980).
- [5] E.A.Kraut and W.A.Harrison, J.Vac.Sci.Technol., B2 (1984) 409.



**MOTTO:**

Ei voi kauhalla ottaa, kun on lusikalla annettu...

Ancient Finnish proverb.